[redacted]

UMRL
050

Studies in Radar Cross-Sections XXI

Radar Cross-Section of a Ballistic Missile - III

by K. M. Siegel, H. Brysk, J. W. Crispin,
R. F. Goodrich, and R. E. Kleinman

Contract AF 04(645)-33

December 1956

2428-19-T

The University of Michigan
Engineering Research Institute
Willow Run Airport
Ypsilanti, Michigan

2428-19-T = RL-2049

CONFIDENTIAL

[redacted]

MISSING PAGE

Declassified IAW E.O. 11652 dated 8March72
Section 5, paragraph D

TABLE OF CONTENTS

		Page
	List of Studies in Radar Cross-Sections	iv
	Preface	vi
I	Introduction and Summary	1
II	The Radar Cross-Section of the Rudolph Warhead	7
III	The Radar Cross-Section of the Perturbations to The Rudolph Warhead	16
IV	The Radar Cross-Section of Conical Bodies of Revolution	30
Appendix A - Rayleigh Cross-Sections of Bodies of Revolution		42
Appendix B - Physical Optics Radar Cross-Section of a Finite Cone For Near Nose-On Aspects		59
Appendix C - The Radar Cross-Section of a Thin Wire Loop For Small Wavelengths		71
Appendix D - Circular Wedge Approximation to Radar Cross-Section of Thin Finite Cones		73
Appendix E - Minimal Cross-Section Shapes		84
Appendix F - The Radar Cross-Section of Finite Cones With Various Base Terminations - A Comparison Between Theory and Experiment		92
Appendix G - The Radar Cross-Section of An Ogive		107
References		122

I

INTRODUCTION AND SUMMARY

The University of Michigan has been working on problems involving defense against ballistic missiles since 1946. One of the major aspects of these problems is the determination of the detectability of a ballistic missile by a search radar. The main parameter in such a discussion is the radar cross-section of the missile. The same parameter is important for those engaged in developing offensive ballistic missiles. Thus, it behooved these people to avail themselves of our studies in order to reduce the radar cross-section of our offensive missiles and thus produce a less detectable and perforce more deadly weapon.

Our first major project for the Ramo-Wooldridge Corporation was to determine theoretically the radar cross-section of six new ballistic missile warhead shapes. One of the assignments under the continuation of this Air Force contract was to have these theoretical values experimentally checked at certain frequencies. This has now been done and the agreement between theory and experiment is excellent.

In order to improve the probability of kill, those working on offensive missiles had to decide how much they could afford to reduce the radar cross-section of the weapon without violating the restrictions placed by other systems parameters, such as weight and aerodynamic considerations. It was conceived (Ref. 1) that it would be possible in the ICBM program to place dummy surfaces around the 3rd stage of our intercontinental ballistic missile as long as these dummy surfaces would vaporize almost immediately on re-entry.

(In Reference 1 and this report we call the warhead Rudolph because of its red nose upon re-entry.) It was then predicted by order-of-magnitude investigations that "conical nose, ogival midsections, and conical tail"-type assemblies would greatly reduce the nose-on cross-section of the 3rd stage ballistic missile and that these reductions would increase with frequency, reaching possibly a factor of 10^5 at S-band.

Since that time, these ideas have been experimentally checked, the theory has been refined, and we have learned that it is definitely feasible, using the ideas presented in Reference 1, to reduce the radar cross-section of a ballistic missile. Of course, in any refinement investigation one learns how to improve his work and he learns a great deal by experiment. We have learned that the rougher approach of Reference 1 gave reductions of 25 to 35 db from 400 Mc through X-band and it is believed this is also true for all higher frequencies. We have found that in the 200 to 400 Mc frequency range a much smoother transition section between the nose and tail surfaces than was proposed previously is required.

Between the time Reference 1 was written (January 1956) and the writing of this report (November 1956) the defensive thinking has changed regarding the lowest frequency of detection. Search radars are being considered for the 380 to 1000 Mc range with much greater weight still being placed on the lower frequencies. As a result, in this report we are concentrating on the lower frequencies in this range. However, the 200 Mc situation will also be considered because of what is primarily a contractual obligation; it should be

noted that the 200 Mc frequency range may again become of prime importance as it was two years ago.

In Section 2 the basic shapes of the 3rd stage ballistic missile as presented in Reference 1 are considered. Theoretical and experimental results in the 350 Mc to 500 Mc frequency range for these shapes are compared. The theoretical values are only average values of the data; the experimental results indicate the oscillations around this average. These experiments were done by Air Force Cambridge Research Center and the Canadian government. We gratefully acknowledge the assistance that the work of R. I. Primich of the Radio Physics Laboratory of the Defence Research Board of Canada and Nelson Logan, B. B. Gorr, and Lt. P. Blacksmith of Air Force Cambridge Research Center has been to our study.

A discussion is presented in Section 2 concerning the effects of a small variation in frequency about any given primary detection frequency. It was found in experimental data obtained at Air Force Cambridge Research Center, that a change of $\pm$ 5% around 400 Mc will produce a 12 db increase in cross-section in the critical null-regions of the patterns. This is very important from the defensive view point as it shows that a factor of more than 10 can be gained in power by using one additional frequency. This means that by increasing transmitted power by a factor of 2 one can gain a factor of 10 in received power, so that operation at two contiguous frequencies is clearly an important new concept in defensive ballistic missile thinking. The critical frequency was raised from 200 Mc to 400 Mc in the hope of mitigating

the difficulties associated with the aurora, propagation effects, and the Faraday effect when looking through the ionosphere and to decrease the number of meteors that would trip the warning system. Also, this change in frequency is expected to be advantageous due to the fact that, while there is expected to be no significant change in cross-section between the two frequencies, the enemy's countermeasure program becomes increasingly difficult, since, at the new frequencies, the powers that must be transmitted by long range propagation are now too large to be considered practical for jamming from Russia. Theoretical and experimental data lead us to believe that some of this reasoning is incorrect, however, this material cannot be released without a special need-to-know. Some answers to this problem will be obtained as an incidental biproduct on contract AF 33(600)34359.

In Section 3 we present data for the perturbed missile shapes presented in Reference 1. The experimental results of the Cornell Aeronautical Laboratory and the Canadian government are presented and compared with theory. These experimental values and an improvement in our theory have indicated that the minimal shape ideas are correct even though small variations in the geometry will be needed in order to reduce the cross-section by as much as was predicted in Reference 1. However, as stated above, for frequencies above 400 Mc one can expect, even with our preliminary shapes, reduction in cross-sections of 25 to 35 db.

In Appendix F we present the radar cross-section of the 3rd stage ballistic missile shape specified as "Carrot" by the Cornell Aeronautical Laboratory.

Section 4 is devoted to a discussion of a new theoretical approach to the determination of the radar cross-section of bodies of revolution. This work is used with the material previously reported in References 1 and 2 to determine the cross-sections of ballistic missile shapes of interest to this contract and to Project Plato.*

The experimental results of the University of California (Ref. 3) and The Ohio State University (Ref. 4) and theoretical work on spheroids (Ref. 5), indicate that for large length-to-width-ratio bodies of revolution the significant resonant region was much greater than had been anticipated from the sphere, infinite cone, paraboloid, and wedge results. It is necessary to find how to determine the length of the resonance region as a function of ka ($k = 2\pi/\lambda$ and a = one-half the maximum dimension in the direction of Poynting's vector). This analysis will allow one to predict the frequency range in which it is sensible to use more than one transmitted frequency - that is, to predict the region (in ka) where there is a sufficient difference in amplitude between the maxima and minima to warrant the extra instrumentation. Clearly, in the optics region the decrease in amplitude at two adjacent

* The investigation presented in Section IV and Appendices A through F was partially supported by Project Plato. Part of the effort reported in "Radar Cross-Sections of Conical Bodies of Revolution" by K. M. Siegel, Engineering Research Institute, The University of Michigan, Report No. 2488-1-T, (31 October 1956), SECRET, was supported by this contract. In this way we could make more basic information available to both projects without extra cost to the United States Government.

frequencies is not sufficient to warrant the extra instrumentation. Thus a theoretical analysis had to be done to determine the location in ka space of the resonance region. This analysis is handled in Section 4 supplemented by the unclassified Appendices A, B, C, D, and G and the classified Appendices E and F.

Appendices A, B, C, and D contain important new unclassified theoretical radar cross-section data. It is of extreme importance that this new information receive proper distribution.

Considerable effort has been expended on the determination of the radar cross-section of the finite cone by the variational method. This work will be reported elsewhere without cost to this contract.

Also, probabilistic methods have been applied to the task of solving unseparable boundary value problems. The results of these investigations will also be reported elsewhere without cost to this contract.

We wish to alert the reader to the fact that the experiments reported here do not constitute the complete body of experimental data on present I.C.B.M. shapes. The authors are familiar with several other sets of experimental data which pertain in an important way to this study. This data is available to the reader with a sufficient need-to-know.

II

THE RADAR CROSS-SECTION OF THE RUDOLPH WARHEAD

Theoretical estimates of the radar cross-sections of six parameterizations of the Rudolph warhead were presented in Reference 1. The six parameterizations of the basic warhead shape are shown in Figures 2-1 and 2-2. The theoretical data presented in Reference 1 cover the aspect range out to sixty degrees off nose and radar frequencies from 200 Mc to 3000 Mc.

Since the publication of Reference 1, experiments have been conducted at the Air Force Cambridge Research Center (Ref. 6) and at the Radio Physics Laboratory of the Defence Research Board of Canada (Ref. 7). The Air Force Cambridge Research Center experiments were conducted at a model frequency of approximately 9300 Mc resulting in equivalent full-scale data at 400 Mc. These Air Force Cambridge Research Center experiments involved each of the six basic configurations. The results of these experiments are shown in Figure 2-3 through 2-8. The theoretical estimates given in Reference 1 for the cross-sections at 350 Mc for the aspect range out to sixty degrees off nose are also presented in Figure 2-3 through 2-8. It can readily be observed that the "average" curves predicted in Reference 1 are in good agreement with the experimental data. Since the AFCRC experimental data gives more information than we attempted to obtain theoretically we recommend that the Cambridge data be used in preference to ours for this reason.

The Radio Physics Laboratory of the Defence Research Board of Canada obtained data for a missile shape very similar to that of Configuration I

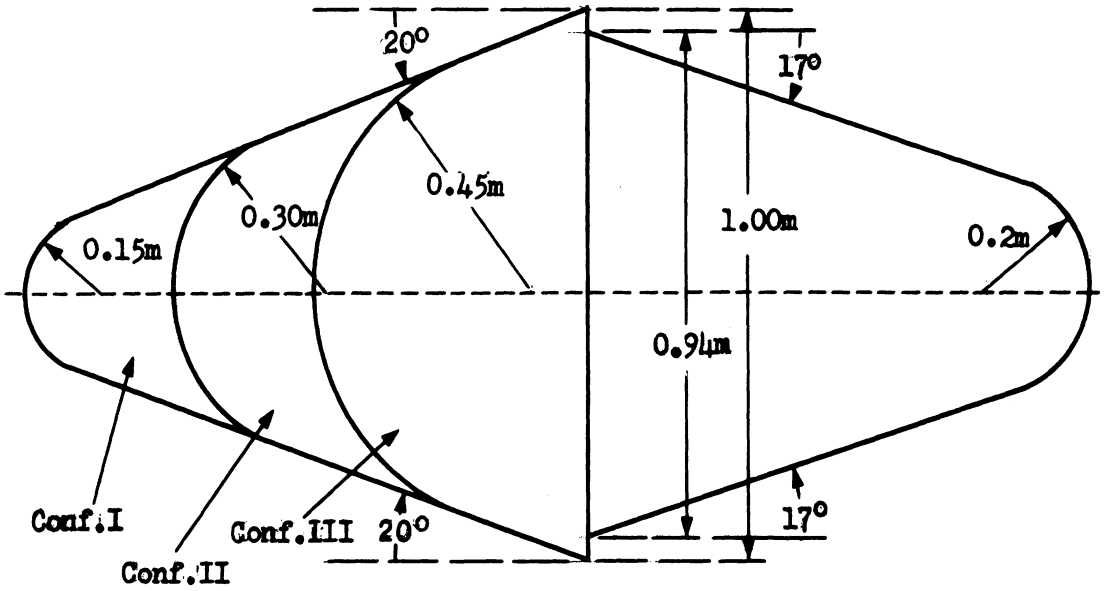

FIG. 2-1 CONFIGURATIONS I, II, AND III

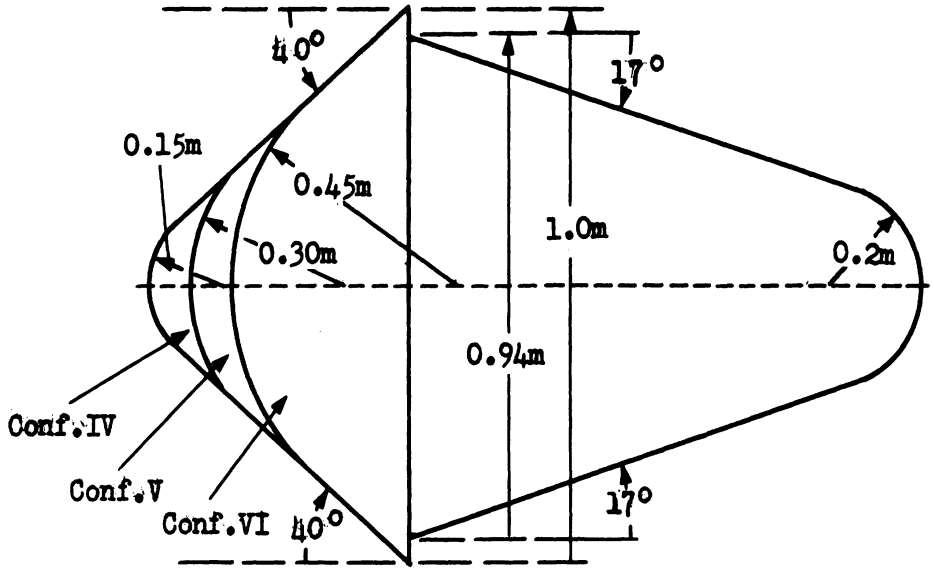

FIG. 2-2 CONFIGURATIONS IV, V, AND VI

SECRET

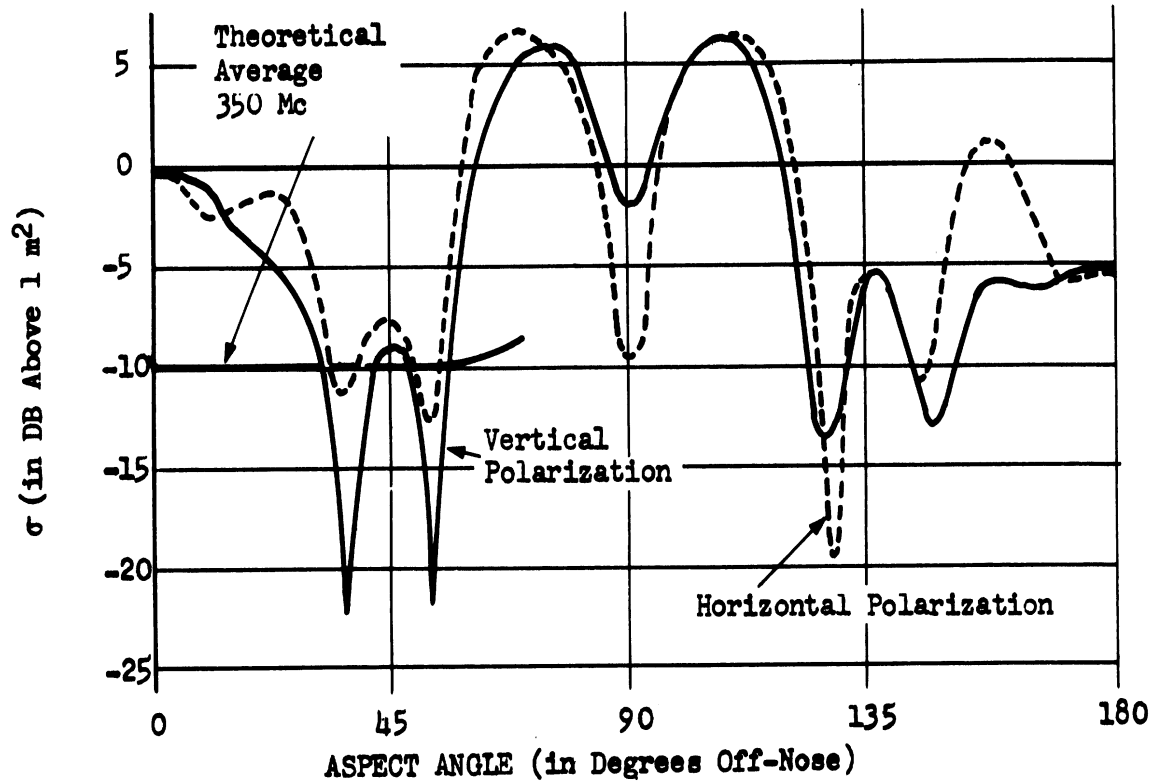

FIG. 2-3 CROSS-SECTION OF CONFIGURATION I AT 400 Mc(AFCRC DATA)

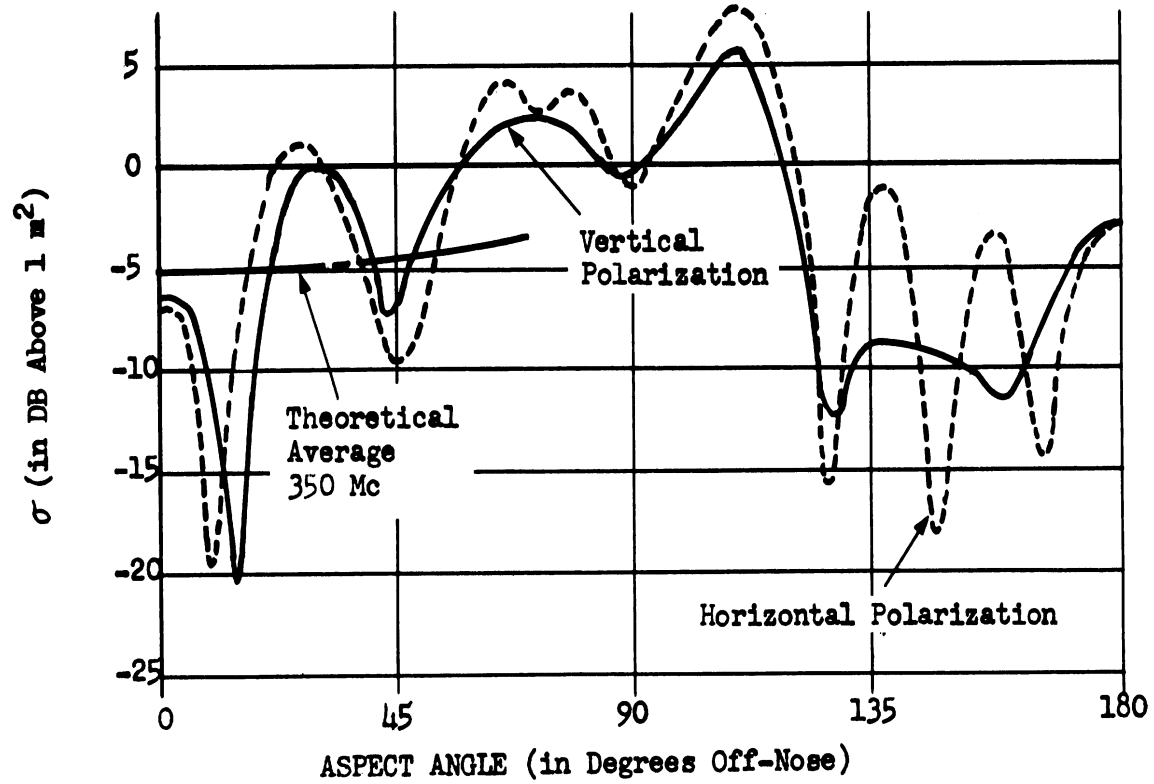

FIG. 2-4 CROSS-SECTIONS OF CONFIGURATION II AT 400 Mc (AFCRC DATA)

SECRET

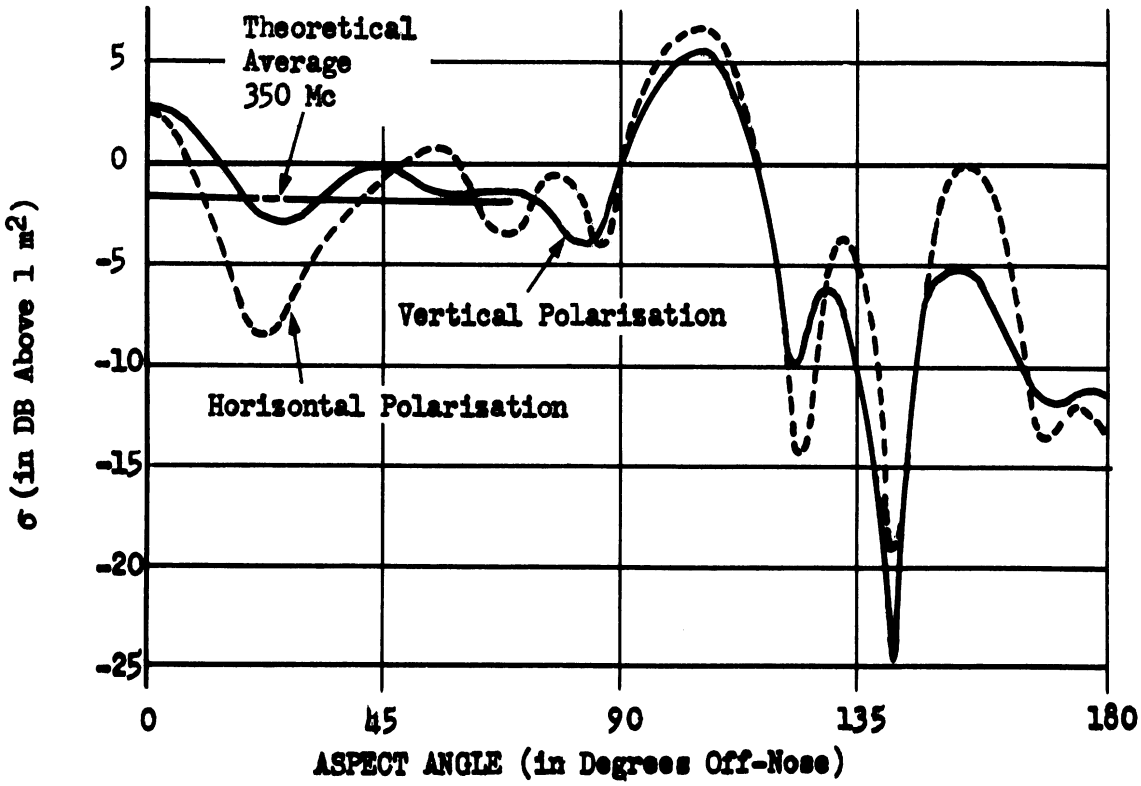

FIG. 2-5 CROSS-SECTION OF CONFIGURATION III AT 400 Mc (AFCRC DATA)

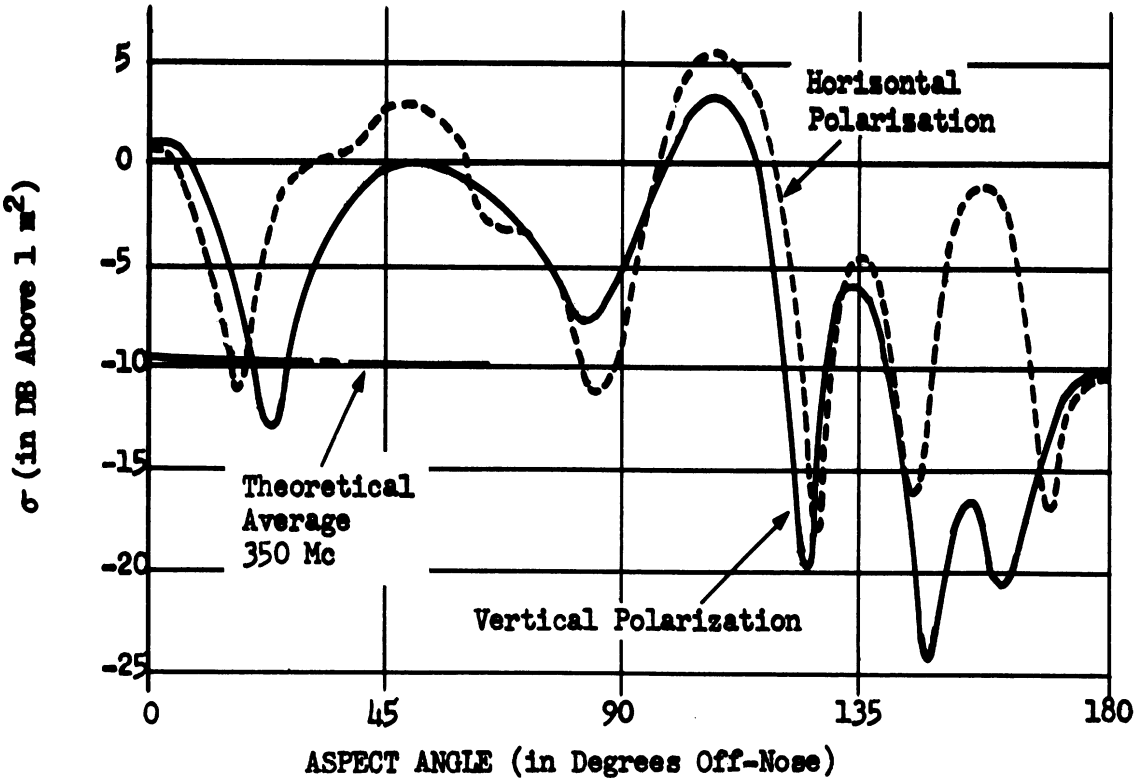

FIG. 2-6 CROSS-SECTIONS OF CONFIGURATION IV AT 400 Mc (AFCRC DATA)

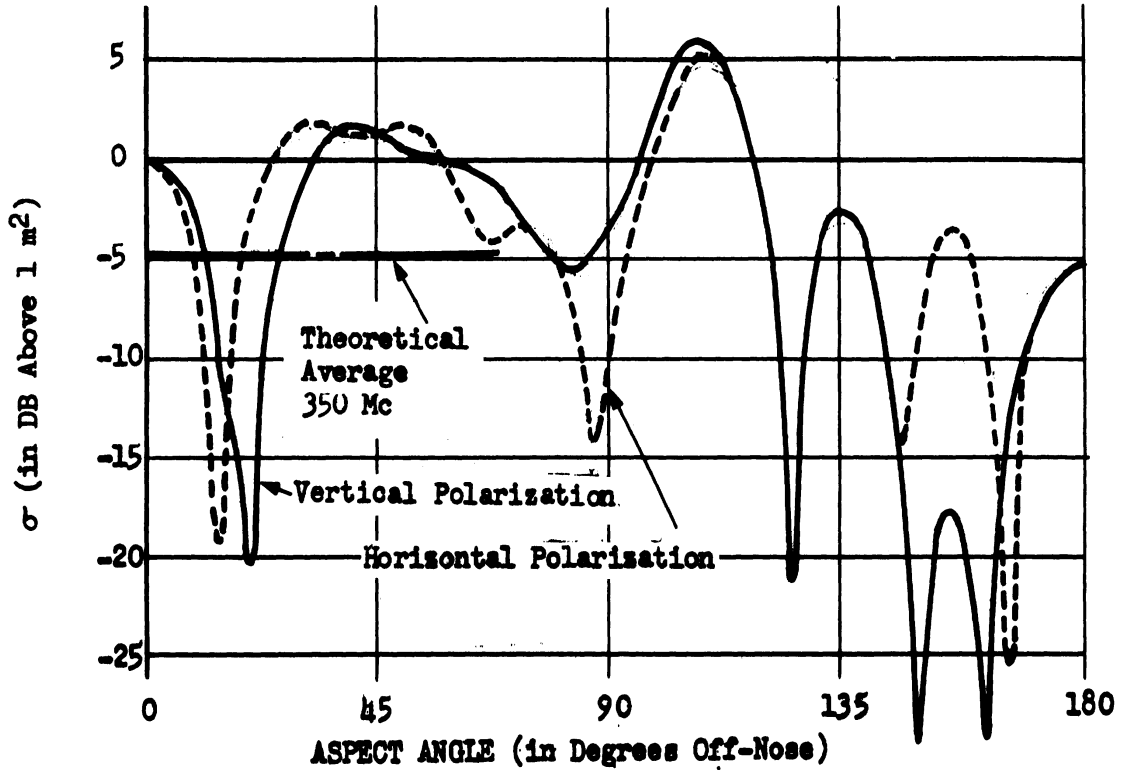

FIG. 2-7 CROSS-SECTION OF CONFIGURATION V AT 400 Mc(AFCRC DATA)

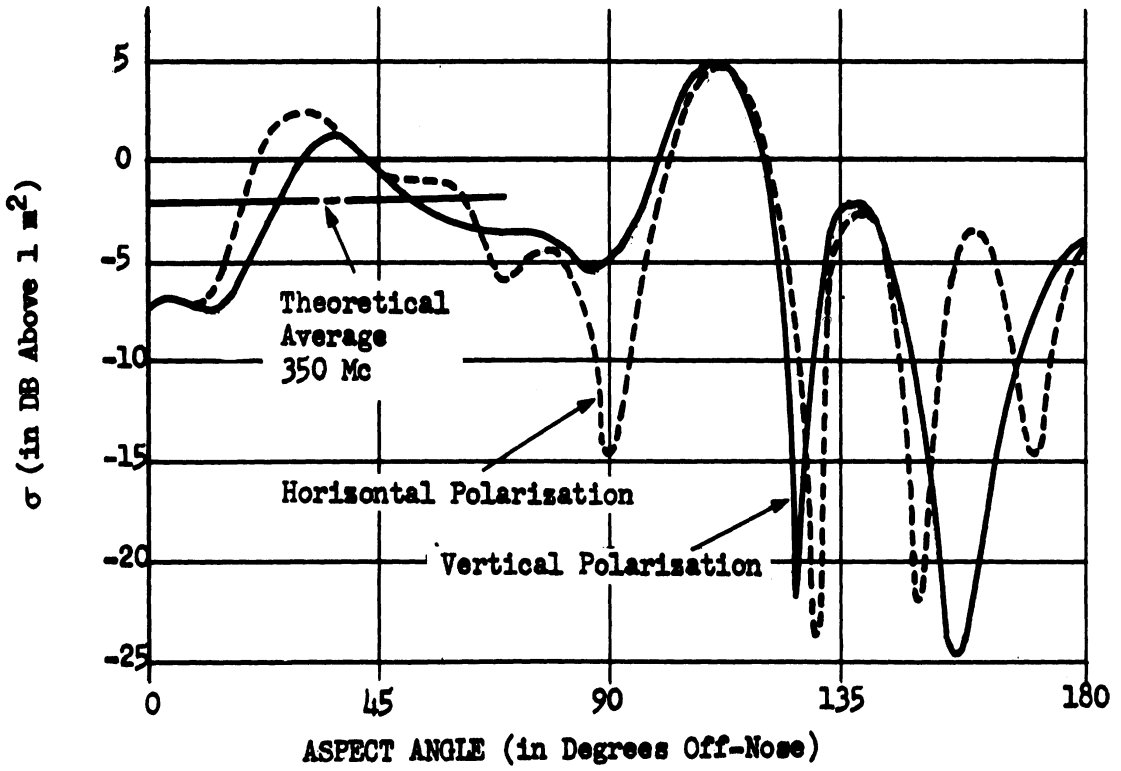

FIG. 2-8 CROSS-SECTIONS OF CONFIGURATION VI AT 400 Mc (AFCRC DATA)

(the only difference being in the radius of curvature at the rear). These data are for vertical polarization only and are for an equivalent full-scale frequency of 500 Mc. These Canadian data are presented in Figure 2-9 where they are compared with the 500 Mc theoretical estimate given in Reference 1 for Configuration I. Again, it is readily seen that the agreement between the theoretical "average" curve and the experimental data is excellent.

Experiments conducted at AFCRC have shown that if one should operate at 380 Mc, at 400 Mc, and at 420 Mc, 12 db power gains in the nulls are easily possible. That is, the cross-section varies as a function of both aspect and frequency, and if the aspect is held fixed, this $\pm 5\%$ variation in frequency at this frequency permits one to fill in the nulls of the pattern obtained from one frequency. The AFCRC experiments conducted for both polarizations and various elevation and azimuth angles have indicated that defensive systems would benefit by 12 db through the use of three frequencies.*

Since the publication of Reference 1 the theoretical techniques have been refined. The theoretical cross-sections predicted by these refined techniques are presented in Table 2.1 for the nose-on cross-sections of these six configurations at 200 Mc, at 400 Mc, and at 500 Mc. Included in the table are the nose-on cross-section values obtained experimentally by AFCRC and RPL-DRB. We consider the agreement between theory and experiment shown in Table 2.1 to be excellent. As in Reference 1, the theoretical estimates consist

*These data were shown to two of the authors (K. M. Siegel and J. W. Crispin) by Lt. Blacksmith of AFCRC at a meeting held at WDD on 15 November 1956.

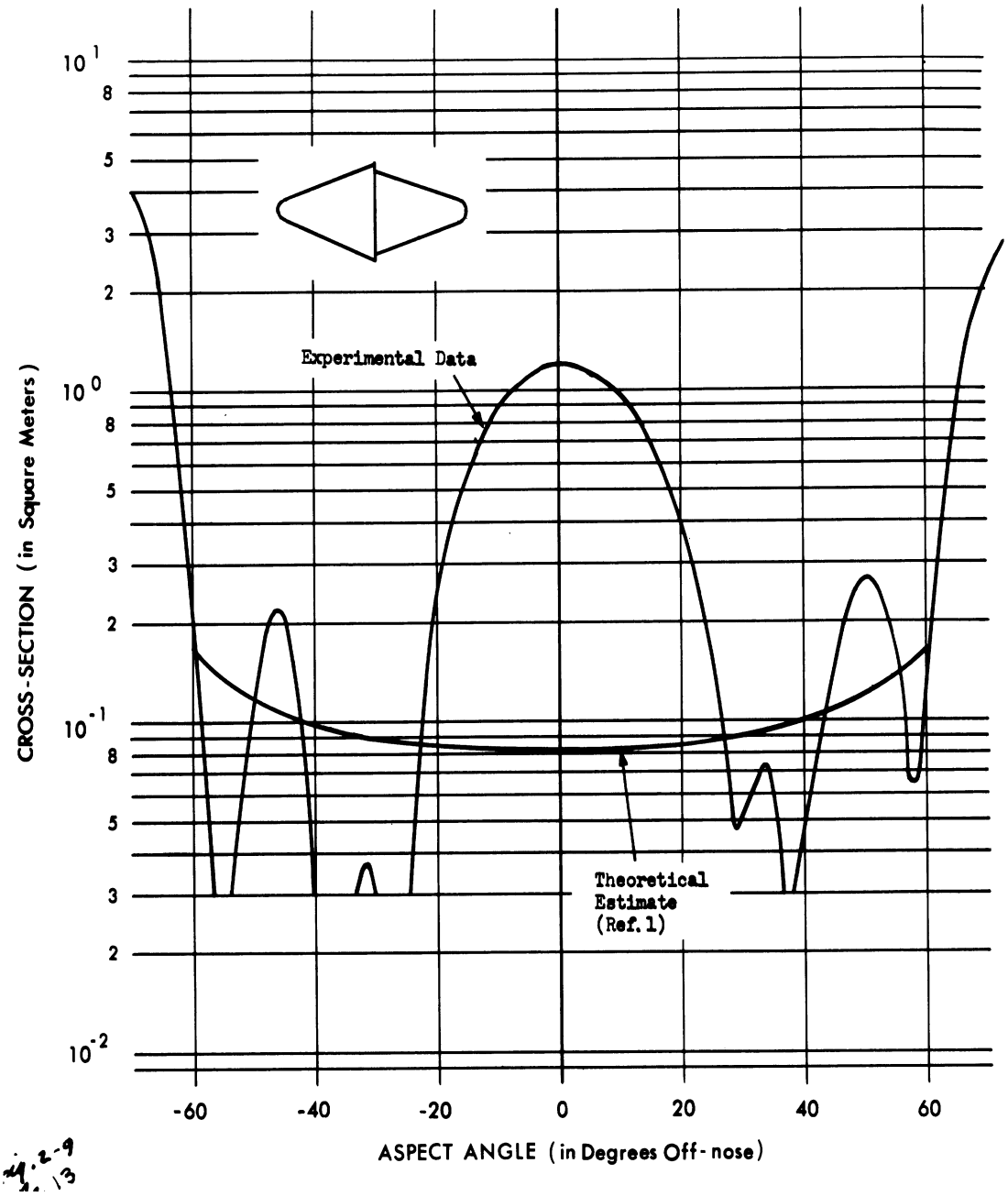

FIG 2-9 RADAR CROSS-SECTION OF CONFIGURATION I AT 500 Mc
(RPL-DRB DATA) (VERTICAL POLARIZATION)

TABLE 2.1: NOSE-ON CROSS-SECTIONS OF CONFIGURATIONS I, II, III, IV, V, AND VI COMPUTED BY REFINED THEORETICAL TECHNIQUES COMPARED WITH EXPERIMENTAL DATA OBTAINED BY AFCRC AND RPL-DRB

Configuration	Frequency	Cross-Section (in m^2)			
		Theoretical Estimate			Experimental Data
		Lower Bound	Av.	Upper Bound	
I	200 Mc	0.58	1.1	1.7	---
II	"	0.26	1.3	2.4	---
III	"	0.04	1.7	3.4	---
IV	"	0.58	1.1	1.7	---
V	"	0.26	1.3	2.4	---
VI	"	0.04	1.7	3.4	---
I	400 Mc	0.23	0.62	1.0	1.0 (1)
I	500 Mc	0.23	0.62	1.0	1.0 (2)
II	400 - 500 Mc	0.05	0.82	1.6	0.2 (1)
III	"	0.005	1.2	2.4	2.0 (1)
IV	"	0.29	0.72	1.1	1.0 (1)
V	"	0.08	0.92	1.7	1.0 (1)
VI	"	6×10^{-4}	1.3	2.6	0.2 (1)

(1) - AFCRC Data

(2) - RPL-DRB Data

of an average value and estimates of upper and lower bounds. These bounds are obtained by assuming that the contributions from the nose and the step are either completely in phase or completely out of phase. The refinement in the theoretical technique consists of a new treatment of the contribution of the step. The details of the procedure are given in Section 4 and in Appendix D.

Though the checking of the basic warhead theoretical values was a very important consideration of this contract we will spend no further time on this part of our study because as theoreticians we are happy with our results. We shall now turn our attention to the perturbed shapes and to the recent theoretical investigations which have led to a modification of our interpretation of the effects to be expected through the use of these perturbations.

III

THE RADAR CROSS-SECTION OF THE PERTURBATIONS TO THE RUDOLPH WARHEAD

Several types of perturbations to the six basic shapes of the Rudolph Warhead were considered in Reference 1. Theoretical estimates were obtained over the frequency range from 200 Mc to 3000 Mc and conclusions reached as to the type of perturbation which would be most effective in reducing the detectability of the warhead. We now know that the ideas presented in Reference 1 for reducing the radar cross-section of the missile warhead are correct. However, for the magnitude of the effect to be in the ball park we predicted requires that the ratio of radius of curvature to wavelength in the transition region must be greater than stated in Reference 1.

In this section we shall examine the experimental data obtained for these perturbed shapes, compare the experimental data with the theoretical estimates given in Reference 1, and present the new theoretical approach for the estimation of the cross-section of the optimum perturbed shape.

The experimental measurements were performed at the Cornell Aeronautical Laboratory, Inc.* and at the Radio Physics Laboratory of the Defence Research Board of Canada. The perturbed shapes involved in the C.A.L. experiments are shown in Figures 3-1 through 3-3.

*The C.A.L. experiments were performed under a University of Michigan subcontract under the prime contract AF04(645)-33.

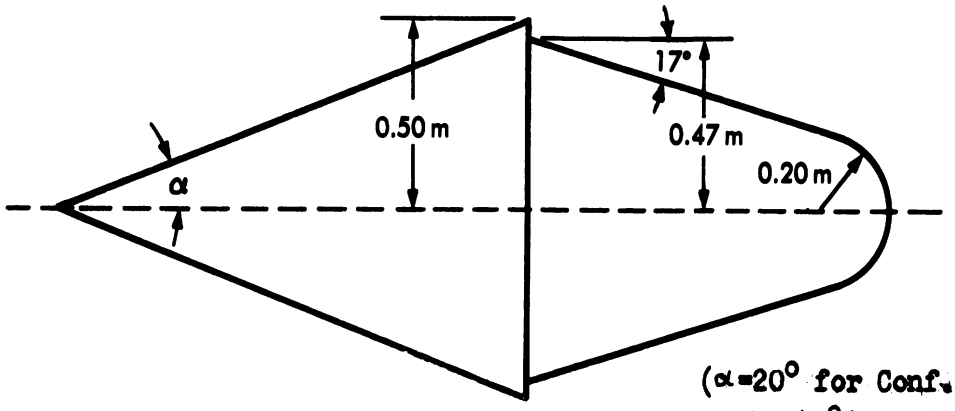

($\alpha = 20^{\circ}$ for Conf. A
and $\alpha = 40^{\circ}$ for Conf. B)

FIG. 3-1 CONFIGURATIONS A AND B

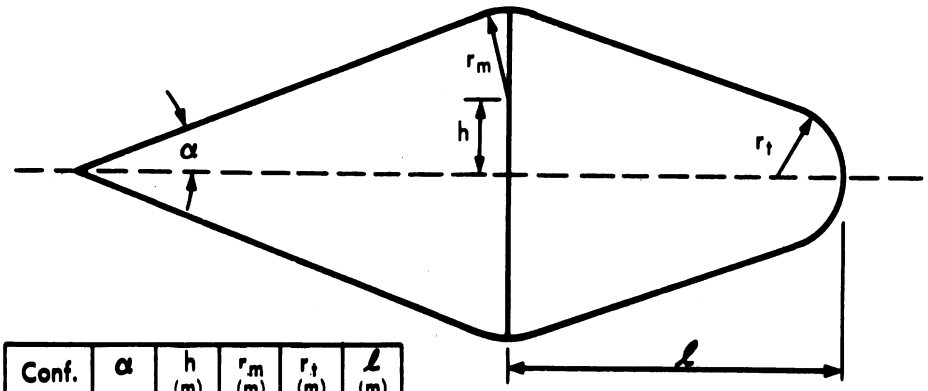

Conf.	α	h (m)	r_m (m)	r_t (m)	ℓ (m)
E	20°	0.22	0.28	0.20	1.03
F	40°	0.43	0.07	0.20	1.03

FIG. 3-2 CONFIGURATIONS E AND F

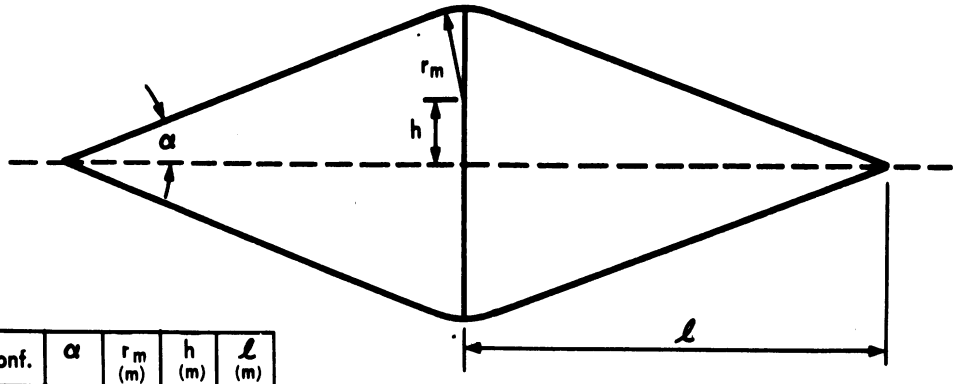

Conf.	α	r_m (m)	h (m)	ℓ (m)
G	20°	0.28	0.22	1.45
H	40°	0.07	0.43	1.45

FIG. 3-3 CONFIGURATIONS G AND H

All of the C. A. L. measurements were made in the aspect range from nose-on out to sixty degrees off-nose. The data are shown in Figure 3-4 through 3-9.

These experiments and a detailed report of the experimental technique employed are reported in Reference 8. It is stated there that

> "... the error involved for the small models, from an equipment standpoint, is estimated to be in the order of .4 db. An additional error occurs in mounting the models in the support--the uncertainty of again regaining the same position from run to run, and from obtaining a true orthogonal coordinate system. With proper set-up care, overall error is estimated to be about 1 db for the group of small models (estimated for the maximum cross-section condition only). With sharp nulls present and the angular resolution only good to $\pm 0.5^{\circ}$, there is a rapid decay until, in the nulls, the error may be as much as of the order of 4 db."

The experiments performed at the Radio Physics Laboratory of the Defence Research Board of Canada are reported in Reference 7. The first of the perturbations considered in these experiments is similar to Configuration A in that the step is present; it differs from Configuration A in that the rear of the body is pointed. The second of these Canadian perturbed shapes is similar to that of Configuration G except that the radius of curvature at the shadow boundary is larger (about twice as large). The results of these experiments (designed to give data for the full-scale configurations at

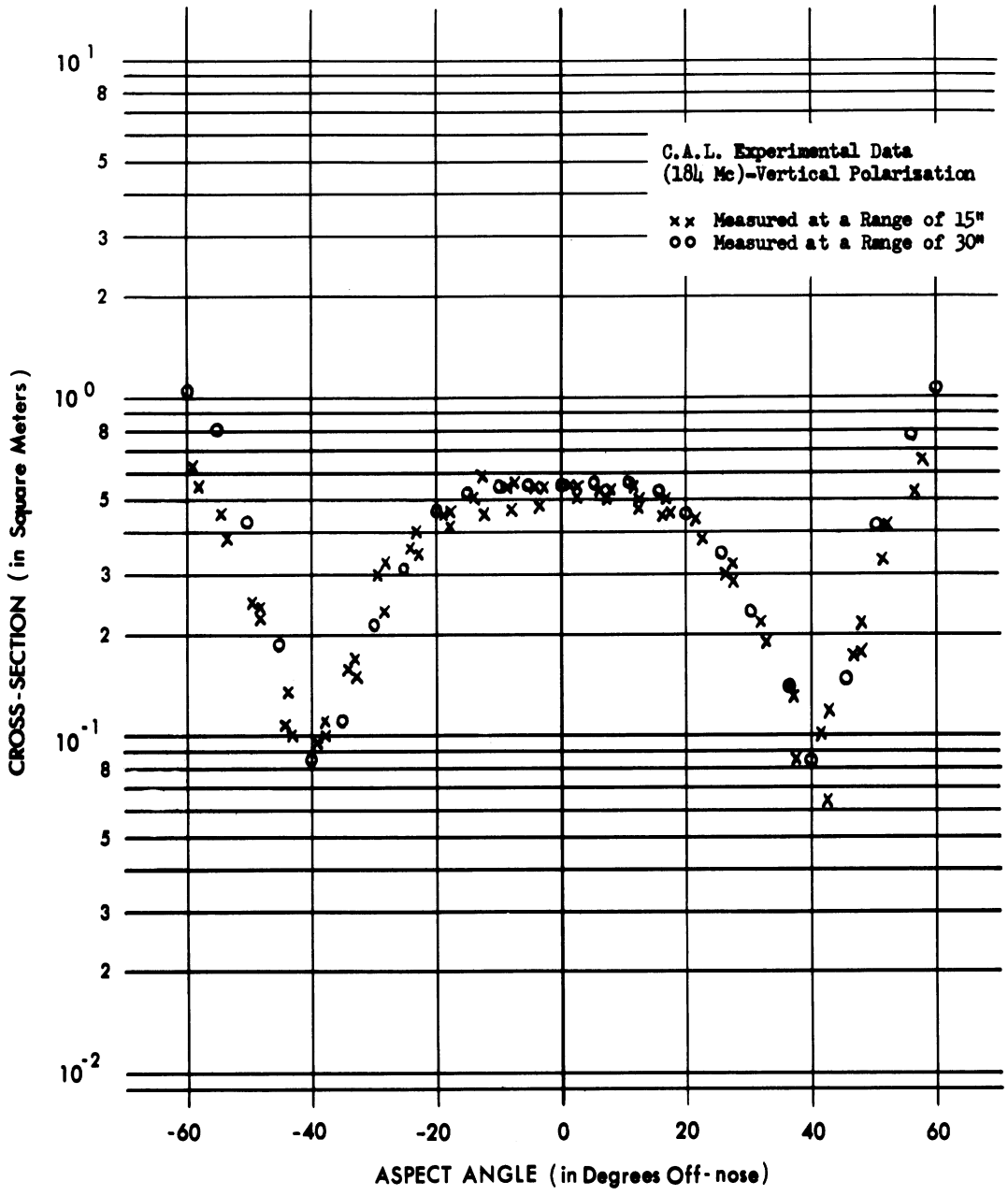

FIG 3-4 RADAR CROSS-SECTION OF CONFIGURATION A AT A FREQUENCY OF APPROXIMATELY 200 Mc

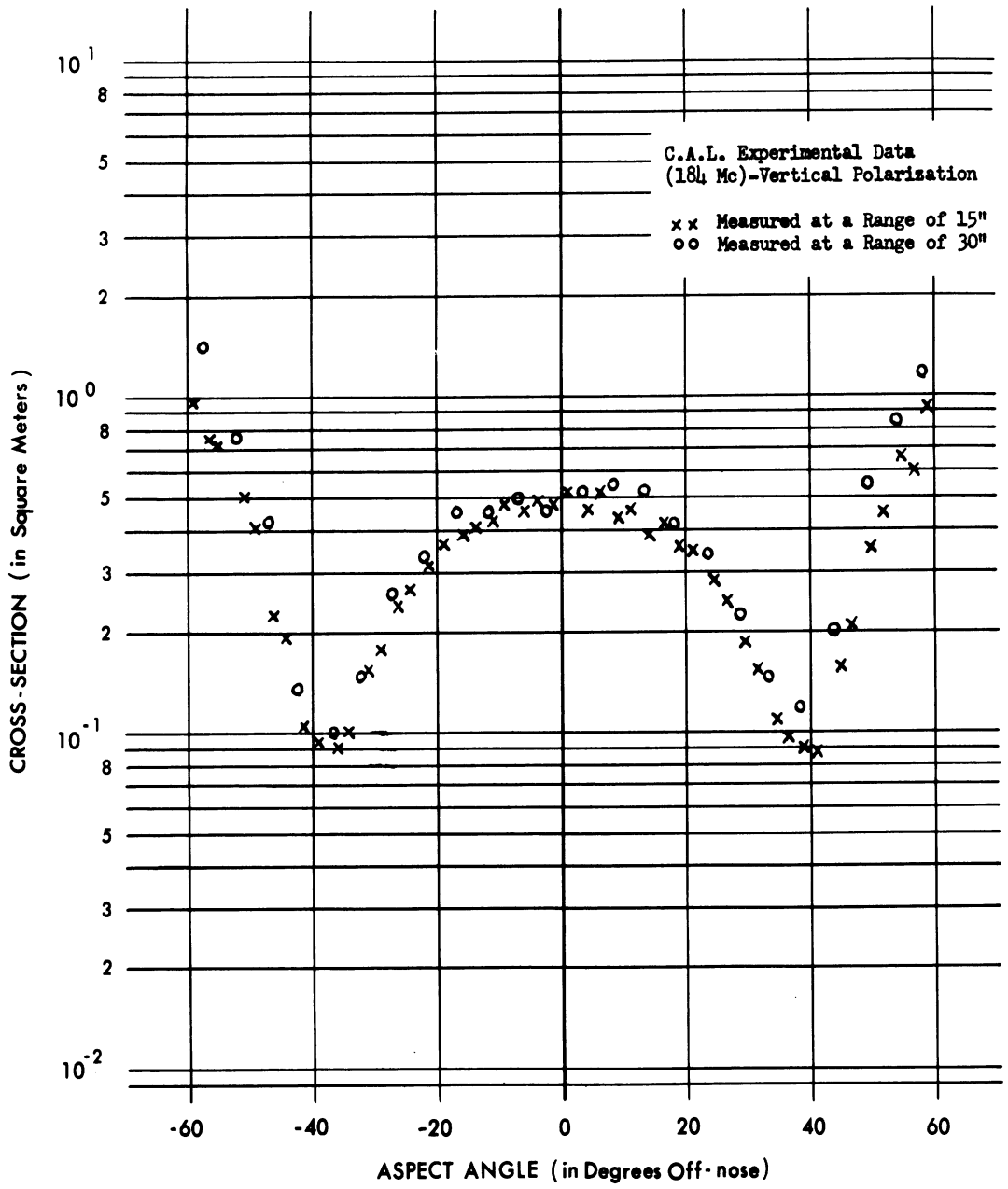

FIG 3-5 RADAR CROSS-SECTION OF CONFIGURATION E AT A FREQUENCY OF APPROXIMATELY 200 Mc.

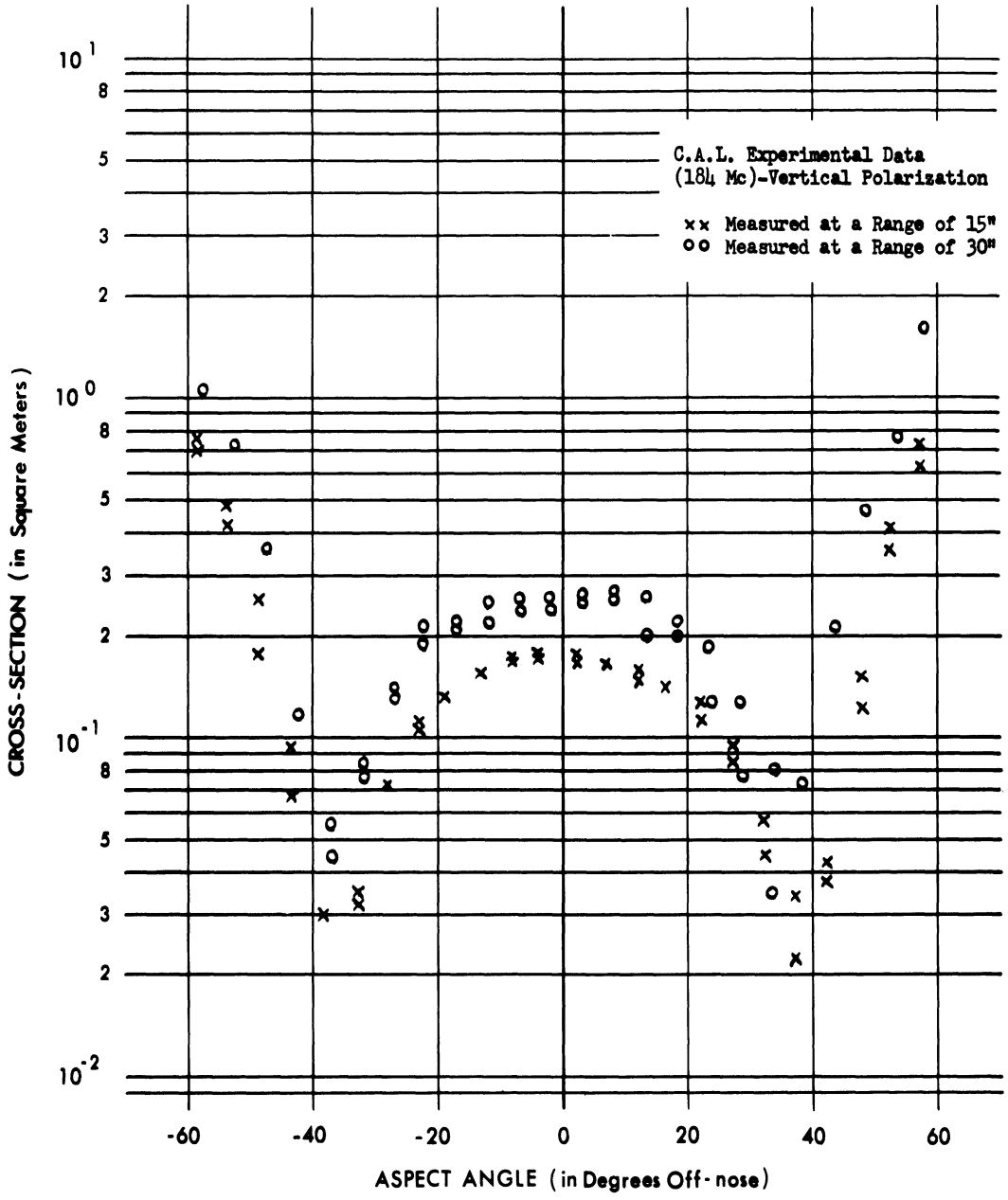

FIG 3-6 RADAR CROSS-SECTION OF CONFIGURATION G AT A FREQUENCY OF APPROXIMATELY 200 Mc.

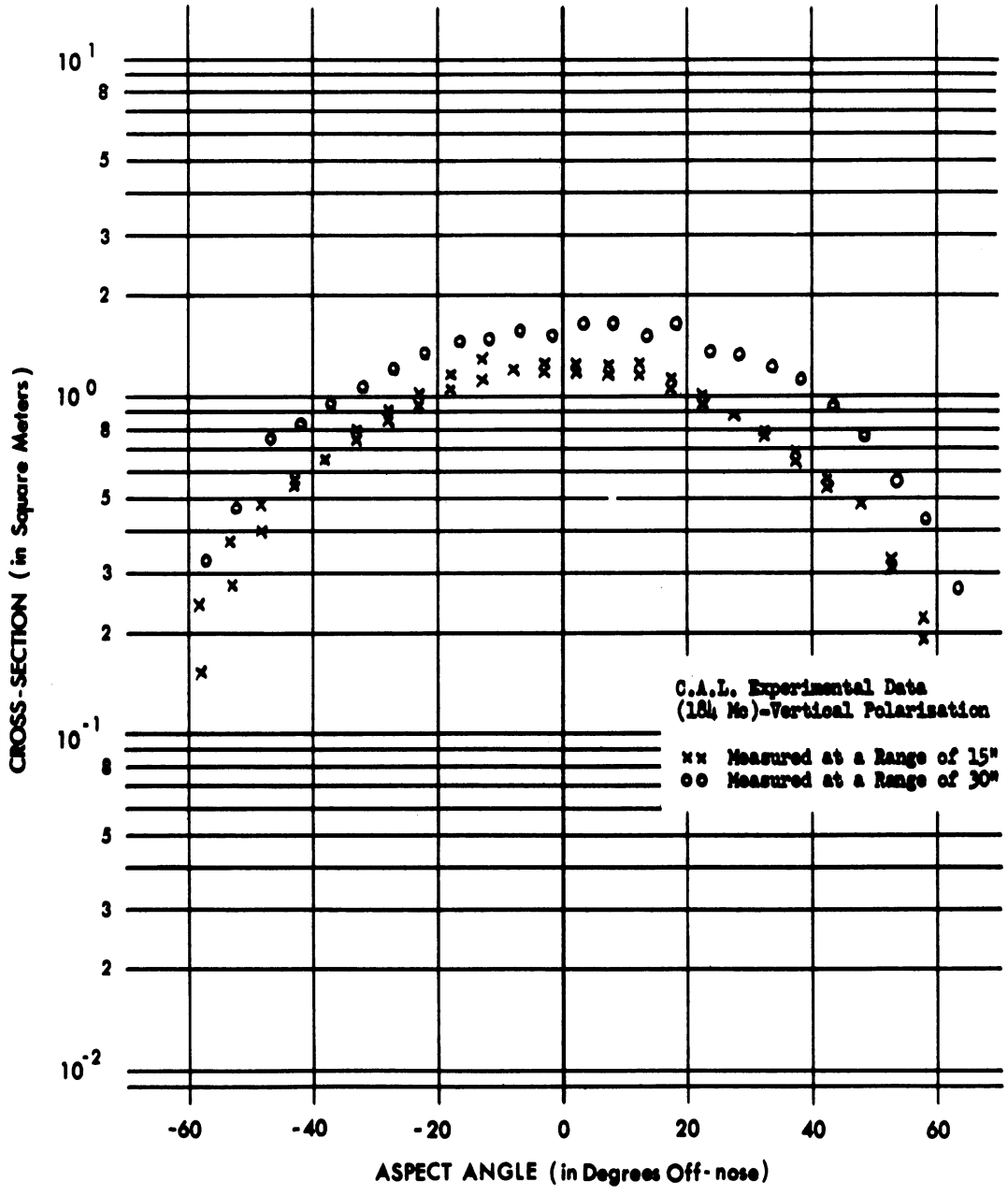

FIG 3-7 RADAR CROSS-SECTION OF CONFIGURATION B AT A FREQUENCY OF APPROXIMATELY 200 Mc.

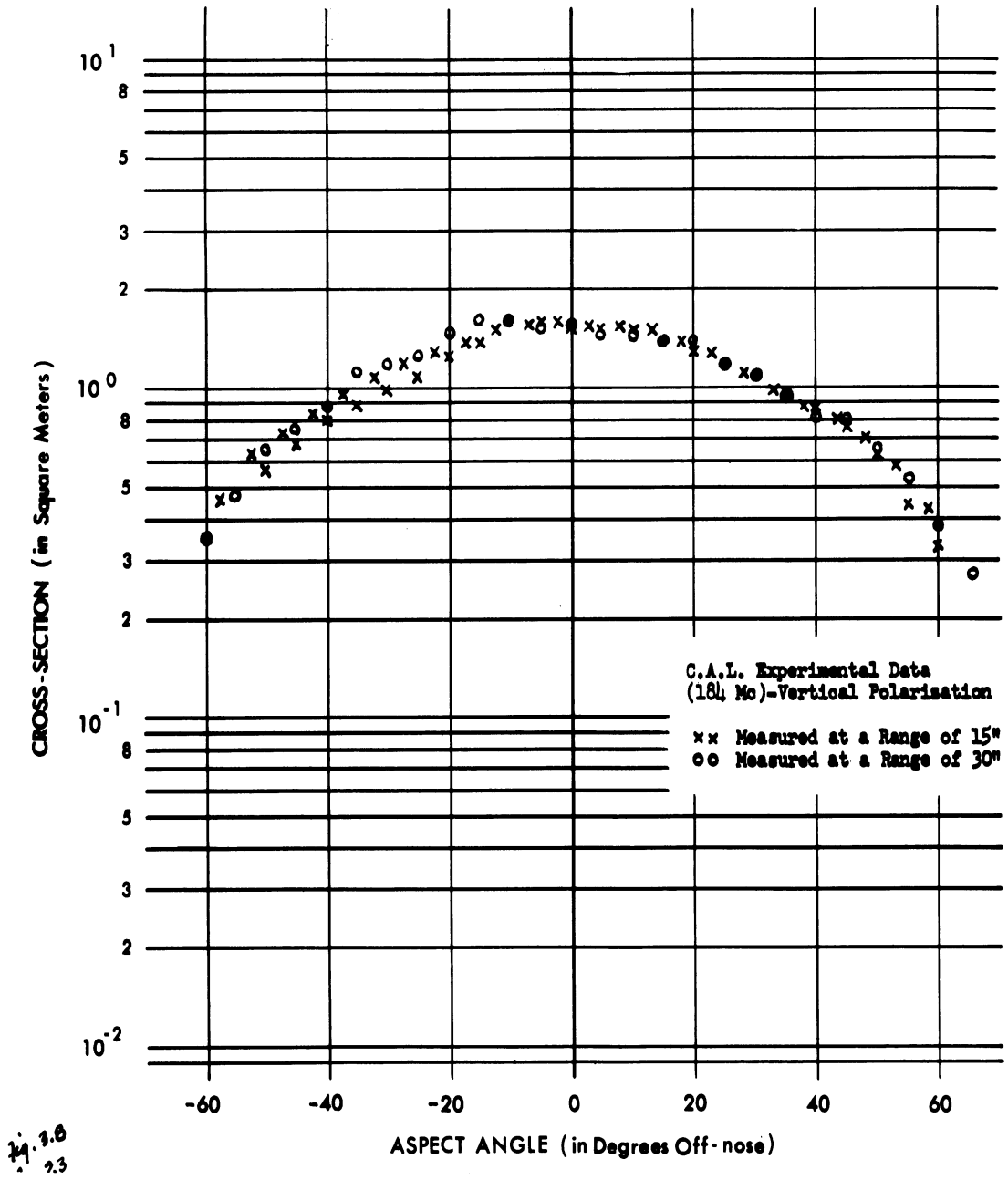

FIG 3-8 RADAR CROSS-SECTION OF CONFIGURATION F AT A FREQUENCY OF APPROXIMATELY 200 Mc.

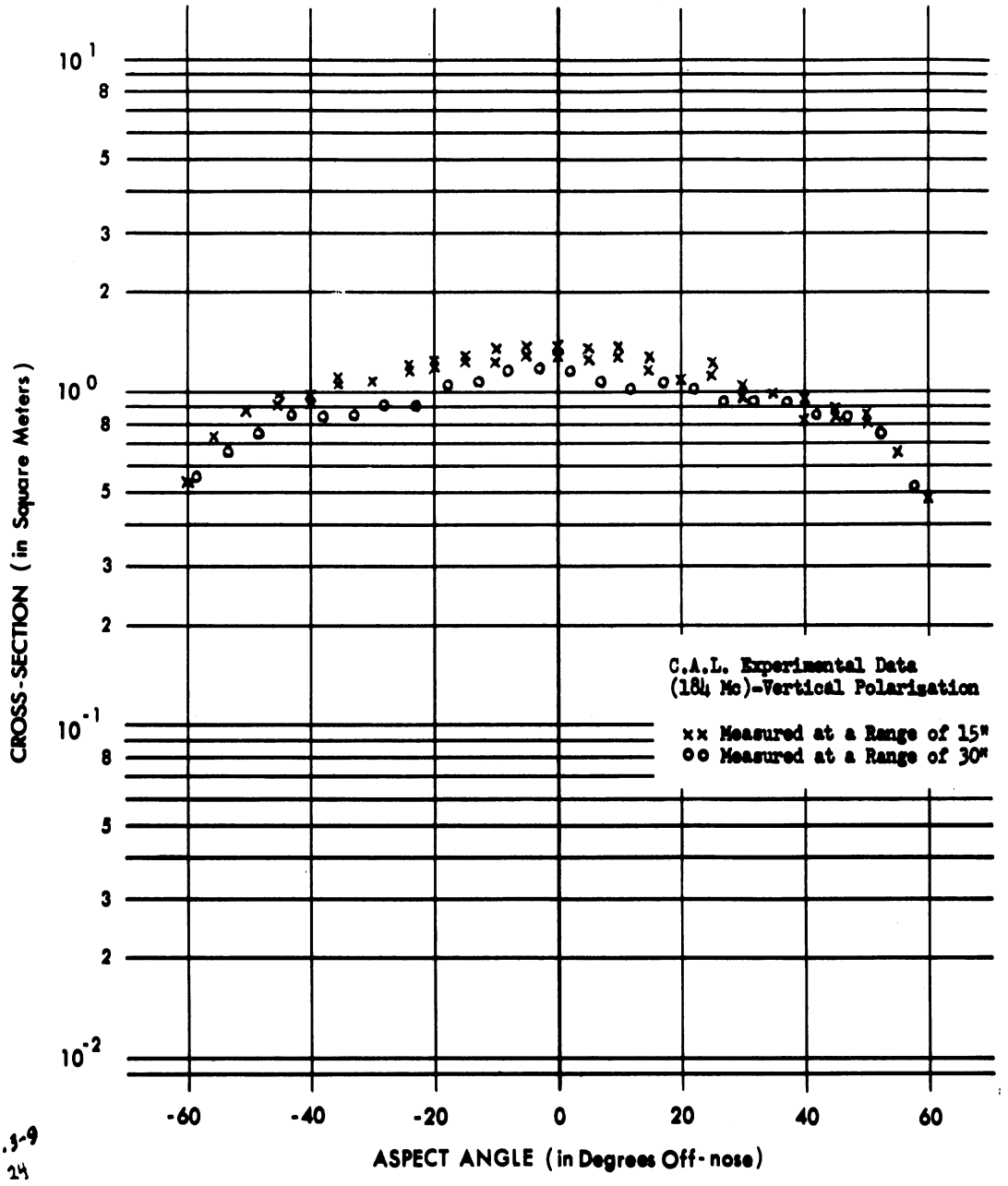

FIG 3-9 RADAR CROSS-SECTION OF CONFIGURATION H AT A FREQUENCY OF APPROXIMATELY 200 Mc.

500 Mc) are shown in Figure 3-10 and 3-11. Additional measurements of the nose-on cross-section of this second shape were made at 250, 1000, and 2000 Mc.

An examination of this RPL-DRB data indicates that if the perturbation still contains the step, then no reductions in cross-section can be expected at 500 Mc. This prediction was made in Reference 1. However, if in addition to capping the nose with a cone, the step is smoothly rounded, appreciable reductions in the cross-section can be obtained, as was also predicted in Reference 1.

Unfortunately, no appreciable reductions at 200 Mc can be achieved with the type of perturbation illustrated by Configuration G. If the radius of curvature at the shadow boundary (i.e, at the step) is made larger, then reductions in the cross-section can be anticipated.

The refinement of theoretical techniques referred to previously in Section II has resulted in a more appropriate approach to the theoretical estimation of the nose-on cross-section of these perturbed shapes.

We were not sure at the time of the writing of Reference 1 whether one had to increase the ratio of the radius of curvature of the perturbation about the step much more than the order of magnitude of the wavelength in order to reduce the step cross-section significantly. We thought this might be the case, so for ease of construction we chose the smallest type of increase in curvature (just to the order of a wavelength). Experiment now shows we must do much better than that to obtain the 20 db reduction we sought. As a result we now know that if our perturbations are to be that good as low as 200 Mc we must increase the radius of curvature considerably. What we have done is sufficient at 400 Mc.

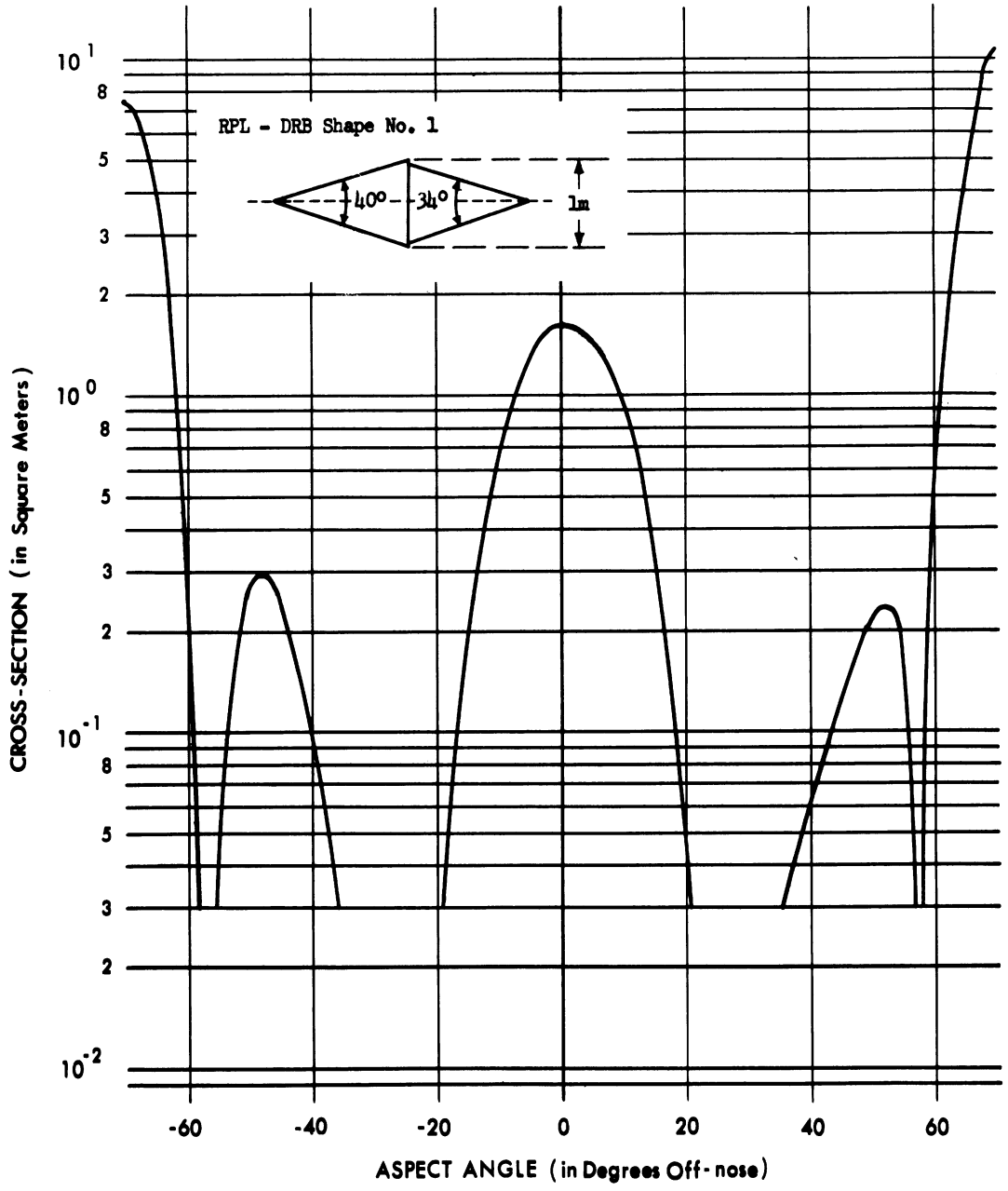

FIG 3-10 RADAR CROSS-SECTION OF RPL-DRB SHAPE No. 1 - 500 Mc. (VERTICAL POLARIZATION)

SECRET

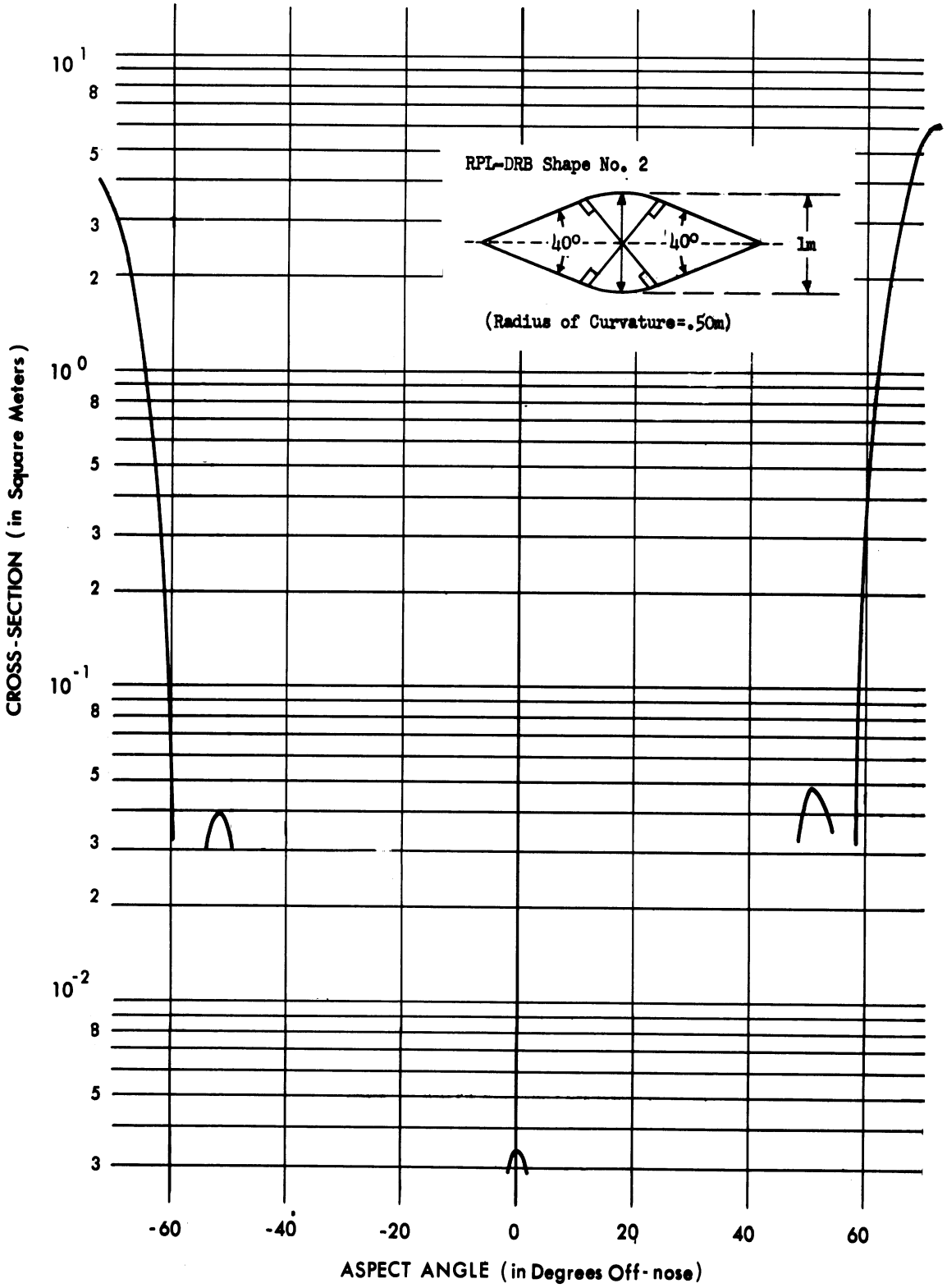

FIG 3-11 RADAR CROSS-SECTION OF RPL-DRB SHAPE No. 2 - 500 Mc.
(VERTICAL POLARIZATION)

SECRET

The effect of the conical tip helped us a great deal near nose-on but did not do what we wanted exactly on the axis. We now know a spheroidal rear would have been a more judicious choice for the perturbed rear.

Thus, a refinement in the method of the treatment of the contribution from the rear has been developed and the new technique applied to the determination of the nose-on cross-section of Configurations E and G and RPL-DRB Shape #2 (see Appendix E). In view of these new theoretical investigations it is seen that the radius of curvature at the shadow boundary used for Configurations F and H is so small with respect to λ for the 200 Mc case that the shape at the shadow boundary is essentially discontinuous (i.e., the normal to the surface has a discontinuity at the shadow boundary). Thus, in computing the cross-sections of Configurations F and H as well as Configurations A and B and RPL-DRB Shape #1, use has been made of the new techniques described in Section 4 and Appendix D for determining the contribution to the cross-section from a ring singularity in the shape of a circular wedge. The results of these new computations are presented in Table 3.1 where these theoretical results are compared with the experimental data obtained by C.A.L. and RPL-DRB.

Appendices E and G contain the details of our recent investigations relative to minimal cross-section shapes.

TABLE 3.1: NOSE-ON CROSS-SECTIONS OF PERTURBATIONS OF THE RUDOLPH WARHEAD AS COMPUTED BY REFINED THEORETICAL TECHNIQUES COMPARED WITH EXPERIMENTAL DATA OBTAINED BY CAL AND RPL-DRB

Configuration	Frequency	Cross-Section (in m^2)	
		Theoretical Est. (Av.)	Experimental Data
A	184-200 Mc	1.1	0.5
B	"	1.1	1.5
E	"	0.18	0.5
F	"	1.0	1.5
G	"	0.18	0.2
H	"	1.0	1.3
RPL-#1	500 Mc	.55	1.5
RPL-#2	250 Mc	.07	.11
"	500 Mc	.01	.003
"	1000 Mc	.002	.004
"	2000 Mc	.0004*	.002

* We note that, if for the RPL shape No. 2 at 2000 Mc, the "exact" value for the creeping wave contribution to the cross-section rather than the "average" value were used (see Figure E-2 in Appendix E), the theoretical and experimental values would agree precisely. This is not unexpected since as λ decreases the assumption of a spherical rear for the RPL shape No. 2 becomes more correct.

IV

THE RADAR CROSS-SECTION OF CONICAL BODIES OF REVOLUTION

In examining the radar reflection characteristics of a perfectly conducting finite body of revolution it is convenient to distinguish between three wavelength regions:

(1) the Rayleigh region, where the wavelength of the radiation is large compared with all characteristic dimensions of the body;

(2) the physical optics region, where the wavelength of the radiation is small compared with almost all characteristic dimensions of the body; *

(3) the resonance region, intermediate between the other two.

In the first two regions good approximations to the cross-section can be obtained without recourse to the exact solution of the electromagnetic theory boundary value problem. This solution is unavailable for all finite bodies except the spheroid, in which case electronic computations are required. Such computations have been carried out in a very few cases. In the Rayleigh region, we develop from Rayleigh's results for spheroids a procedure for approximating the cross-sections of other bodies of revolution, and illustrate the method for several of the more common shapes. In the physical optics region, the cross-sections of a number of bodies of revolution have previously been given (Ref. 9); we present here several new results. In the resonance region, we indicate how a qualitative description of the cross-section can be obtained in the absence of a direct

* A noteworthy exception is a conical point.

solution by combining our knowledge of the cross-section in the other two regions with the results of certain physical arguments; in some cases the cross-section in the resonance region can thus be pretty well delineated.

Explicitly, we find for the Rayleigh region that the backscattering cross-section of an elongated body of revolution for incidence along the axis of symmetry is given by

$$\sigma = \frac{4}{\pi} k^4 V^2$$

where k is the wave number, and V the volume of the body. For bodies that cannot be considered elongated (along the axis of symmetry) a correction factor must be applied to the above expression to obtain more accuracy. We alter V to VF where

$$F = 1 + \frac{1}{ny} e^{-y}$$

and the elongation factor y is the ratio of the characteristic dimension along the axis of symmetry to the characteristic dimension perpendicular to the axis of symmetry. For geometrical configurations that allow this transformation, y is determined by contracting the body to a disc and requiring that it assume the correct cross-section in the limit; this is illustrated for several of the more common shapes. For scattering in other directions, the Rayleigh cross-section is obtained by approximating the body by the equivalent spheroid - i.e., replacing it by a spheroid with the same axis of symmetry, volume, and elongation factor. The Rayleigh cross-section of a spheroid for slant incidence is derived. Details will be found in Appendix A.

To determine radar cross-sections using physical optics, certain simplifying assumptions are made about the nature of the incident wave and the scattering body. One of these assumptions restricts the possible bodies to those whose normals vary continuously over the surface. In practice, however, failure to satisfy this requirement has proven to be no bar to successful application of the method. It is not the intent here to explain why the optics approximation can be successfully applied in a wider range of cases than is indicated by its derivation, but merely to present some heuristic criteria for determining the validity of the physical optics results, whether or not the continuity requirement is met, with particular emphasis on the finite cone.

Those bodies with point discontinuities or sharp edges that have been treated as scatterers using physical optics include cones (finite and semi-infinite), ogives, wedges, cylinders, and flat plates and discs. The semi-infinite cone and the thick ogive, considering just the tip result, are the most outstanding examples of the successful application of physical optics to bodies outside the purported range of validity. As for the other bodies, it was expected and has indeed been verified that in spite of the existence of a sharp edge, the physical optics approximation is a good one when the normal to the surface is parallel to the direction of incidence. This condition is nearly present for very thick cones.* Indeed, in the limit as the cone approaches a disc, the physical optics cone result approaches the physical optics disc result. Thus, at least for thick cones,

* The designations "thick" and "thin" are, of course, quite arbitrary. For the present, a cone half-angle of 15° will be taken to delimit "thick" and "thin" cones.

it is expected that the physical optics approximation will yield good results. In the case of thin cones viewed nose-on, however, the situation is one where the incident and surface normal directions are considerably separated. This is an example in which one should improve upon the results predicted by physical optics. The physical optics result for the finite cone, generalized to include incidence at small angles off nose-on, is derived in Appendix B. In view of the comments above, specifying that the wavelength be small is not sufficient to assure the validity of the optics approximation and, therefore, these results should be used with caution.

Reasoning from known exact solutions one can predict where one would expect pitfalls in using physical optics. If one considers the source and observer near one of the plane faces of a wedge but far from the wedge edge one finds the return from the wedge edge is considerable. This is not predicted by physical optics! One then realizes that as finite cones become longer and thinner, the same pitfall can be expected to exhibit itself. This, in fact, occurs, as can be observed from all known experimental results. We now present a method which enables one to obtain good theoretical estimates of the cross-sections of cones for such a situation. The advantage of this method lies in that it is a more accurate representation of the physical situation and is readily extended into the small wavelength or "optics" side of the resonance region. It is expected that due to the behavior of surface currents in the neighborhood of corners and edges, the dominant contribution to the cross-section of thin cones at nose-on aspects should come from the ring singularity at the base. (The tip contribution is known to be small from the exact solution of the semi-infinite cone

problem). Thus an adequate treatment of the base of the cone should provide a good approximation to the behavior of the entire cone. In essence, the procedure is to approximate the base by an array of straight segments, find the scattered field due to each segment (neglecting end effects), and integrate around the base. (This is similar to defining a circle as a polygon whose number of sides increases without limit.) This has been done by treating each segment as a thin wire (Appendix C) and also by treating each segment as a wedge (Appendix D). The small wavelength restriction still must be met.

For the resonance region we achieve a qualitative description by extending the results obtained in the Rayleigh and physical optics regions by means of some assumptions based on experience as to the behavior of the cross-section as the resonance region is approached from either end, and also from the general ideas about the resonance region proper. Let us consider for brevity of expression that the important characteristic dimensions in the resonance region are the maximum length in the direction of Poynting's vector and the maximum dimension perpendicular to this direction. If the characteristic dimensions are comparable, the resonance region is small; if they differ considerably from each other, it may be large.* The ratio of characteristic dimensions also determines the general character of the variation of the cross-section with wavelength. It is convenient to use the concept of a major maximum - defined as a maximum whose amplitude equals or exceeds that of the first maximum on the Rayleigh side. The first maximum on the Rayleigh side is thus always a major maximum. The cross-section of an elongated body

*Thus as one moves the transmitter and receiver off the axis of a long thin body the ratio of characteristic dimensions decreases and we obtain a smaller effective resonance region thus the optics approximations will hold for smaller and smaller values of ka.

can be expected to have several major maxima, and thus to be difficult to approximate; the cross-section of a sufficiently flatter body should have only one, and it should be possible to bound it fairly narrowly. For instance, (see Fig. 4-1), the exact theory solution for the 10:1 prolate spheroid shows several major maxima, while the sphere and the disc* have only one. There is then some critical spheroid whose dimensions are such that all spheroids with greater $\frac{a}{b}$ (ratio of semi-major to semi-minor axis) have more than one major maximum and all spheroids with smaller $\frac{a}{b}$ have only one major maximum. In acoustics the situation is reversed. The sphere curve has several major maxima while the 10:1 spheroid has only one (see Fig. 4-2). In this case, there will be a critical spheroid such that all spheroids with greater $\frac{a}{b}$ ratios will have only one major maximum and all spheroids with smaller $\frac{a}{b}$ ratios will have several major maxima.

On the Rayleigh side of the resonance region, the Rayleigh cross-section is expected to provide a good upper bound to the actual cross-section, which falls gradually and monotonically below the Rayleigh result until the first maximum is reached. The initial behavior of this deviation can be obtained by Stevenson's (Ref.10) method (an expansion of the Maxwell equations in a power series in k, and solution of the resultant coupled equations for the coefficients) but this approach fails before the first maximum is reached. On the Rayleigh side of the resonance region, the cross-section is expected to depend on the major large

*This is a mathematical concept. As soon as one gives the disc thickness, bumps occur when the wavelength is the order of the edge.

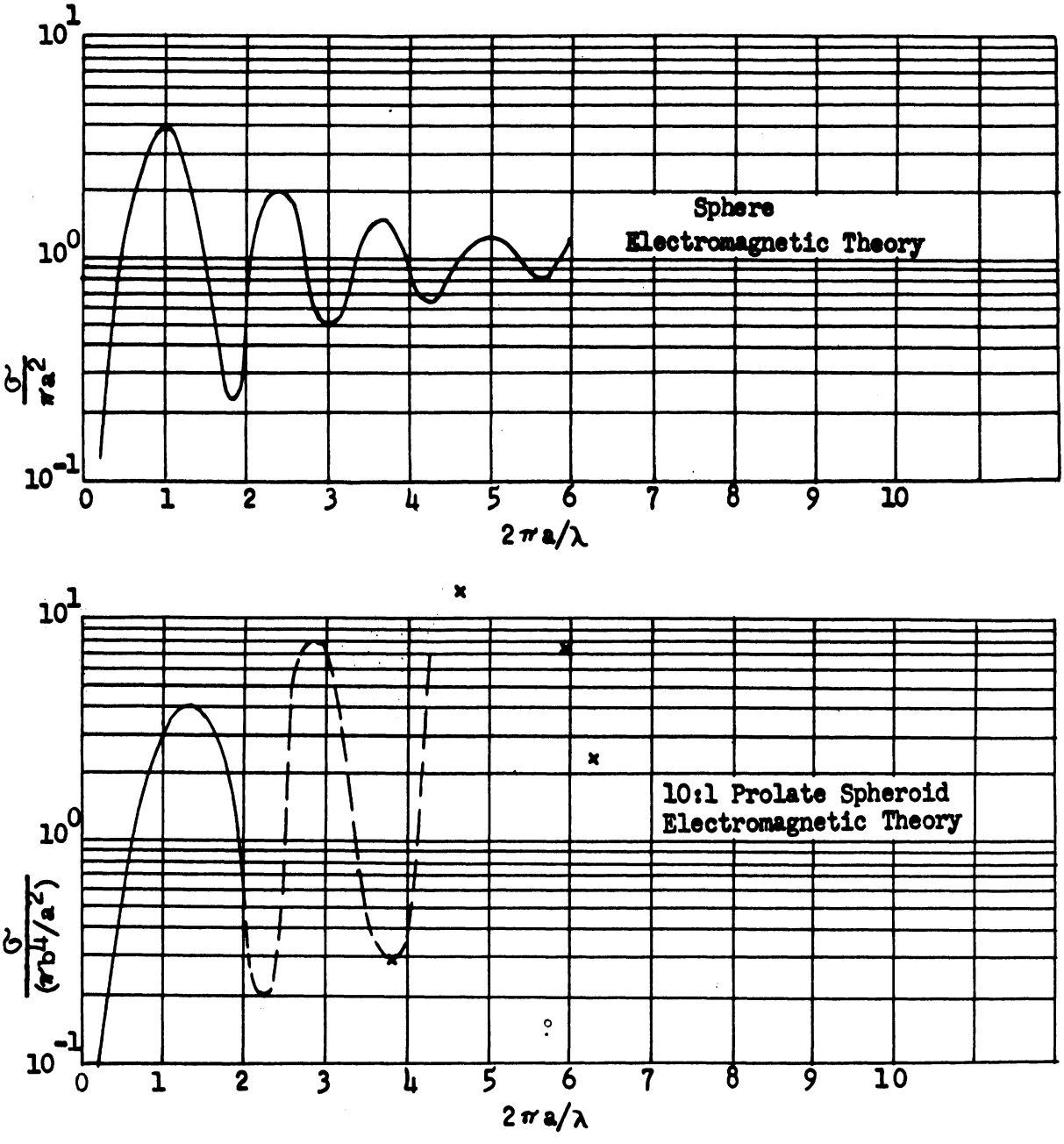

FIG 4-1 CROSS-SECTIONS OF THE SPHERE AND THE 10:1 PROLATE SPHEROID (ELECTROMAGNETIC THEORY)

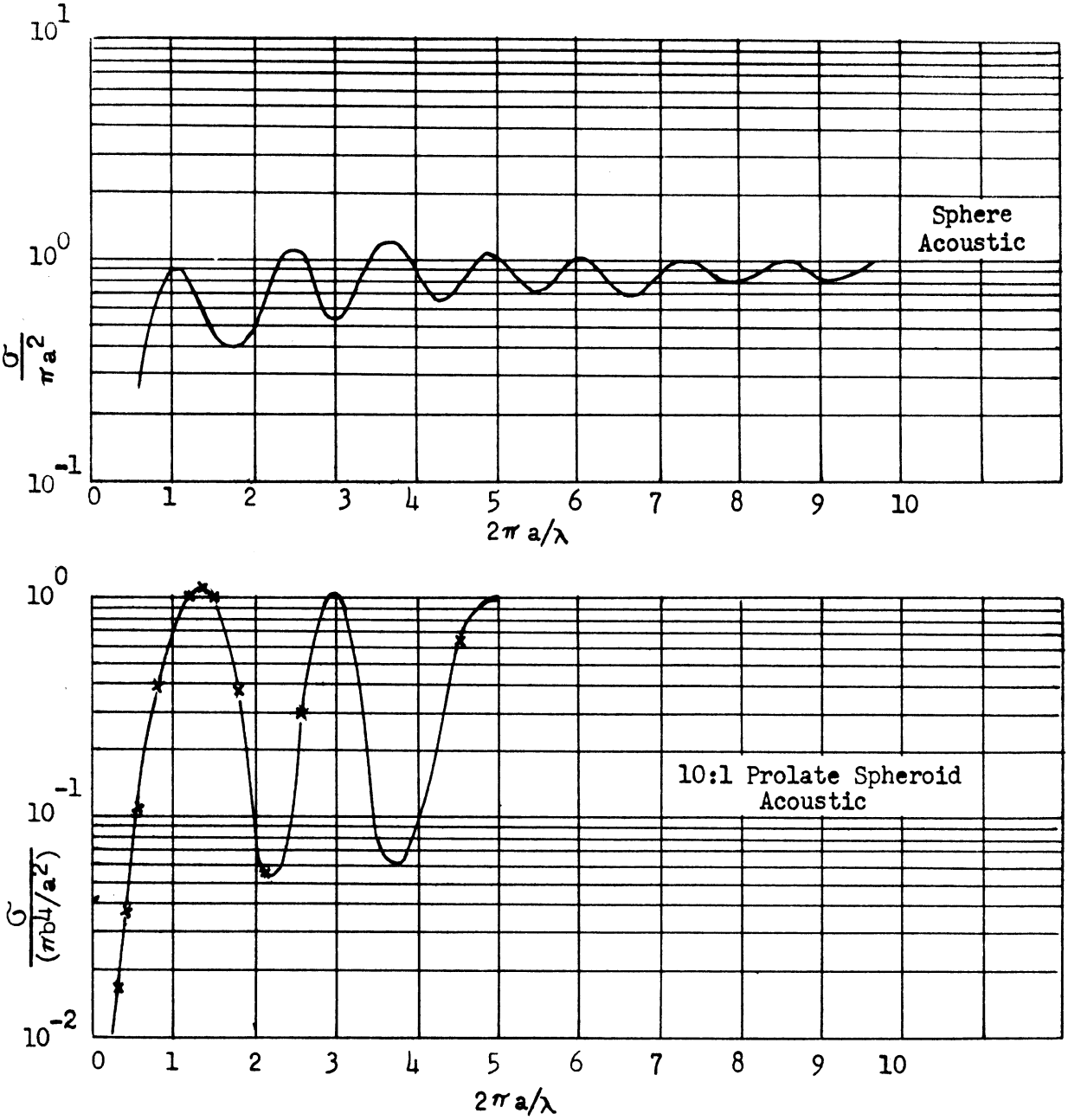

FIG 4-2 CROSS-SECTIONS OF THE SPHERE AND THE 10:1 PROLATE SPHEROID (ACOUSTIC THEORY)

linear characteristic dimensions of the body and not upon fine details of structure; this is in contract to the dependence in the Rayleigh region where the dependence is on the volume of the body. A thin elongated body will behave like an antenna, i.e., its cross-section will have maxima whenever its length is equal to an integral number of half-wavelengths.

Assuming that the base is still the dominant feature of a thin finite cone as the resonance region is entered from the physical optics side, the resonance maximum of the ring singularity would approximate, in both position and amplitude, the last large maximum of the cone. Since in any physically realizable situation, the edge of the base of a cone will have a non-zero radius of curvature, b, ($b \ll \lambda$), the only difference between it and a wire loop (wire radius$<<\lambda$) relative to incident electromagnetic energy is that currents can exist "inside" the loop but not "inside" the base of the cone.

When one looks at the axially symmetric cross-section of a ring as a function of wavelength one finds that there are no minima.* This, then, allows one to predict that the contribution of the inner edge is negligible in comparison to the outer edge when the wavelength is equal to the order of the loop radius but greater than the wire radius. (If there were non-negligible contributions from both the outer and inner edges, then at some wavelengths they would add in phase and at some wavelengths they would add out of phase. But there are no noticeable minima in this region !)

*See page 35.

Thus the cross-section of a loop here looks like a Rayleigh side-type answer, depending only on the loop radius but not on the wire radius. This, then, gives added justification for using an analogy between the conical base and the wire loop. Kouyoumjian's variational results (Ref.12) for wire loops in the resonance region, can then be utilized. His results (as a function of wire radius and loop radius) indicate that the resonant peak is fairly insensitive to changes in wire radius but that as the wavelength decreases the wire radius becomes important. In the region of small wavelengths, the wire loop result can be used to furnish an upper bound on the cone result, since bounding the loop result will, in general, bound the cone result. (The small wavelength wire loop result is derived in Appendix C.)

There is another cone result in the small wavelength region that is obtained by treating the base of the cone, locally, as a wedge. Using physical optics to compute the fields due to the local wedges, and integrating, one obtains precisely the usual physical optics cone result (see Appendix D). Thus, even though physical optics is of dubious applicability, the two physical optics approximations yield consistent results. The wedge-type approximation is then carried out using for the scattered fields expressions generally more exact than physical optics. The resulting wedge-type cone answer is meant to apply only to thin cones and does not compete with the physical optics approximation for thick cones. This result, like the physical optics result, is independent of both polarization and wavelength; however, the two answers differ considerably for

thin cones, as we expected. Since Kouyoumjian has computed the wire loop cross-section in the resonance region, numerical values are available to match the "wedge" result for thin cones in the small wavelength region with the wire loop result in the resonance region. This yields an estimate of the cross-section from the last large maximum out to the zero wavelength limit.

Consolidating all these considerations, we obtain an approximate description of the cross-section of the finite cone, covering the complete range of wavelengths for nose-on incidence. In the Rayleigh region, the cross-section is given by

$$\sigma = \frac{4}{9}\pi h^2 (kr)^4 \left(1 + \frac{1}{\pi h/4r} e^{-(h/4r)}\right)^2 ,$$

h = height, and
r = radius of base.

For a thin cone, the second term is negligible. In the resonance region, a thick cone should behave like a disc, which has a single major maximum. A thin cone can be expected to have more than one major maximum. The last large maximum on the optics side will be given by the wire loop. For all cones, subsidiary maxima may occur on the optics side of the wire loop (or disc) maximum.

In the optics region the cross-section for a thick cone is

$$\sigma = \frac{\pi \tan^4 \alpha}{k^2} \left| \frac{1}{2} + ikh - \frac{e^{2ikh}}{2} \right|^2 , \quad \alpha = \frac{1}{2} \text{ cone angle},$$

which for λ very small in respect to both r and h becomes

$$\sigma = \pi r^2 \tan^2 \alpha .$$

The cross-section for a thin cone is

$$\sigma = \frac{\pi^3 r^2}{\left(\frac{3\pi}{4} + \frac{\alpha}{2}\right)^2} \cot^2\left(\frac{\pi^2}{3\pi + 2\alpha}\right) .$$

APPENDIX A

RAYLEIGH CROSS-SECTION OF BODIES OF REVOLUTION

Rayleigh scattering (Ref. 13) describes the scattering of electromagnetic radiation by a body whose dimensions are much smaller than the wavelength of the radiation. Thus the Rayleigh limit describes the scattered field, due to an incident plane wave, approximated at a large distance from the body by the field of radiating electric and magnetic dipoles located at the scatterer (the magnetic dipole contribution is comparable to that of the electric dipole only for a perfect conductor). To evaluate the electric (magnetic) dipole moment, the static electric (magnetic) field induced on the body by an applied constant field must be known. In other words, the electrodynamic boundary-value problem has been reduced to a corresponding static problem.

Although the solution of the Laplace Equation is in principle simpler than the solution of the Maxwell Equations, there are very few geometrical cases for which even the former is manageable. The question, therefore, arises whether any approximate information can be obtained as to the Rayleigh cross-section when a solution of the Laplace Equation is not available. That this should be possible is heuristically plausible. When the wavelength is much longer than the dimensions of a body, one cannot discern details of the structure of the body - the observed effect depends more on the size of the body than on its shape. Thus, knowledge of the size of the body, modified by a rough indication of shape, should suffice

for a good approximation to the Rayleigh cross-section. It is the purpose of the present discussion to explore this possibility.

For simplicity, consider the scatterer to be a body of revolution, and examine backscattering of a plane wave incident along the axis of symmetry. (Thus, the direction of incidence will be denoted by z, the incident electric vector direction by x, and the length of the body along the symmetry axis by L.) The electric dipole moment $\vec{p}$ is given by

$$\vec{p} = \int_S \omega \vec{r}\, dS \tag{A.1}$$

where ω is the charge density, $\vec{r}$ the position vector, and S is the surface of the body. The boundary condition yields

$$\omega = \epsilon \vec{E} \cdot \hat{n} = \epsilon E \tag{A.2}$$

where ϵ = dielectric constant, $\hat{n}$ = outward normal to the surface, and $\vec{E}$ = electric field strength.

Using cylindrical coordinates,

$$dS = \rho\, d\phi\, dz \tag{A.3}$$

where ρ is a function of z but not of ϕ, so that

$$\vec{p} = \epsilon \int_0^L \rho \int_0^{2\pi} E \vec{r}\, d\phi dz \quad . \tag{A.4}$$

From uniqueness and symmetry considerations, we can write

$$E = \sum_{n=0}^{\infty} a_n(z) \cos n\phi \quad . \tag{A.5}$$

Then $p_y = 0$, as it should, p_z does not concern us as it cannot contribute to the radiation (being along the direction of propagation), and

$$p_x = \epsilon \int_0^L dz \rho^2 \int_0^{2\pi} d\phi \cos\phi \sum_{n=0}^{\infty} a_n(z) \cos n\phi \tag{A.6}$$

$$= \epsilon \int_0^L dz \ \pi\rho^2 \ a_1(z) \quad .$$

Apart from the factor $a_1(z)$, the integral is just the volume of the body, V. In fact, the whole determination of the electric dipole moment resolves itself into the determination of the factor $a(z)$ in

$$E = a(z) \cos\phi \tag{A.7}$$

since the other terms in the series do not contribute. If the body is elongated along the axis of symmetry (i.e., if $L \gg \rho$), $a(z)$ will be a slowly varying function of z and can be removed from the integral and replaced by a mean value (or actually by an estimate of its value). To estimate $a(z)$, we resort to an analogy with reflection from a plane. In the latter case, the amplitude of the total field is twice that of the incident field. Thus we choose $a = 2E_o$ (phase differences in the incident field at various points on the body can be neglected) to obtain

$$\vec{p} = \hat{x} \ 2\epsilon E_o V \quad . \tag{A.8}$$

The far-zone electric field due to the electric dipole is (Ref. 14)

$$\vec{E} = -\frac{k^2}{4\pi\epsilon}\ \hat{z}\ x\ (\hat{z}\ x\ \hat{p})\ \frac{e^{i(kR-\omega t)}}{R}\ . \qquad (A.9)$$

For a conductor, analogous treatment of the magnetic dipole yields an equal contribution in phase. Altogether, we have in the far-zone

$$\vec{E} = \hat{x}\ \frac{k^2}{\pi}\ E_o\ V\ \frac{e^{i(kR-\omega t)}}{R}\ . \qquad (A.10)$$

The cross-section is given by

$$\sigma = 4\pi R^2\ \left|\frac{\vec{E}}{\vec{E}_o}\right|^2 = \frac{4}{\pi}\ k^4\ V^2\ . \qquad (A.11)$$

This, then, is the value of the cross-section to be expected for an elongated body of revolution.* As the flatness of the scatterer increases, the approximation is expected to get worse, in fact an infinitely flat body (infinite radii of curvature) has a non-zero cross-section.

Let us now compare this pseudo-derivation with the exact answer for the special case we do know, the spheroid (Ref. 13). Let us define for convenience the quantity

$$F = \frac{\pi R\ |\vec{E}|}{k^2\ E_o V}\ . \qquad (A.13)$$

* It should be noted that for the acoustic case the treatment would be equivalent except that instead of the two components (electric and magnetic) there would be only one, and thus the cross-section would be

$$\sigma = \frac{1}{\pi}\ k^4\ V^2\ . \qquad (A.12)$$

$F = 1$ yields the magnitude of $\vec{E}$ given by Equation A.10. Modifying Rayleigh's notation slightly,

$$F = \frac{1}{2}\left(\frac{1}{L} + \frac{1}{2-L}\right) = \frac{1}{L(2-L)} \qquad (A.14)$$

where, for a prolate spheroid, (Ref. 13),

$$L = \left(\frac{1}{e^2} - \frac{1-e^2}{2e^3} \log \frac{1+e}{1-e}\right) \qquad (A.15)$$

where e = eccentricity -- i.e., the semi-axes are a, a, $\frac{a}{\sqrt{1-e^2}}$.

For an elongated spheroid ($e \to 1$), $L \to 1$ and $F \to 1$, checking the approximation.

Next, let us inquire into the shape correction by first examining its form for the spheroid. We already know the prolate result; for the oblate spheroid,

$$L = \left(\frac{\sqrt{1-e^2}}{e^3} \sin^{-1} e - \frac{1-e^2}{e^2}\right) \quad \text{(Ref. 13)} \qquad (A.16)$$

where the semi-axes are now a, a, $a\sqrt{1-e^2}$. As these expressions are quite complicated, it is profitable to examine their limiting values.

Consider a sphere ($e = 0$): From (A.15)

$$\log \frac{1+e}{1-e} = 2\left(e + \frac{1}{3}e^3 + \ldots\right) \qquad (A.17)$$

$$L \approx \frac{1}{e^2}\left[1-(1-e^2)\left(1+\frac{1}{3}e^2\right)\right] \approx \frac{1}{e^2}\left[1-1+e^2-\frac{1}{3}e^2\right] = \frac{2}{3} \qquad (A.18)$$

$$F \approx \left(\frac{2}{3}\left(2-\frac{2}{3}\right)\right)^{-1} = \left(\frac{2}{3}\cdot\frac{4}{3}\right)^{-1} = \frac{9}{8} \quad . \qquad (A.19)$$

It is easily demonstrated that F is monotone decreasing as we progress from a sphere to an elongated prolate spheroid. Hence, it ranges from $\frac{9}{8}$ to 1 -- very nearly constant, of the form 1 + decaying term.

Examine the disc limit (e→1 for oblate spheroid):

Let

$$e = \sin x \quad . \qquad (A.20)$$

Then $L = \cos x \csc^2 x\,(x \csc x - \cos x)$. (A.21)

Let

$$y = \frac{\pi}{2} - x \quad . \qquad (A.22)$$

Then $L = \sin y \sec^2 y \left[\left(\frac{\pi}{2} - y\right) \sec y - \sin y\right]$. (A.23)

Expand near y = 0 (equivalent to e → 1):

$$L \approx y\left[\left(\frac{\pi}{2} - y\right) - y\right] = \frac{\pi y}{2} - 2y^2 = \frac{\pi}{2} y\left(1-\frac{4}{\pi}y\right) \qquad (A.24)$$

$$F = \frac{1}{L(2-L)} \approx \frac{1}{\frac{\pi}{2}y\left(1-\frac{4}{\pi}y\right)\left(2-\frac{\pi}{2}y\right)} \approx \frac{1}{\pi y}\left(1+\frac{4}{\pi}y+\frac{\pi}{4}y\right) \quad . \qquad (A.25)$$

For small y, $y \approx \sqrt{1-e^2}$; if we call the semi-axes a, a, b, then $y = \frac{b}{a}$.

Combine the information about F. In the oblate case, F is again monotone, increasing toward the disc limit. The prolate spheroid discussion indicates that we should split off from F a unity term, and that the remaining term should decay as $y = \frac{b}{a} \to \infty$. Thus,

$$F \approx 1 + \frac{1}{\pi y}\left[1 + \left(\frac{4}{\pi} + \frac{\pi}{4} - \pi\right) y\right] \approx 1 + \frac{1}{\pi y}(1 - y) \approx 1 + \frac{1}{\pi y} e^{-y} \quad . \tag{A.26}$$

We postulate, then, that for all spheroids (with semi-axes a, a, b), the shape correction factor is approximately

$$F = 1 + \frac{1}{\pi y} e^{-y} \tag{A.26}$$

where $y = \frac{b}{a}$. Numerical comparison indicates that the approximation is valid to within one percent. The Rayleigh cross-section of a spheroid for back-scattering along the axis of symmetry is

$$\sigma = \frac{4}{\pi} k^4 V^2 \left(1 + \frac{1}{\pi y} e^{-y}\right)^2 \quad . \tag{A.27}$$

The cross-section of the spheroid depends on its volume and on a correction factor involving $y = \frac{b}{a}$. Except for very flat oblate spheroids, the shape correction factor can be neglected. Where it is not neglected, the shape correction factor is a simple function of y, which is a measure of the elongation.

The natural extension of the discussion is to postulate that for all bodies of revolution the Rayleigh cross-section for backscattering along the axis of symmetry can be expressed as

$$\sigma = \frac{4}{\pi} k^4 V^2 \left(1 + \frac{1}{\pi y} e^{-y}\right)^2 \qquad (A.27)$$

where y is a measure of the elongation (characteristic dimension along the axis of symmetry)/(characteristic dimension in the perpendicular direction). For elongated bodies, the term in y drops out and there is no ambiguity. For flattened bodies, the answer is sensitive to the choice of characteristic dimensions, but a good approximation should still be attainable. The ambiguity can be eliminated in a number of cases by imposing a restriction on the choice of characteristic dimensions: in the limit of extreme flattening, the cross-section must tend to the value for the appropriate disc.

Illustration I: Finite Cone

Consider a right circular cone of altitude h and radius of base r. As $h \to 0$, the cross-section of the cone must go into the cross-section of a disc of radius r --- i.e., we must have

$$VF = \frac{1}{3} \pi r^2 h \left(1 + \frac{1}{\pi y} e^{-y}\right) \to \frac{r^2 h}{3y} = \frac{4}{3} r^3 \quad . \qquad (A.28)$$

Thus, the appropriate ratio of characteristic dimensions to be used in Equation A.27 is

$$y = \frac{h}{4r} \quad . \qquad (A.29)$$

Hence, the cone has the same cross-section as a spheroid of equal volume whose semi-axes are (r, r, h/4).

Illustration II: Lens

Consider a symmetrical convex lens of radius of curvature R (the body of revolution obtained by rotating the shaded area in Figure A-1 about the η-axis). In the disc limit (d constant, $c \to 0$):

$$VF \to \frac{V}{\pi y} = \frac{4}{3} d^3 \qquad (A.30)$$

Hence, we take for the lens

$$y = \frac{3V}{4\pi d^3} = \frac{3V}{4\pi R^3 \sin^3 \theta} \quad . \qquad (A.31)$$

The volume of the lens is

$$V = \frac{2\pi}{3} R^3 (1-\cos\theta)(1-\cos\theta + \sin^2\theta) \quad . \qquad (A.32)$$

As $\theta \to \frac{\pi}{2}$ (sphere limit), we reproduce the previous spheroid result, as expected.

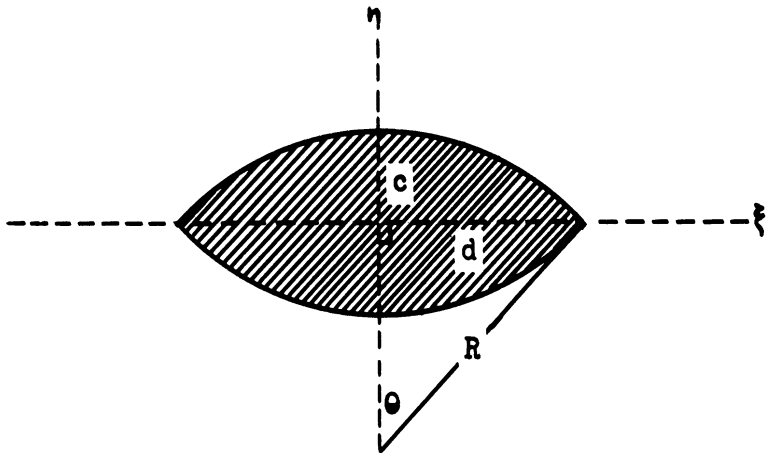

Figure A-1

Illustration III: Elliptic Ogive

Inasmuch as the circular ogive is more elongated than a sphere, the argument from the disc limit connot be applied to it directly.

Instead, we consider the elliptic ogive obtained by rotating the shaded area of Figure A-2 (a portion of an ellipse) about the η -axis (which is taken parallel to the minor axis). For this body, in the disc limit (d constant, $c \to 0$):

$$VF \to \frac{V}{\pi y} = \frac{4}{3} d^3 \quad . \tag{A.33}$$

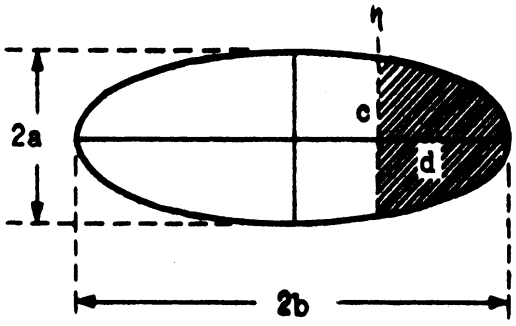

FIG A-2

From the equation for the ellipse,

$$\frac{c^2}{a^2} + \frac{(b-d)^2}{b^2} = 1, \tag{A.34}$$

which suggests use of the parameter θ:

$$\sin \theta = \frac{c}{a} \quad . \tag{A.35}$$

Then

$$y = \frac{3V}{4\pi d^3} = \frac{3V}{4\pi b^3 (1-\cos\theta)^3} \quad . \tag{A.36}$$

The volume of the elliptic ogive is

$$V = 2\pi ab^2 (\sin\theta - \theta\cos\theta - \frac{1}{3}\sin^3\theta) \quad . \tag{A.37}$$

As $\theta \to \frac{\pi}{2}$, we reproduce the previous spheroid result, as expected.

Special Case: Circular Ogive. To obtain the cross-section of the circular ogive, we now merely take the special case of the elliptic ogive with a = b. From geometry, ω can now be identified with the ogive half-angle. Now

$$y = \frac{3}{2} \frac{\sin\theta - \theta\cos\theta - \frac{1}{3}\sin^3\theta}{(1-\cos\theta)^3} \quad . \tag{A.38}$$

Illustration IV: Spindle

Consider the body of revolution obtained by rotating the shaded area of Figure A-3 (bounded by a parabola and a straight line perpendicular to the axis of the parabola) about the η-axis. Using the disc limit exactly as before, we have

$$y = \frac{3V}{4\pi d^3} \tag{A.39}$$

where the volume is

$$V = \frac{16}{15}\pi cd^2 \tag{A.40}$$

so that

$$y = \frac{4}{5}\frac{c}{d} \quad . \tag{A.41}$$

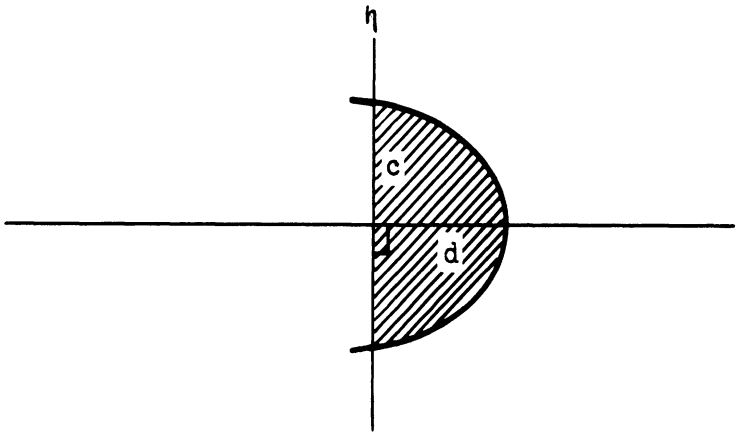

Figure A-3

Illustration V: Finite Cylinder

Consider a cylinder of radius r and height h. From the disc limit,

$$y = \frac{3V}{4\pi r^3} = \frac{3h}{4r} \qquad (A.42)$$

To evaluate the Rayleigh cross-section of a body of revolution (for any transmitter and receiver directions) the body is approximated by the equivalent spheroid. The equivalent spheroid is a spheroid with the same axis of symmetry, the same volume, and the same elongation factor, y, as the body. The simplification found for the backscattering along the symmetry axis provides a reasonable way to arrive at an elongation factor for many bodies.

Rayleigh quotes the far-zone scattered field for an ellipsoid for incidence along one principal axis (with coefficients evaluated for the special case of a spheroid) (Ref. 13). A simple permutation of coordinates

leads to the far-zone scattered field of a spheroid for incidence along any principal axis. The extension to slant incidence is not difficult, but requires a little more care. To take the polarization into account correctly, it is necessary to treat the contributions to the far-zone scattered field from the electric and magnetic incident fields separately. Using Rayleigh's results and appropriate rotations (with some slight changes of notation), the contributions to the far-zone scattered field from the various components of the incident field are:

(A.43)

$$\vec{E}_o = \hat{x}E_o \;:\; \vec{E} = -\frac{k^2 e^{i(kr-\omega t)}}{2\pi R}\frac{E_o V}{L_x}\left(-\frac{y^2+z^2}{R^2}, \frac{xy}{R^2}, \frac{xy}{R^2}\right)$$

$$\vec{E}_o = \hat{y}E_o \;:\; \vec{E} = -\frac{k^2 e^{i(kR-\omega t)}}{2\pi R}\frac{E_o V}{L_y}\left(\frac{xy}{R^2}, -\frac{x^2+z^2}{R^2}, \frac{yz}{R^2}\right)$$

$$\vec{E}_o = \hat{z}E_o \;:\; \vec{E} = -\frac{k^2 e^{i(kR-\omega t)}}{2\pi R}\frac{E_o V}{L_z}\left(\frac{xz}{R^2}, \frac{yz}{R^2}, -\frac{x^2+y^2}{R^2}\right)$$

$$\vec{H}_o = \hat{x}\epsilon c E_o \;:\; \vec{E} = -\frac{k^2 e^{i(kR-\omega t)}}{2\pi R}\frac{E_o V}{2-L_x}\left(0, -\frac{z}{R}, \frac{y}{R}\right)$$

$$\vec{H}_o = \hat{y}\epsilon c E_o \;:\; \vec{E} = -\frac{k^2 e^{i(kR-\omega t)}}{2\pi R}\frac{E_o V}{2-L_y}\left(\frac{z}{R}, 0, -\frac{x}{R}\right)$$

$$\vec{H}_o = \hat{z}\epsilon c E_o \;:\; \vec{E} = -\frac{k^2 e^{i(kR-\omega t)}}{2\pi R}\frac{E_o V}{2-L_z}\left(-\frac{y}{R}, \frac{x}{R}, 0\right)$$

If the z-axis is the axis of symmetry of the spheroid, we can take $\phi = 0$ without loss of generality. Then

$$x = R \sin\theta \qquad y = 0 \qquad z = R\cos\theta \tag{A.44}$$

The L's have been evaluated by Rayleigh. For our geometry,

$$L_x = L_y = L \tag{A.45}$$

where L is the quantity given by Equations A.15 and A.16. The expressions for L_z can be written in terms of those for L; the relation is

$$L_z = 2\,(1-L) \quad . \tag{A.46}$$

Consider now an incident plane wave traveling toward the origin in the direction θ_T. For arbitrary polarization, it can be expressed as a linear combination of the following two cases:

a) $\vec{E}_o$ in the plane defined by the Poynting vector and the axis of symmetry - i.e.,

$$\vec{E}_{oa} = (-\hat{x}\cos\theta_T + \hat{z}\sin\theta_T)E_o \quad , \quad \vec{H}_{oa} = \hat{y}\,\epsilon\, cE_o \quad . \tag{A.47a}$$

b) $\vec{E}_o$ perpendicular to this plane - i.e.

$$\vec{E}_{ob} = \hat{y}\,E_o \quad , \quad \vec{H}_{ob} = (\hat{x}\cos\theta_T - \hat{z}\sin\theta_T)\,\epsilon\, cE_o \quad . \tag{A.47b}$$

In each case, the far-zone scattered field is obtained by adding up the contributions (as given by Equation A.43) due to the components of the incident electric and magnetic fields that are present. In the direction of observation θ_R the results for the two cases are

$$\vec{E}_a = \frac{k^2 E_o V e^{i(kR-\omega t)}}{2\pi R}\left(\frac{1}{2-L} + \frac{\cos\theta_R\cos\theta_T}{L} + \frac{\sin\theta_R\sin\theta_T}{2-2L}\right) \qquad (A.48a)$$

$$x\left(-\cos\theta_R,\ 0\ ,\ \sin\theta_R\right)$$

and

$$\vec{E}_b = \frac{k^2 E_o V e^{i(kR-\omega t)}}{2\pi R}\left(\frac{1}{L} + \frac{\cos\theta_R\cos\theta_T}{2-L} + \frac{\sin\theta_R\sin\theta_T}{2L}\right)$$

$$x\left(0,\ 1,\ 0\right)\ . \qquad (A.48b)$$

If we again write

$$\sigma = \frac{4}{\pi}\ k^4\ V^2\ F^2 \qquad (A.49)$$

we now have

$$F_a = \frac{1}{2}\left(\frac{1}{2-L} + \frac{\cos\theta_R\cos\theta_T}{L} + \frac{\sin\theta_R\sin\theta_T}{2-2L}\right) \qquad (A.50a)$$

$$F_b = \frac{1}{2}\left(\frac{1}{L} + \frac{\cos\theta_R\cos\theta_T}{2-L} + \frac{\sin\theta_R\sin\theta_T}{2L}\right)\ . \qquad (A.50b)$$

As an example, Figure A-4 exhibits F as a function of aspect angle for backscattering by a 10 : 1 prolate spheroid, for both polarizations.

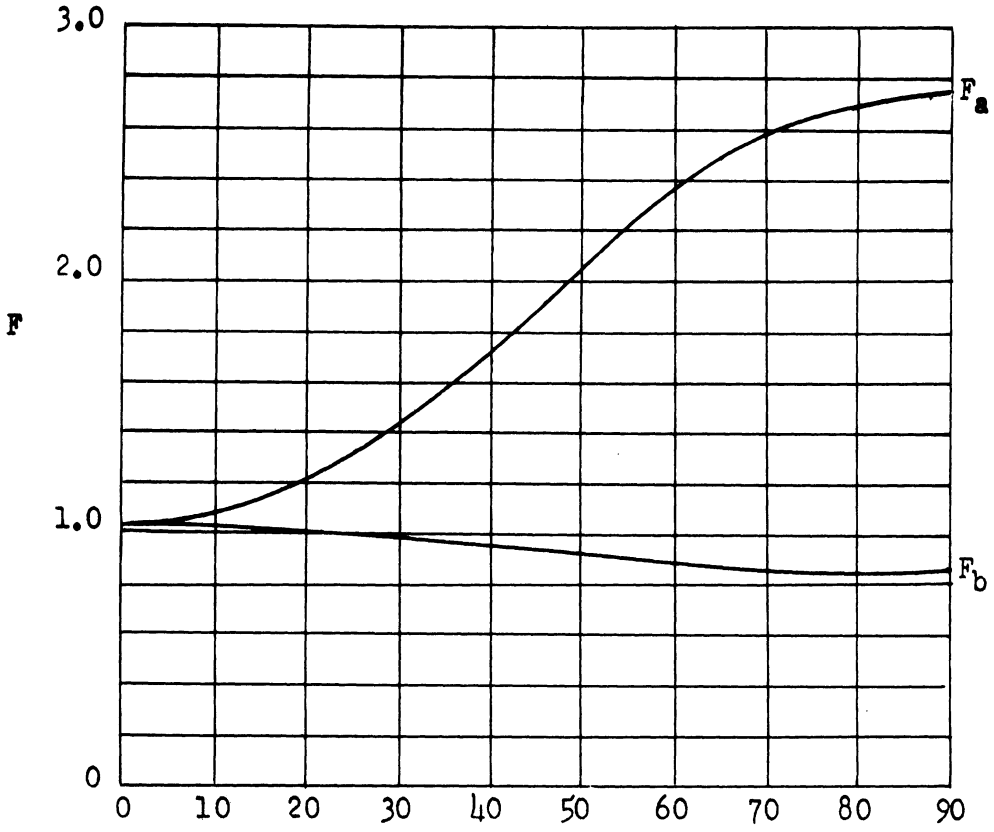

FIG. A-4

Similarly, though more simply, Rayleigh's results for the scattering of a plane scalar wave by a spheroid (Ref. 13) can be generalized to arbitrary incidence. Thus, for a wave of unit amplitude incident along the x - axis, Rayleigh obtains for the Neumann problem (vanishing normal derivative at the body) a scattered wave

$$\psi = -\frac{k^2 V e^{i(kR-\omega t)}}{4\pi R}\left(1+\frac{x}{R}\;\frac{2}{2-L_x}\right) . \qquad (A.51)$$

For a direction of incidence denoted by (θ_T , ϕ_T) and a direction of observation denoted by (θ_R , ϕ_R), this becomes

$$\psi = -\frac{k^2 V e^{i(kR-\omega t)}}{4\pi R}\left(1+\frac{2\sin\theta_R \sin\theta_T \cos\phi_R \cos\phi_T}{2-L_x} + \frac{2\sin\theta_R \sin\theta_T \sin\phi_R \sin\phi_T}{2-L_y} + \frac{2\cos\theta_R \cos\phi_T}{2-L_z}\right). \qquad (A.52)$$

Using (A.45) and (A.46), there results a cross-section

$$\sigma' = \frac{4\pi V^2}{4\pi}\left(1+\frac{2\sin\theta_R \sin\theta_T \cos(\phi_R-\phi_T)}{2-L} + \frac{\cos\theta_R \cos\theta_T}{L}\right)^2 . \qquad (A.53)$$

APPENDIX B

PHYSICAL OPTICS RADAR CROSS-SECTION OF A FINITE CONE FOR NEAR NOSE-ON ASPECTS

To obtain the monostatic physical optics cross-section of a finite cone for incidence at a small angle, ε, to the axis of symmetry of the cone, we proceed as follows.

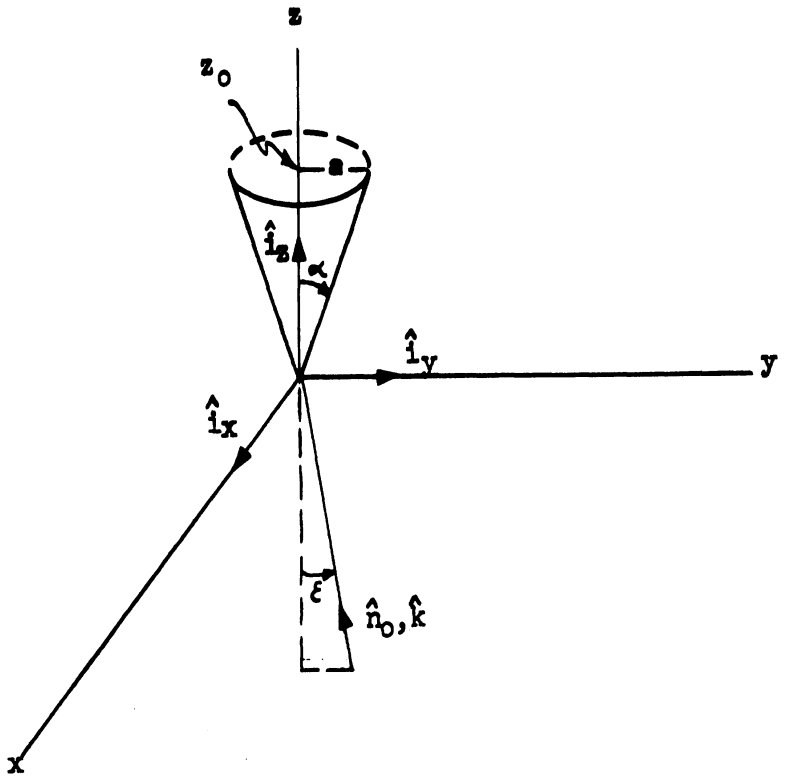

FIG. B-1

Utilizing the physical optics expression for the radar cross-section as given in Reference 9, we obtain

$$\sigma = \frac{4\pi}{\lambda^2} \left| \int\limits_{\substack{\text{illum.} \\ \text{region}}} \hat{n}_o \cdot \hat{n}\ e^{-ik\vec{r}} \cdot (\hat{n}_o + \hat{k})\ dS \right|^2 \qquad \text{(B.1)}$$

where

$\hat{k} = \hat{n}_o = \cos\varepsilon\, \hat{i}_z + \sin\varepsilon\, \hat{i}_y$ (unit vectors to origin from receiver and transmitter),

a = radius of the base of the cone,

$\hat{n} = -\sin\alpha\, \hat{i}_z + \cos\alpha\cos\phi\, \hat{i}_x + \cos\alpha\sin\phi\, \hat{i}_y$ (normal to cone),

$k = \frac{2\pi}{\lambda}$,

$\vec{r} = z\, \hat{i}_z + z\tan\alpha\cos\phi\, \hat{i}_x + z\tan\alpha\sin\phi\, \hat{i}_y$ (vector from origin to any point on cone),

$\alpha = \frac{1}{2}$ cone angle,

ϕ = angular variable in x-y plane

and

$$dS = \frac{z\tan\alpha}{\cos\alpha}\, d\phi dz.$$

Because of symmetry, $\hat{n}_o$ and $\hat{k}$ can be chosen in the y-z plane with positive components. From the definitions of $\hat{k}$, $\hat{n}_o$, $\hat{n}$, and $\vec{r}$ we have

$$\hat{n}_o \cdot \hat{n} = -\cos\varepsilon\sin\alpha + \cos\alpha\sin\varepsilon\sin\phi$$

and

$$\vec{r} \cdot (\hat{n}_o + \hat{k}) = 2z(\cos\varepsilon + \tan\alpha\sin\varepsilon\sin\phi).$$

Substituting in Equation B.1 and restricting ε so that $\varepsilon < \alpha$, we obtain

$$\sigma = \frac{4\pi}{\lambda^2}\left|\int_0^{2\pi}\int_0^{z_o} \frac{z\tan\alpha}{\cos\alpha}(\cos\alpha\sin\varepsilon\sin\phi - \cos\varepsilon\sin\alpha)e^{-2ikz(\cos\varepsilon+\tan\alpha\sin\varepsilon\sin\phi)}\,dz\,d\phi\right|^2. \tag{B.2}$$

Setting $b = 2\sin\varepsilon\tan\alpha$ and $c = 2\cos\varepsilon$, we get

$$\sigma = \frac{4\pi}{\lambda^2}\left|\int_0^{2\pi}\tan\alpha(\sin\varepsilon\sin\phi - \tan\alpha\cos\varepsilon)\int_0^{z_o} z\,e^{-ikz(c+b\sin\phi)}\,dz\,d\phi\right|^2. \tag{B.3}$$

The integration with respect to z can be performed exactly, yielding

$$\sigma = \frac{4\pi}{\lambda^2}\left|\int_0^{2\pi}\tan\alpha(\sin\varepsilon\sin\phi - \tan\alpha\cos\varepsilon)\left(\frac{e^{-ikz_o(b\sin\phi+c)}}{k^2(b\sin\phi+c)^2} + \frac{iz_o e^{-ikz_o(b\sin\phi+c)}}{k(b\sin\phi+c)} - \frac{1}{k^2(b\sin\phi+c)^2}\right)d\phi\right|^2. \tag{B.4}$$

For $\varepsilon = 0$, (B.4) becomes

$$\sigma = \frac{4\pi}{\lambda^2}\left|\tan^2\alpha\int_0^{2\pi}\left(\frac{e^{-2ikz_o}}{4k^2} + \frac{iz_o e^{-2ikz_o}}{2k} - \frac{1}{4k^2}\right)d\phi\right|^2 \tag{B.5}$$

or upon integrating

$$\sigma = \frac{\pi\tan^4\alpha}{k^2}\left|\frac{1}{2} + ikz_o - \frac{e^{2ikz_o}}{2}\right|^2, \tag{B.6}$$

which is the complete nose-on physical optics cross-section. Neglecting terms of order one in respect to kz_o, Equation B.6 becomes,

$$\sigma = \pi z_o^2 \tan^4 \alpha = \pi a^2 \tan^2 \alpha \quad , \tag{B.7}$$

the well-known nose-on optics approximation.

Returning to the off-nose case, we find that neglecting terms in kb and kc with respect to terms in $(kb)^2$, $(kc)^2$, and k^2bc Equation B.4 becomes

$$\sigma \approx \frac{4\pi}{\lambda^2} \left| \int_0^{2\pi} \frac{z_o \tan\alpha (\sin\varepsilon \sin\phi - \tan\alpha \cos\varepsilon) e^{-ikz_o(b \sin\phi + c)}}{k(b \sin\phi + c)} \, d\phi \right|^2 . \tag{B.8}$$

Factoring out $\frac{z_o}{k}$ and remembering that

$$b = 2 \sin\varepsilon \tan\alpha, \text{ and}$$

$$c = 2 \cos\varepsilon,$$

we can rewrite Equation B.8 as follows:

$$\sigma \approx \frac{z_o^2}{4\pi} \left| \int_0^{2\pi} \left(1 - \frac{c \sec^2\alpha}{b \sin\phi + c}\right) e^{-ikz_o(b \sin\phi + c)} \, d\phi \right|^2 \tag{B.9}$$

or, since $\left| e^{-ikz_o c} \right| = 1$

$$\sigma \approx \frac{z_o^2}{4\pi} \left| \int_0^{2\pi} \left(1 - \frac{c \sec^2\alpha}{b \sin\phi + c}\right) e^{-ikz_o b \sin\phi} \, d\phi \right|^2 . \tag{B.10}$$

It remains to evaluate the integrals

$$\int_0^{2\pi} e^{-ikz_o\, b \sin\phi}\, d\phi \quad \text{and} \quad \int_0^{2\pi} \frac{e^{-ikz_o b \sin\phi}}{b \sin\phi + c}\, d\phi \ .$$

The first integral is immediately recognizable as a Bessel function.

$$\int_0^{2\pi} e^{-ikz_o\, b \sin\phi}\, d\phi = 2\pi J_o(k\, z_o\, b) \ . \qquad \text{(B.11)}$$

Thus,

$$\sigma = \frac{z_o^2}{4\pi} \left| 2\pi J_o(k\, z_o b) - \int_0^{2\pi} \frac{c \sec^2\alpha\, e^{-ikz_o\, b \sin\phi}}{b \sin\phi + c}\, d\phi \right|^2 \qquad \text{(B.12)}$$

or

$$\frac{\sigma}{\pi a^2} = \frac{1}{\tan^2\alpha} \left| J_o(k\, z_o\, b) - \frac{c \sec^2\alpha}{\pi} \int_0^{\pi} \frac{e^{ikz_o\, b \cos\phi}}{c - b \cos\phi}\, d\phi \right|^2 \qquad \text{(B.13)}$$

which can also be written

$$\frac{\sigma}{\pi a^2} = \frac{1}{\tan^2\alpha} \left| J_o\left(\frac{4\pi z_o \sin\varepsilon \tan\alpha}{\lambda}\right) - \frac{\cos\varepsilon \sec^2\alpha}{\pi} \int_0^{\pi} \frac{e^{i\frac{4\pi z_o \sin\varepsilon \tan\alpha \cos\phi}{\lambda}}}{\cos\varepsilon - \sin\varepsilon \tan\alpha \cos\phi}\, d\phi \right|^2 \qquad \text{(B.14)}$$

For values of $\frac{z_o \sin\varepsilon \tan\alpha}{\lambda} > 1$, the integral in Equation B.8 can be evaluated by the method of stationary phase, yielding

$$\sigma = \frac{\lambda z_0 \tan\alpha}{2\pi \sin\varepsilon(\sin^2\varepsilon\tan^2\alpha - \cos^2\varepsilon)^2}\left\{\tan^2\alpha\cos^2\left(\frac{4\pi z_0 \sin\varepsilon\tan\alpha}{\lambda} - \frac{\pi}{4}\right)\right. \qquad \text{(B.15)}$$

$$\left. + \frac{\sin^2\varepsilon\cos^2\varepsilon}{\cos^4\alpha}\sin^2\left(\frac{4\pi z_0 \sin\varepsilon\tan\alpha}{\lambda} - \frac{\pi}{4}\right)\right\}$$

which we observe is the asymptotic form of

$$\frac{\sigma}{\pi a^2} = \frac{\tan^2\alpha\left[J_0\left(\frac{4\pi z_0 \sin\varepsilon\tan\alpha}{\lambda}\right)\right]^2 + \frac{\sin^2\varepsilon\cos^2\varepsilon}{\cos^4\alpha}\left[J_1\left(\frac{4 z_0 \sin\varepsilon\tan\alpha}{\lambda}\right)\right]^2}{(\sin^2\varepsilon\tan^2\alpha - \cos^2\varepsilon)^2}. \qquad \text{(B.16)}$$

It is noted that while the nose-on physical optics cross-section is independent of wavelength, the stationary phase result indicates that the near nose-on cross-section varies linearly with wavelength. However, it must be remembered that for small values of ε, α and $\frac{z_0}{\lambda}$ ($\varepsilon < \alpha$, $\alpha < 10^0$, $\frac{z_0}{\lambda} < 10$) the integrand in Equation B.8 or B.14 does not oscillate rapidly enough for valid application of stationary phase. The integral in Equation B.14 was therefore evaluated on an analog computer for various values of α, ε, and z_0/λ. The results are compared with the results computed from Equations B.15 and B.16 in the Figures B-2 through B-7.

The figures indicate that the modified form of the stationary phase result, Equation B.16, is a better approximation than the stationary phase result itself, Equation B.15. The figures also indicate that the requirement

$$\frac{4\pi z_0 \sin\varepsilon\tan\alpha}{\lambda} \gg 1$$

can be relaxed considerably.

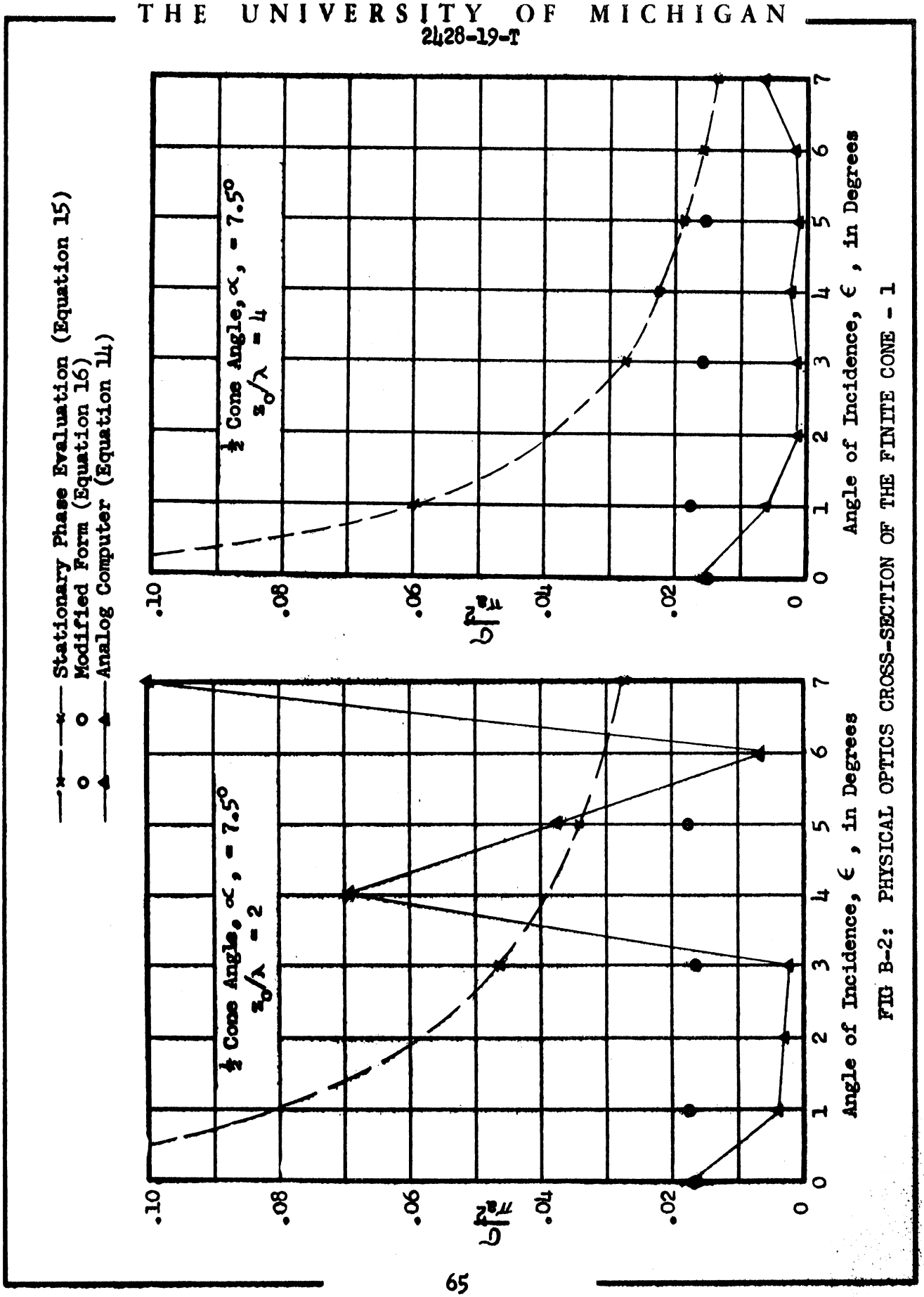

FIG B-2: PHYSICAL OPTICS CROSS-SECTION OF THE FINITE CONE - 1

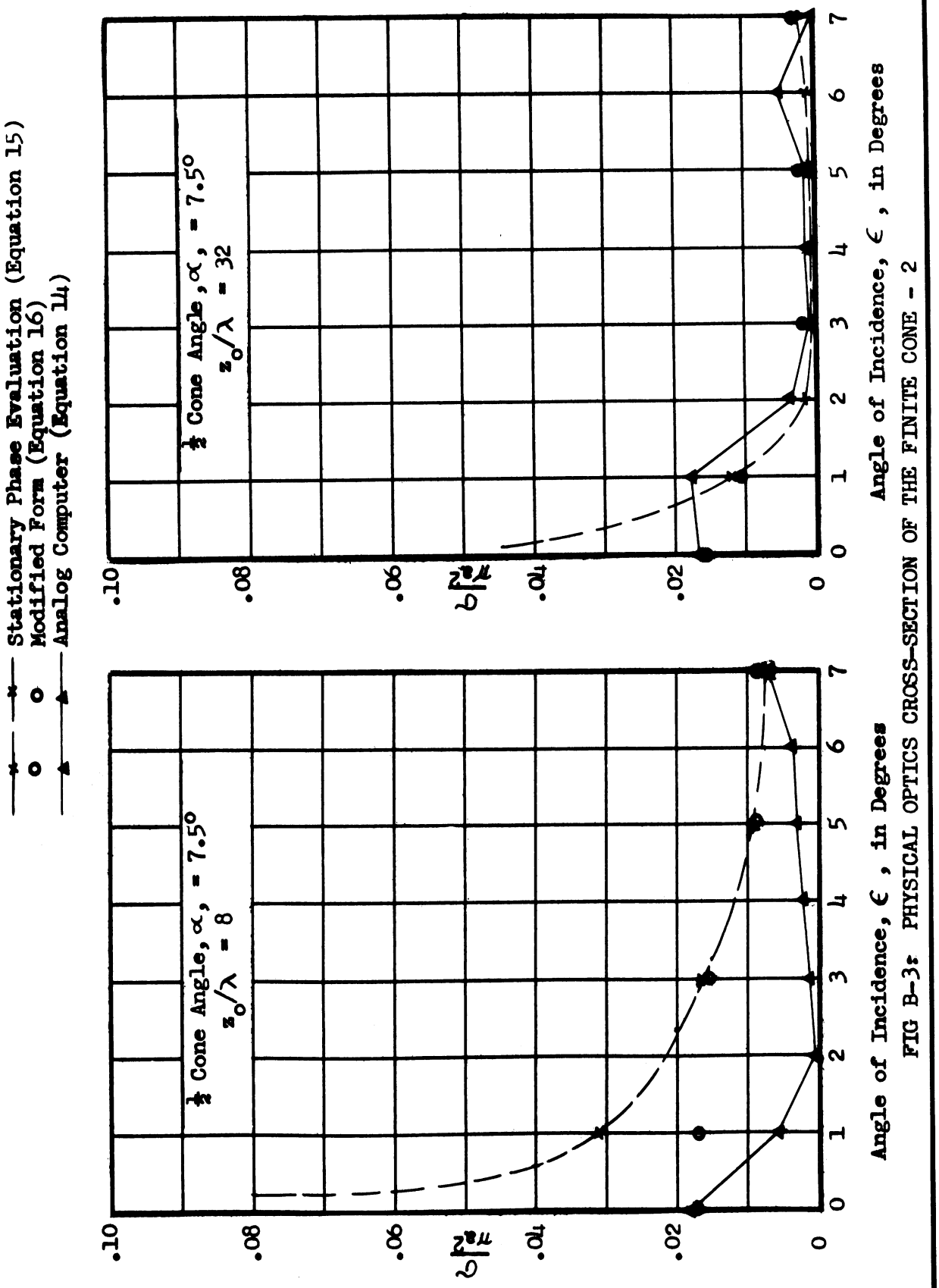

FIG B-3: PHYSICAL OPTICS CROSS-SECTION OF THE FINITE CONE - 2

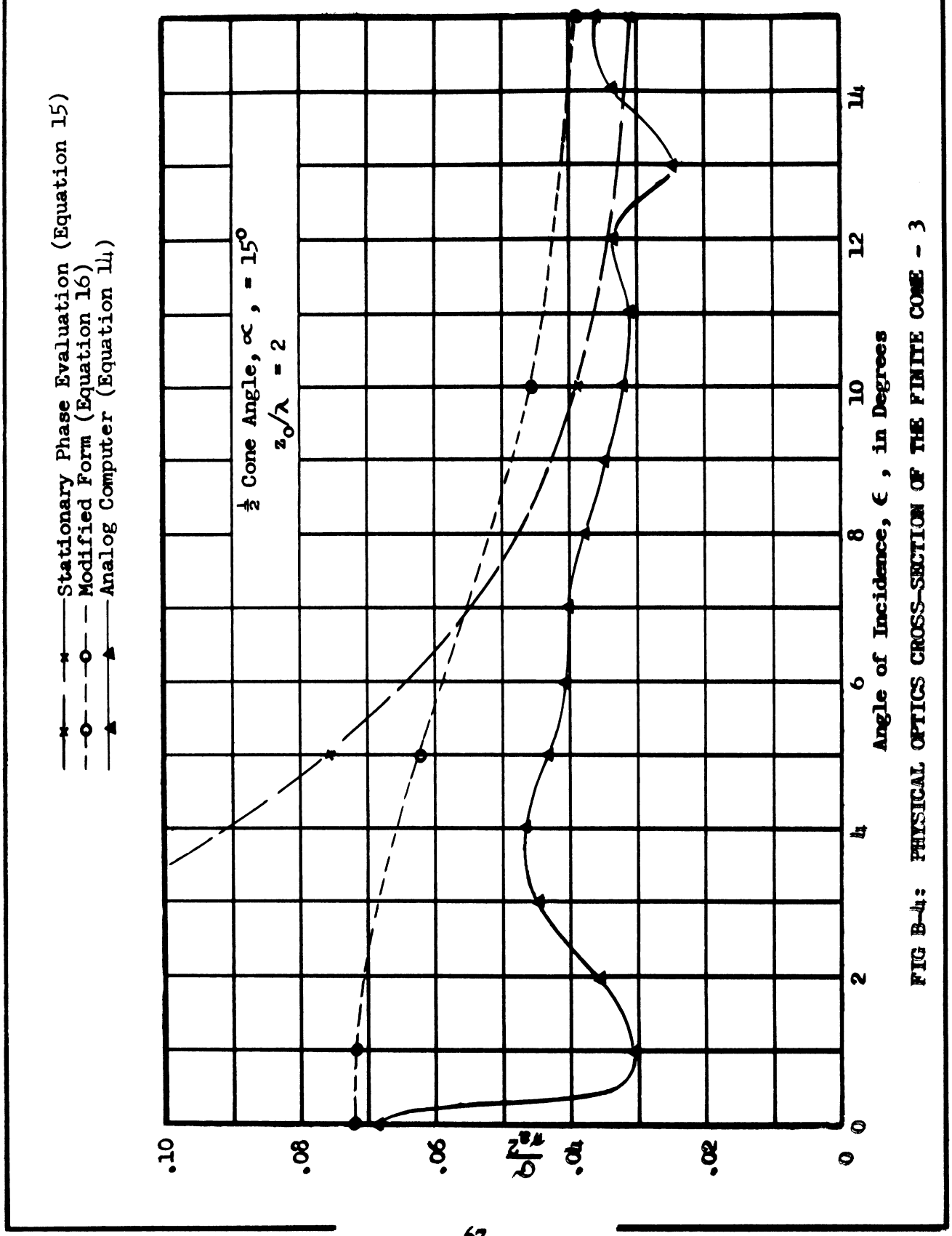

FIG B-4: PHYSICAL OPTICS CROSS-SECTION OF THE FINITE CONE - 3

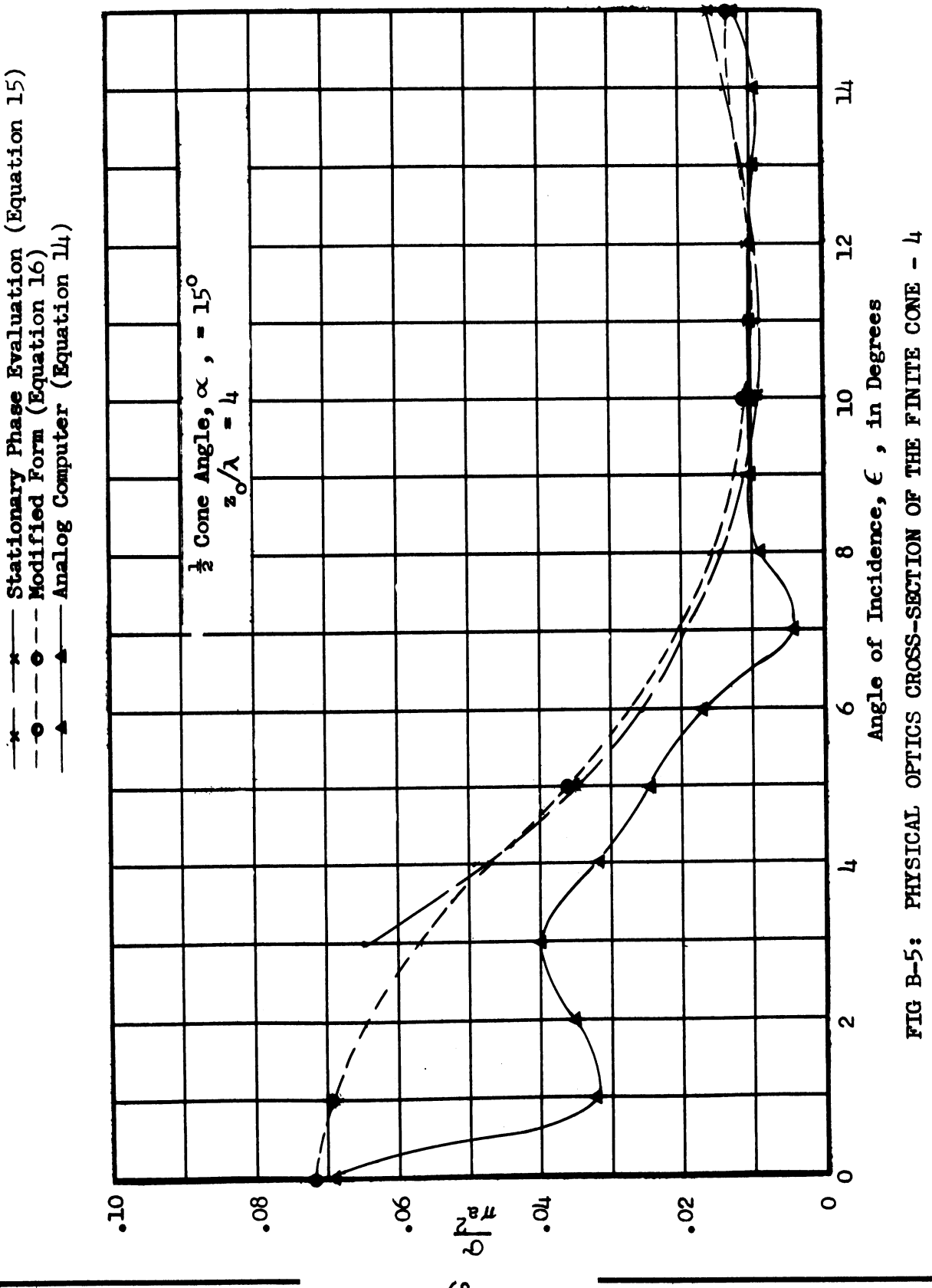

FIG B-5: PHYSICAL OPTICS CROSS-SECTION OF THE FINITE CONE - 4

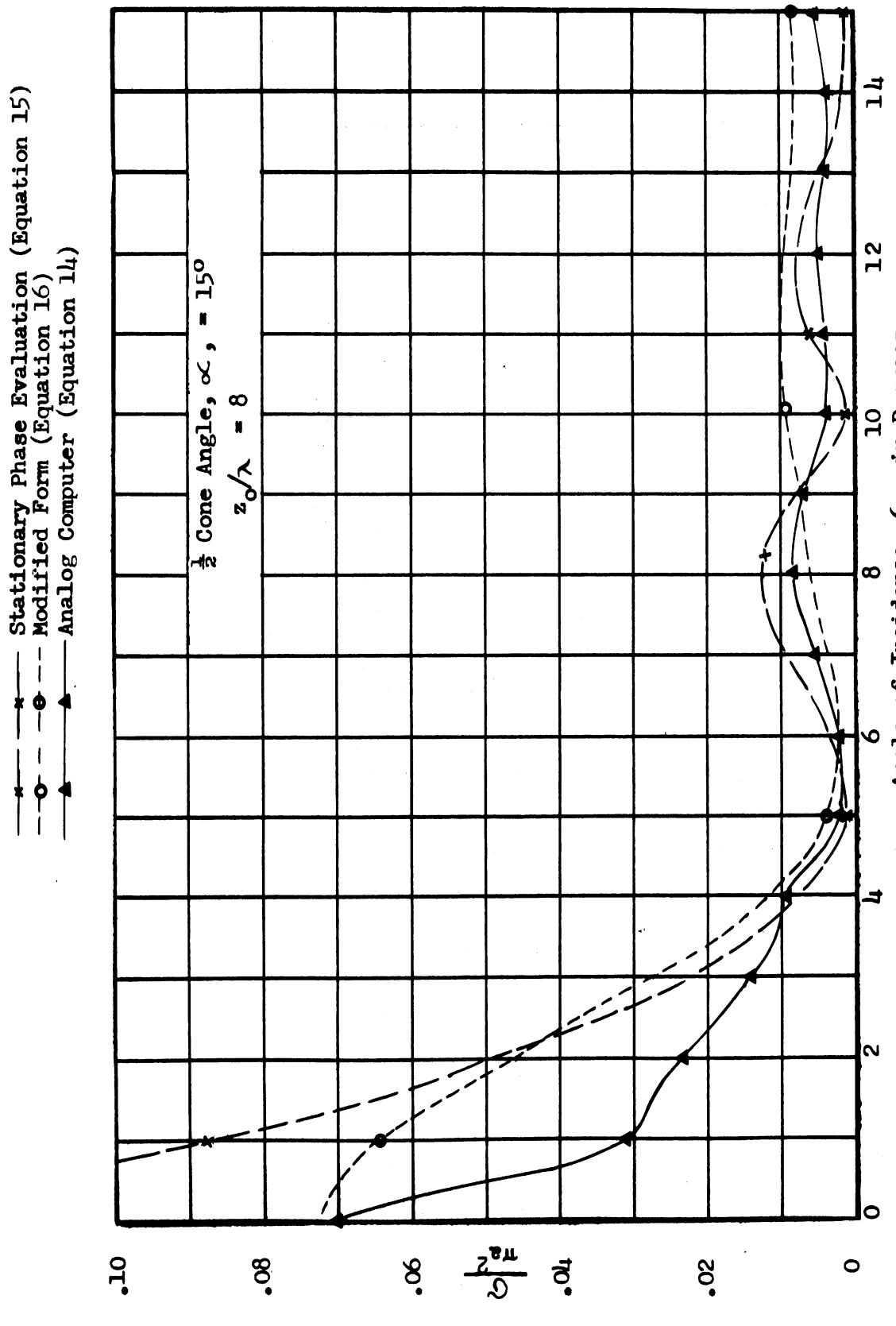

FIG B-6: PHYSICAL OPTICS CROSS-SECTION OF THE FINITE CONE - 5

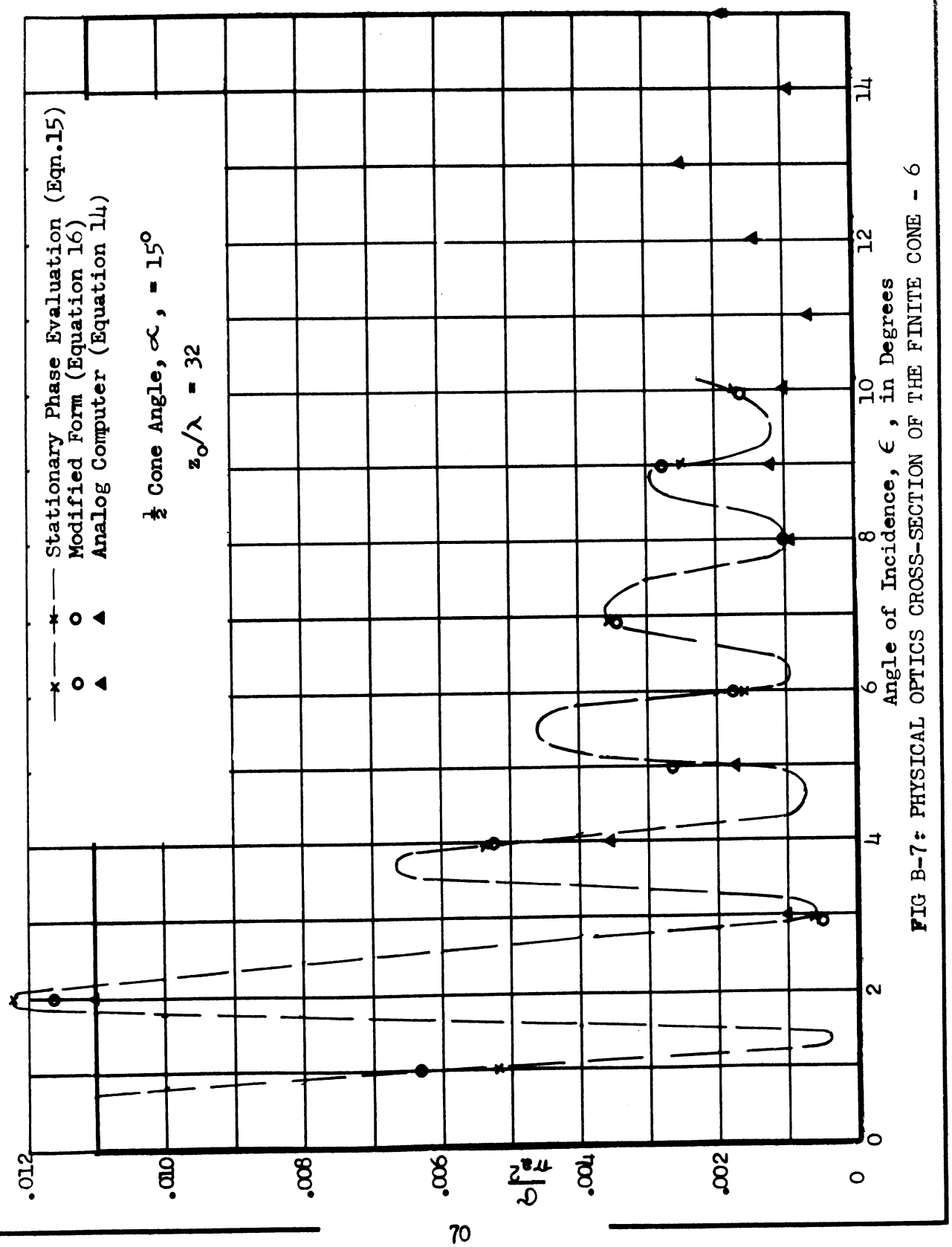

FIG B-7: PHYSICAL OPTICS CROSS-SECTION OF THE FINITE CONE - 6

APPENDIX C

THE RADAR CROSS-SECTION OF A THIN WIRE LOOP FOR SMALL WAVELENGTHS

The radar cross-section of a thin wire loop is derived, for wavelengths which are small compared with the radius of the loop and large compared with the radius of the wire, using an expression due to Chu (Ref.11) for straight wires.

Chu's expression, for incidence normal to the wire becomes

$$\sigma = \frac{\pi L^2 \cos^4 \phi}{\left(\frac{\pi}{2}\right)^2 + \left(\log \frac{\lambda}{\gamma \pi b}\right)^2} \qquad (C.1)$$

where

L = length of wire,

ϕ = angle between electric vector and the plane of the wire and the incident direction,

γ = Euler's constant ≈ 1.78 and

b = radius of wire.

Since $\sigma = 4\pi r^2 \left| \frac{\vec{E}_s}{\vec{E}_i} \right|^2$, we can obtain an expression for $\vec{E}_s$ except for phase from (C.1) assuming $|\vec{E}_i| = 1$ and Huygen's principle holds.

$\vec{E}_s$ then has the form

$$\vec{E}_s = \frac{\vec{s}\, L \cos^2 \phi}{2\left\{\left(\frac{\pi}{2}\right)^2 + \left(\log \frac{\lambda}{\gamma \pi b}\right)^2\right\}^{\frac{1}{2}}} \frac{e^{ikr}}{r}$$

where $\vec{s}$ is a unit vector in an arbitrary direction.

Setting $L = a d\phi$ (where a is the radius of the loop) and integrating around the loop we obtain

$$\vec{E}_s = \frac{\hat{s}\ e^{ikr}\ a}{2r\left\{\left(\frac{\pi}{2}\right)^2 + \left(\log \frac{\lambda}{\gamma \pi b}\right)^2\right\}^{1/2}} \int_0^{2\pi} \cos^2\phi\, d\phi$$

$$= \frac{\hat{s}\ \pi\ a\ e^{ikr}}{2r\left\{\left(\frac{\pi}{2}\right)^2 + \left(\log \frac{\lambda}{\gamma \pi b}\right)^2\right\}^{1/2}} .$$

The cross-section of the loop can then be written

$$\sigma = 4\pi r^2 \left| \frac{\vec{E}_s}{\vec{E}_i} \right|^2$$

$$= \frac{\pi^3\ a^2}{\left(\frac{\pi}{2}\right)^2 + \left(\log \frac{\lambda}{\gamma \pi b}\right)^2} .$$

APPENDIX D

CIRCULAR WEDGE APPROXIMATION TO RADAR CROSS-SECTION OF THIN FINITE CONES

The radar cross-section of a thin finite cone is determined by considering only the contribution from the base which is approximated by a circular wedge shape. That this approximation retains the essential scattering characteristics of the cone is indicated by first computing the cross-section of the approximating wedge shape using physical optics. It is seen that the result thus obtained and the physical optics thin cone result (Equation B.7) agree exactly.

The circular wedge cross-section is then computed using a method suggested by C. E. Schensted (Ref. 15). Expressions for the field due to a straight wedge, which are in general more exact than physical optics, are employed.

Proceeding as outlined, using the physical optics expressions in Reference 9, we obtain the following expressions for the scattered magnetic field from a semi-infinite wedge of length L with incidence perpendicular to the back face as shown in Figure D-1:

$$\vec{H}_s = \frac{e^{-ikR'}}{R'} \left[-\frac{ik}{2\pi} \left(\hat{n}_o \cdot \vec{f} \right) \hat{a} \right]$$

where

$$\vec{f} = \int_{\text{illuminated area}} \hat{n}\, e^{-ik\vec{r}\left(\hat{n}_o + \hat{k}\right)} dS ,$$

$\vec{H}_i$ = unit incident field = $\hat{a}$,

$\hat{n}_o = \hat{k} = \hat{i}_z$,

$\hat{n}$ = normal to wedge = $\hat{i}_x \sin\gamma - \hat{i}_z \cos\gamma$,

γ = included wedge angle,

and $dS = \frac{dydx}{\cos\gamma}$

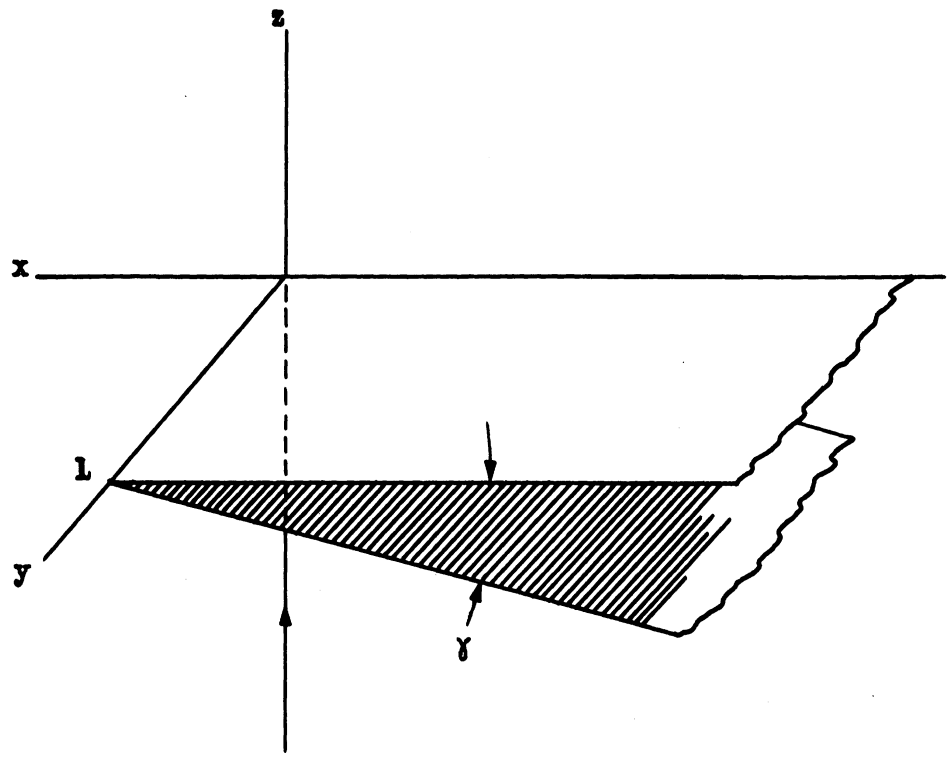

FIG D-1

Hence $\vec{r} = \hat{i}_x x + \hat{i}_y y + \hat{i}_z (x \tan\gamma)$,

$\hat{n} \cdot \vec{n}_o = - \cos\gamma$,

and $\vec{r} \cdot (\vec{n}_o + \vec{k}) = 2x \tan\gamma$.

Thus,

$$\vec{n}_o \cdot \vec{f} = - \int_0^{-\infty} \int_0^{L} e^{-i2kx\tan\gamma} \, dy dx$$

$$= L \int_0^{\infty} e^{+i2kx\tan\gamma} \, dx$$

$$= + L \left[\frac{e^{+i2kx\tan\gamma}}{i2k\tan\gamma} \right]_0^{\infty} .$$

Associating the edge contribution with the value at the lower limit (just as in the infinite cone case we obtain the "tip" contribution) we have finally

$$\vec{n}_o \cdot \vec{f} = \frac{- L}{i2k\tan\gamma}$$

and

$$\vec{H}_s = + \frac{L \hat{a}}{4\pi \tan\gamma} \frac{e^{-ikR'}}{R'} .$$

Now letting $L = ad\beta$, where a = radius of base, and integrating around the base (a = constant vector), we obtain

$$\vec{H}_s = \int_0^{2\pi} \frac{\hat{a}\, e^{-ikR'}}{4\pi R \tan\gamma}\, a\,d\beta = \frac{a\,\hat{a}\, e^{-ikR'}}{2R' \tan\gamma}$$

$$\sigma = 4\pi R'^2 \left| \frac{\vec{H}_s}{\vec{H}_i} \right|^2$$

$$= 4\pi R'^2 \left| \frac{a\ e^{-ikR'}}{2R' \tan\gamma}\ \hat{a} \right|^2$$

$$= \frac{\pi a^2}{\tan^2\gamma} \quad .$$

But $\gamma = \frac{\pi}{2} - \alpha$ (see Fig. D-2) where α is half the cone angle; thus,

$$\tan\alpha = \tan\left(\frac{\pi}{2} - \gamma\right)$$

$$= \cot\gamma$$

and finally

$$\sigma = \pi a^2 \tan^2\alpha \quad ,$$

which is precisely the nose-on result obtained for the cone directly with physical optics.

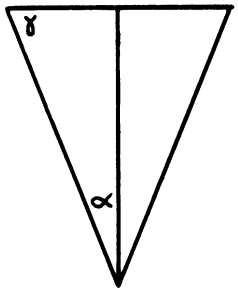

FIG D-2

Now instead of using the physical optics field for a wedge, we use the generally more exact expression as presented in Reference 15, and proceed exactly as before. For linear polarization the scattered field for a wedge of length L is

$$\vec{E}_s = \frac{L\, e^{ikr}}{4r\phi_0} \sin\frac{\pi^2}{2\phi_0} \left[\frac{E(a)\hat{\phi} - E(b)\hat{k}}{A} - \frac{E(a)\hat{\phi} + E(b)\hat{k}}{B} \right], \qquad (D.1)$$

where

E(a) = component of the incident field perpendicular to the edge of the wedge,

E(b) = component of the incident field parallel to the edge of the wedge,

$A = \cos\frac{\pi\theta}{\phi_0} + \cos\frac{\pi^2}{2\phi_0}$

$B = 1 - \cos\frac{\pi^2}{2\phi_0}$

ϕ_0 = wedge angle (see Fig. D-3) where in terms of the half cone angle

$$\phi_0 = \frac{3\pi}{4} + \frac{\alpha}{2}$$

θ = angle of incidence, and

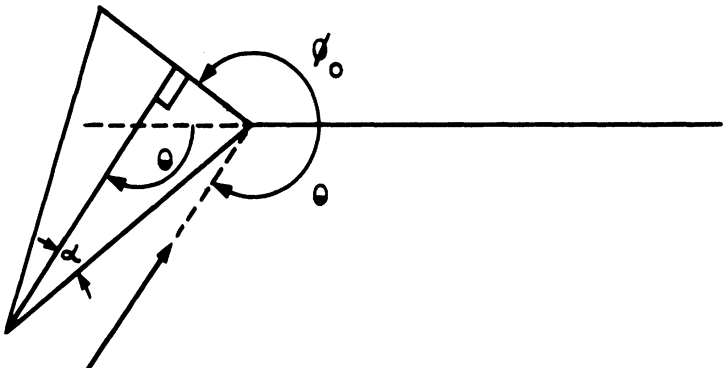

FIG D-3

$\hat{\beta}$ and $\hat{k}$ are unit vectors perpendicular and parallel, respectively, to the edge of wedge (or circumference of the cone base) (see Fig. D-4)

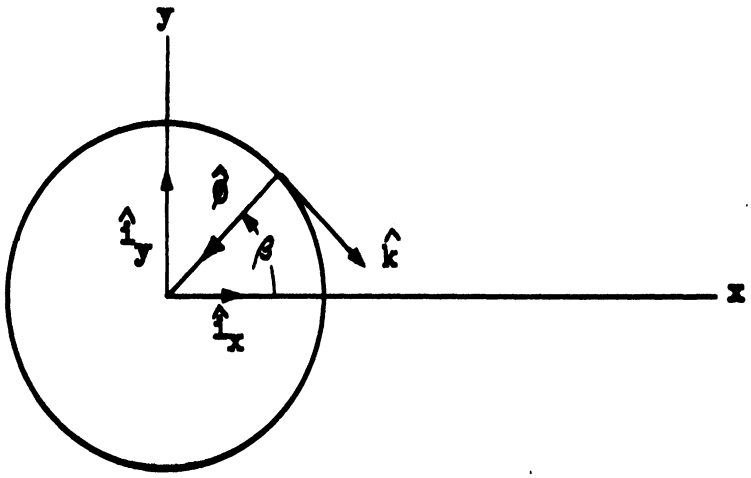

Figure D-4

The quantities $\hat{\beta}$ and $\hat{k}$ are related to $\hat{i}_x$ and $\hat{i}_y$ as follows:

$$\hat{\beta} = -\hat{i}_x \cos\beta - \hat{i}_y \sin\beta \qquad \hat{i}_x = -\hat{\beta}\cos\beta + \hat{k}\sin\beta \qquad (D.2)$$

$$\hat{k} = \hat{i}_x \sin\beta - \hat{i}_y \cos\beta \qquad \hat{i}_y = -\hat{\beta}\sin\beta - \hat{k}\cos\beta$$

Since the incident electric vector lies in the x-y plane and since the base of the cone is symmetric about the origin in the x-y plane, we may choose $\hat{E}_{incident}$ to lie along $\hat{i}_x$.

Thus,

$$\hat{E}_i = \hat{i}_x = -\hat{\beta}\cos\beta + \hat{k}\sin\beta = E(a)\hat{\beta} + E(b)\hat{k} \quad . \qquad (D.3)$$

To obtain the total scattered field we compute the field for a wedge of length $L = ad/\beta$ where a is the radius of the base of the cone, and integrate around the base.

Thus, we have from (D.1) and (D.3)

$$\vec{E}_s = \int_0^{2\pi} \frac{a\, e^{ikr}}{4r\phi_o} \sin\frac{\pi^2}{2\phi_o} \left[\frac{-\cos\beta\,\hat{\phi} - \sin\beta\,\hat{k}}{\cos\frac{n\theta}{\phi_o} + \cos\frac{\pi^2}{2\phi_o}} - \frac{-\cos\beta\,\hat{\phi} + \sin\beta\,\hat{k}}{1 - \cos\frac{\pi^2}{2\phi_o}} \right] d\beta$$

Using Equations (D.2) we get

$$\vec{E}_s = \frac{a\, e^{ikr}}{4\, r\, \phi_o} \sin\frac{\pi^2}{2\phi_o} \int_0^{2\pi} \left[\frac{\hat{i}_x \cos 2\beta + \hat{i}_y \sin 2\beta}{\cos\frac{\pi\theta}{\phi_o} + \cos\frac{\pi^2}{2\phi_o}} - \frac{\hat{i}_x}{1 - \cos\frac{\pi^2}{2\phi_o}} \right] d\beta$$

$$= -\frac{a\pi e^{ikr}}{2\, r\, \phi_o} \sin\frac{\pi^2}{2\phi_o} \frac{\hat{i}_x}{1 - \cos\frac{\pi^2}{2\phi_o}} \quad .$$

The effective radar cross-section is defined by

$$\sigma = \lim_{r \to \infty} 4\pi r^2 \left| \frac{\vec{E}_s \cdot \hat{p}}{\vec{E}_i} \right|^2$$ where $\hat{p}$ = receiver polarization vector.

In the case being considered, $\hat{p} = \hat{i}$ and $|\vec{E}_i| = 1$. Thus,

$$\sigma = \lim_{r \to \infty} 4\pi r^2 \left| \vec{E}_s \right|^2 \quad .$$

Substituting for $\vec{E}_s$, we get

$$\sigma = \frac{a^2 \pi^3}{\phi_o^2} \frac{\sin^2 \frac{\pi^2}{2\phi_o}}{\left(1 - \cos \frac{\pi^2}{2\phi_o}\right)^2}$$

$$= \frac{a^2 \pi^3}{\phi_o^2} \cot^2 \frac{\pi^2}{4\phi_o}$$

or, in terms of the half cone angle, α,

$$\frac{\sigma}{\pi a^2} = \frac{\pi^2}{\left(\frac{3\pi}{4} + \frac{\alpha}{2}\right)^2} \cot^2 \left(\frac{\pi^2}{3\pi + 2\alpha}\right) . \qquad (D.4)$$

This result is compared with the physical optics result in Figure D-7. This method can be applied to any body with a ring singularity. Consider, for example, a cone-cylinder combination (Fig. D-5) viewed nose-on.

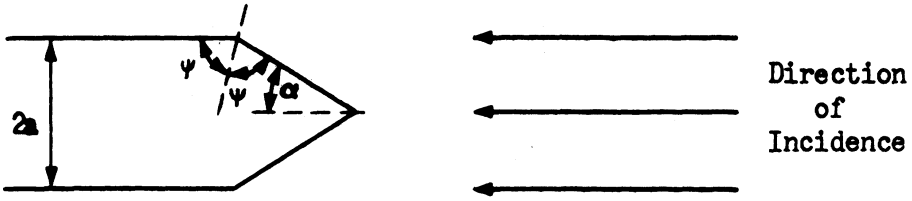

$\psi = \pi - \phi_o$

Figure D-5

The expression derived for the cross-section

$$\frac{\sigma}{\pi a^2} = \frac{\pi^2}{\phi_o^2} \cot^2 \frac{\pi^2}{4\phi_o} \qquad (D.5)$$

still applies. In terms of the half cone angle, α, we have

$$\frac{\sigma}{\pi a^2} = \frac{\pi^2}{\left(\frac{\pi}{2} + \frac{\alpha}{2}\right)^2} \cot^2\left(\frac{\pi^2}{2(\pi + \alpha)}\right) . \qquad (D.6)$$

Similarly, for the contribution from any ring singularity, Equation D.5 holds where ϕ_0 is the supplement of half of the included wedge angle (Fig. D-6)

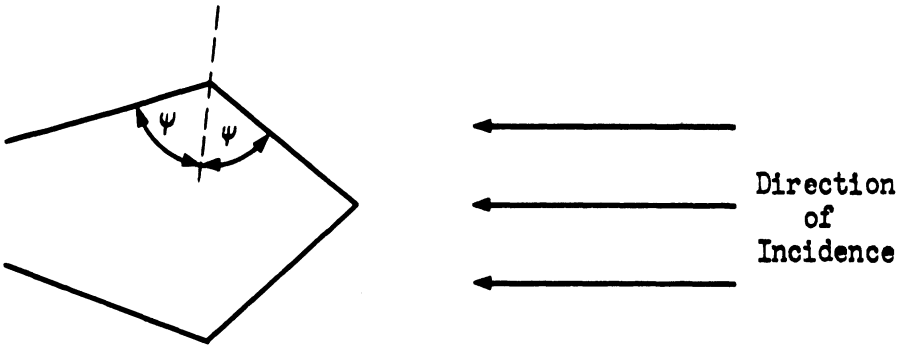

$\psi = \pi - \phi_0$

Figure D-6

Equations D.4, D.5, and D.6 are plotted in Figure D-8.

$$Y_1 = \frac{\pi}{\left(\frac{3\pi}{4} + \frac{\alpha}{2}\right) \tan\left(\frac{\pi^2}{3\pi + 2\alpha}\right)} = \sqrt{\frac{\sigma_{wedge}}{\pi a^2}}$$

$$Y_2 = \tan \alpha = \sqrt{\frac{\sigma_{phys.\ op.}}{\pi a^2}}$$

$\alpha = \frac{1}{2}$ cone angle

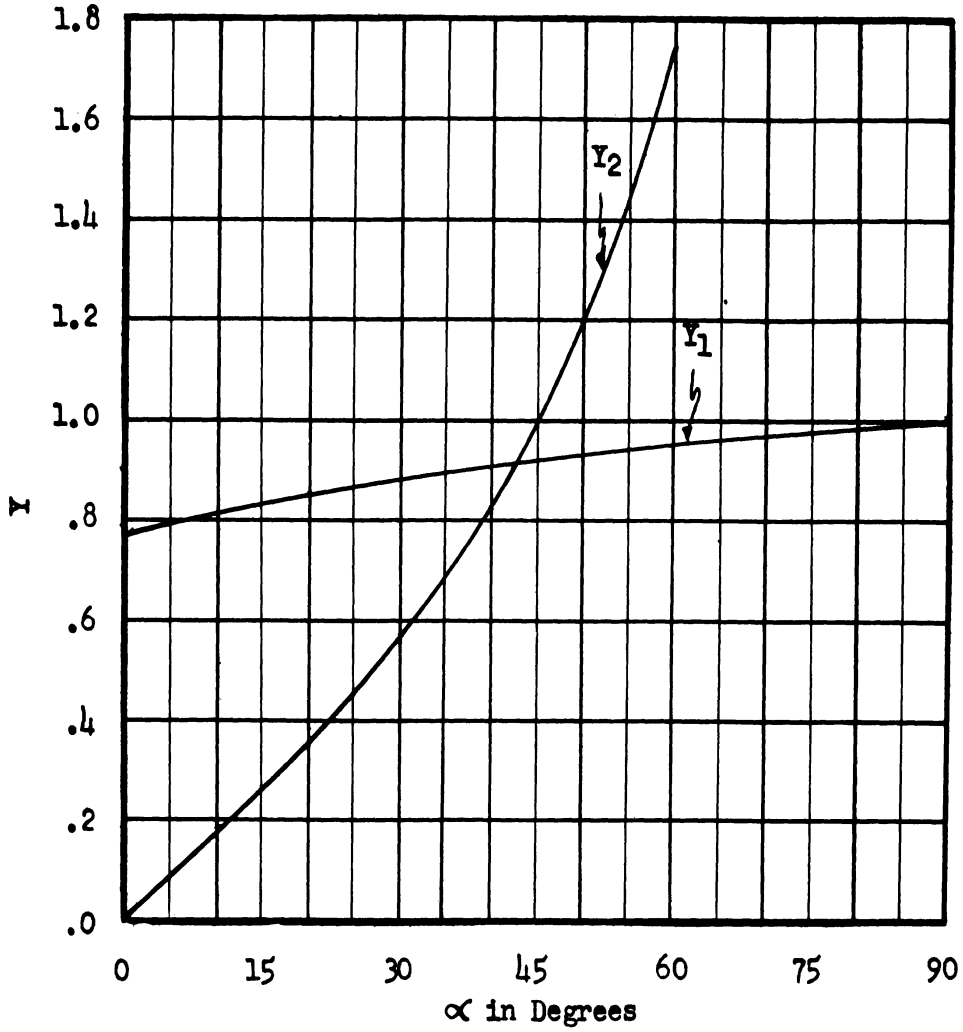

FIG. D-7 NOSE-ON FINITE CONE CROSS-SECTIONS AS COMPUTED BY PHYSICAL OPTICS AND CIRCULAR WEDGE APPROXIMATIONS.

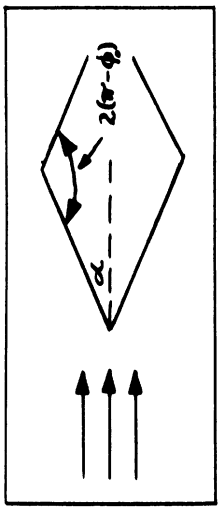

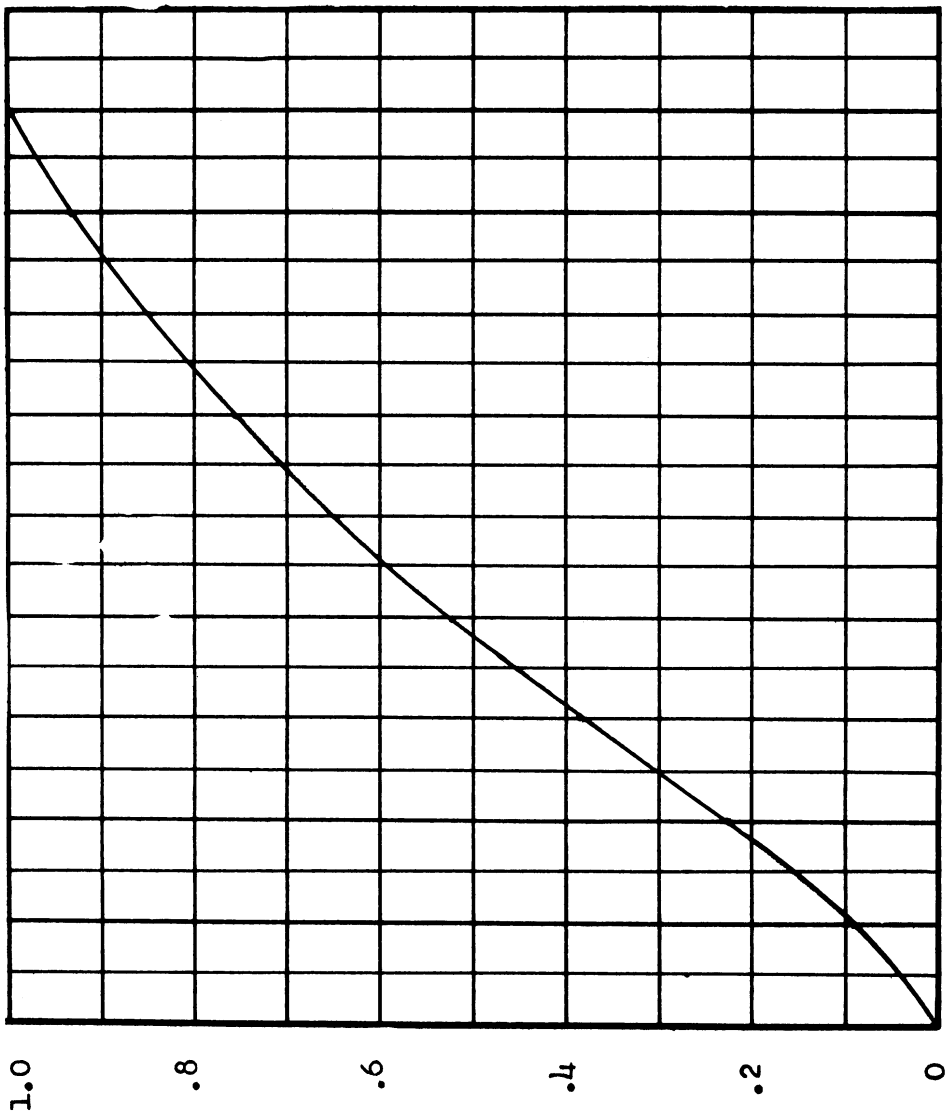

FIG. D-8 NOSE-ON CROSS-SECTION OF CIRCULAR WEDGE

APPENDIX E

MINIMAL CROSS-SECTION SHAPES

For many years the authors have advocated that missile design should be conducted from a radar cross-section point of view. The objective would be to design an offensive missile whose cross-section is minimal for any set of Coefficients of Drag and Lift vs. Mach Number and Reynolds Number given as restrictions which the geometry must obey. It was pointed out that the minimum nose-on cross-section one could expect a missile made of a conducting material to equal or approach was (for small wavelengths) the radar cross-section of an infinite cone. It was believed that infinite cones would give the same results as smoothly terminated* bodies for which the cone was the tangent surface.

This belief was verified theoretically for small wavelengths by Schiff (Ref. 16) for the ogive, and experimentally for thick ogives by Sletten (Ref. 17). The question remained as to how sharply one could terminate the conical body and still obtain a nose-on answer which was of the same order of magnitude as the cross-section of an infinite cone,

$$\sigma = \frac{\lambda^2 \tan^4 \alpha}{16\pi} \quad .$$

For thick bodies it was found that the termination could involve much smaller radii of curvature than for thin bodies. In fact for thin ogives the Fock reasoning (discussed below) is only valid for very small λ/R ratios, where R is the radius of curvature in the plane of Poynting's vector at the shadow boundary (the curve on the body which separates the

*In terms of wavelength.

lit region of the body from the shadow region). This has been indicated by recent experiments conducted at The Ohio State University (Ref. 4), which give nose-on cross-sections for thin ogives much different from the infinite cone answer, and by recent Air Force Cambridge Research Center experiments. Thus, the cross-sections of thin bodies for which $\lambda/R > 0.1$ are not predictable by physical optics. The cross-sections of such bodies are expected to be larger on the average than those predicted by optics formulas. Nevertheless such smooth terminations tend to reduce the cross-section.

Here we shall consider the back-scattering cross-section of a finite cone with various base terminations for illumination along the cone axis. This cross-section will depend critically on the method of termination at the base of the cone. Hence, we attempt to isolate the contribution of the cap of the cone from that of the tip. Quite generally we find that the contribution of the base depends upon the rapidity of the transition from light to shadow measured in terms of the wavelength.

The finite cone itself has been discussed in the preceding appendices; here we will examine a finite cone smoothly fitted with a spherical cap. For a wavelength of the same order as the length of the cone we cannot treat the contributions of the tip and the base as uncoupled. However, if the wavelength is decreased so that the distance between the tip and the shadow boundary is several wavelengths, we expect to be able to treat the contributions as virtually uncoupled.

If the radius of curvature at the shadow boundary is large with respect to the wavelength, the base contribution to the cross-section is found

by Schiff (Ref. 16) to be of higher order in λ than that from the tip. As the radius of curvature of the shadow boundary decreases in terms of wavelength, the base contribution becomes increasingly important until in the limit of vanishing radius of curvature (i.e., an ordinary finite cone) the dominant contribution to the cross-section comes from the base.

In applying the physical optics approximation to the finite cone, it is found that there is one term that can be identified as the tip contribution. There is also a term arising from the assumption that the current on the body is discontinuous at the shadow boundary. This latter term, the base contribution, is present even when the body is smoothly terminated and the discontinuity in current is known to be nonexistent. However, the tip contribution is still valid. Thus the cross-section of smoothly terminated cones will consist of the physical optics tip contribution plus a contribution arising from an adequate treatment of the base. This base contribution, it will be recalled, increases in relation to the complete cross-section as the radius of curvature at the shadow boundary decreases to the order of a wavelength.

One method of determining the base contribution, in the special case when the cone has a spherical cap (see Fig. E-1) is obtained from a consideration of the exact sphere solution.

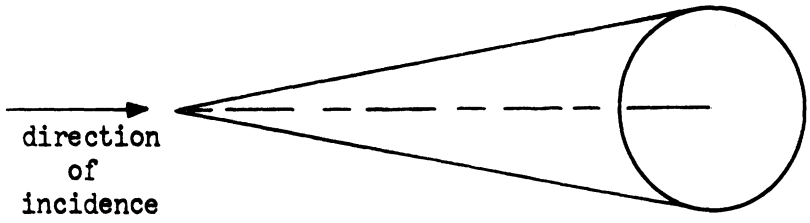

FIG E-1: A CONE CAPPED BY A SPHERE

The sphere cross-section can be decomposed into a geometrical optics term plus a diffraction term. This has been done by Franz, Deppermann, and Imai (Refs. 18 and 19). The optics term comes from the region of specular reflection and the diffraction term from the effects of the currents induced in the shadow and near the shadow boundary. This consideration leads us to attempt to approximate the base contribution of the spherically capped cone by determining the differences between the total field due to the sphere and its geometric optics field. This approach was carried out by Pound recently at the Cornell Aeronautical Laboratory, Inc. (Ref. 20) and here at The University of Michigan in 1954 (Ref 2). These two estimates are shown graphically in Figure E-2.

No such ready solutions to the problems posed by a smoothly fitted convex cap which is otherwise arbitrary are available. However, Fock (Ref. 21) has developed a modification of geometric optics which arises from a local analysis of the field in the shadow region and leads to a smooth transition from light to shadow for the field induced on the surface. From the work of both Franz and Fock we see that the important parameter in determining the contribution of the diffraction term is the radius of curvature at the shadow boundary as compared with the wavelength.

An equivalent spherical cap is thus determined and its contribution to the cross-section can be found using the technique as outlined previously. If the radius of curvature at the shadow boundary does not change rapidly as the shadow region is entered, this approximation will yield good results.

Using the "average" expression for the contribution from the base as

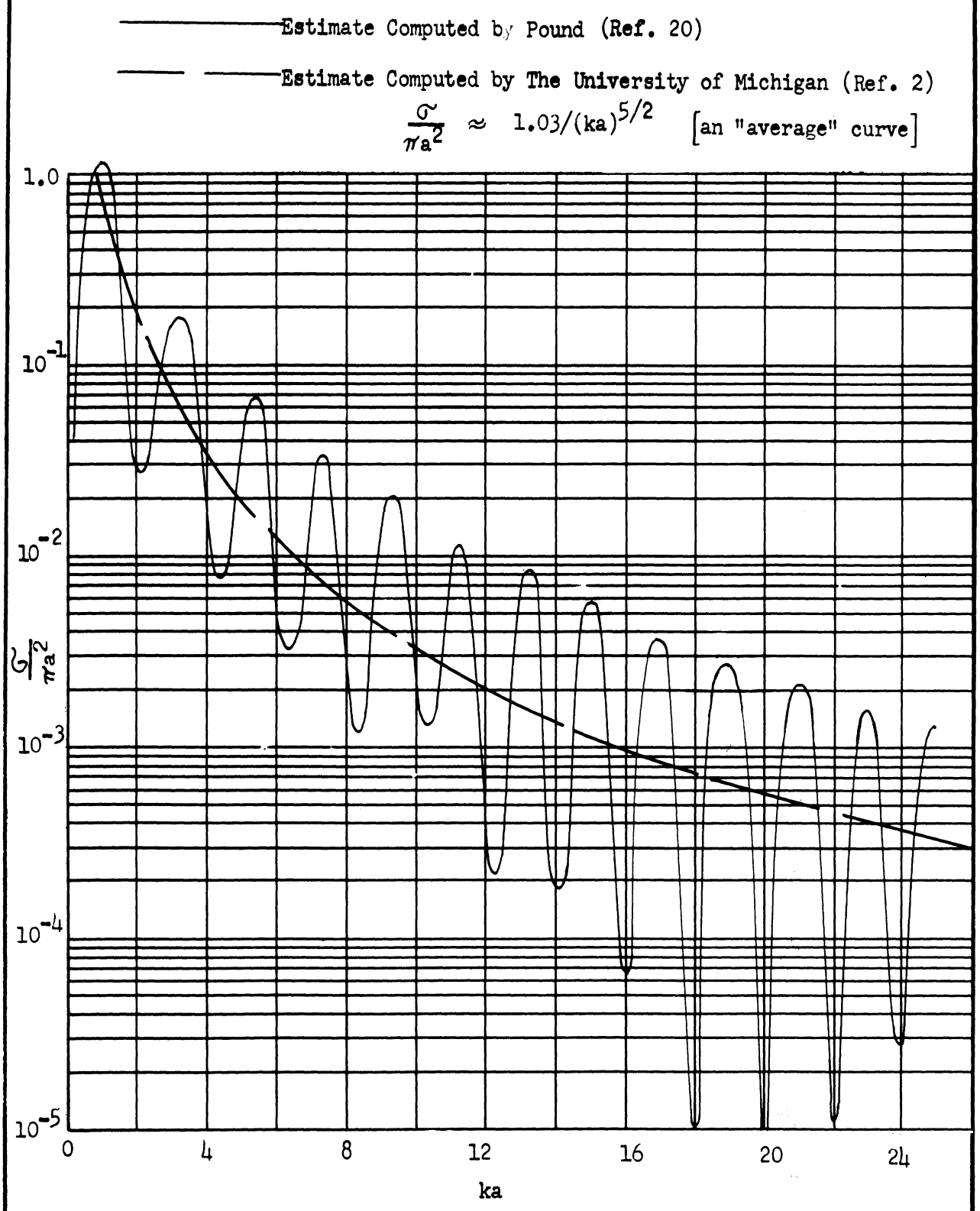

FIG E-2: CONTRIBUTION FROM THE REAR OF A SPHERE OF RADIUS a.

shown in Figure E-2, estimates of the nose-on cross-section of certain thin cones smoothly terminated by spheres or near sphere-like caps are determined in Appendix F and the results so obtained are compared with experiment. In connection with those comparisons between theory and experiment it will be noted from Figure E-2 that over the range of ka involved in the computations, the estimates of Pound deviate from the "average" curve by factors as large as 5 and thus differences of factors of 3 or 4 between theory and experiment are not particularly unexpected. Due to the rapid oscillation of this contribution as a function of ka, it is believed that the "average" curve is more appropriate for the purpose of the comparisons given in Appendix F, since the cap placed upon the cone in these experiments is not truly spherical. It is to be noted in applying this "average" curve that a/λ is restricted by the inequality $\sim 1 < 2\pi a/\lambda < \sim 15$. This restriction is applied since the "average" curve was obtained by a curve fitting process in which a/λ was limited as above.

For large values of ka ($ka > \sim 15$) it is known that physical optics, although it does not correctly predict the positions of the maxima for the sphere, does predict values for the amplitude of the maxima which are in close agreement with exact theory. Thus the "average" curve can be extended into the region of large ka in the following manner.

According to physical optics the cross-section of the sphere is given for large ka by

$$\sigma \sim \pi a^2 \left[1 - \frac{\sin(2ka)}{ka} + \frac{1-\cos(2ka)}{2(ka)^2} \right] \qquad \text{(E-1)}$$

This expression takes on "maximum" values whenever $2ka = (4N+3)\frac{\pi}{2}$ remembering $ka > \sim 15$ where N is an integer greater than 3. For these cases assuming that the maximum cross-section is given by

$$\sigma_{max} \approx (\sqrt{\sigma_f} + \sqrt{\sigma_R})^2 \qquad \text{(E-2)}$$

where σ_f = the contribution for the first Fresnel zone $= \pi a^2$

and σ_R = the contribution from the transition region and/or from creeping waves,

we obtain

$$(\sqrt{\pi a^2} + \sqrt{\sigma_R})^2 \approx \pi a^2 \left[1 + \frac{1}{2(ka)}\right]^2 . \qquad \text{(E-3)}$$

Thus, σ_R, the contribution from the rear, becomes

$$\sigma_R \approx \frac{\pi a^2}{4(ka)^2} , \qquad \text{(E-4)}$$

which also can be expressed in the form

$$\frac{\sigma_R}{\lambda^2} \approx \frac{1}{16\pi} . \qquad \text{(E-5)}$$

A maximum value of σ_R can be obtained by assuming that $\sigma = \pi a^2 + \sigma_R$ in equation E-1 and maximizing the right hand side of E-1, obtaining

$$\sigma_{R_{max}} \approx \frac{a\lambda}{2} . \qquad \text{(E-6)}$$

It is seen that the values predicted by equation (E-5) and the "average" curve in Fig. E-2 are equal for ka $\sim$ 15, thus:

1) For $1 < ka < \sim 15$ the value of the contribution from the rear is approximated by

$$\frac{\sigma_R}{\pi a^2} \approx \frac{1.03}{(ka)^{5/2}} ;$$

2) For $ka > \sim 15$

$$\frac{\sigma_R}{\pi a^2} \approx \frac{1}{4(ka)^2} .$$

For bodies of revolution which have at the shadow boundary a fixed radius of curvature in the plane of Poynting's vector which is smaller than the wavelength then that part of the body acts like a ring discontinuity and should be treated by the methods of Appendix D.

APPENDIX F

THE RADAR CROSS-SECTION OF FINITE CONES WITH VARIOUS BASE TERMINATIONS A COMPARISON BETWEEN THEORY AND EXPERIMENT

F.1. Introduction

This appendix gives an account of experimentally determined radar cross-sections of finite cones with various base terminations. Wherever possible, these experimental values are compared with theoretical estimates determined by the methods discussed in the preceding portions of this report. In Section F.2 three finite cones and three cones smoothly capped in the rear ("carrots") are considered. In Section F.3 information on the cross-sections of 7-OC type warheads is presented. In Section F.4 experimental data on other conical shapes is considered. In Section F.5 conclusions are presented.

F.2. The Radar Cross-Section of Carrots and Cones

The Microwave Radiation Company, Inc., performed experimental radar cross-section measurements for the Cornell Aeronautical Laboratory, Inc., on the carrot and cone configurations shown in Figure F-1 (Ref.22). The results obtained in these experiments are summarized in Figures F-2 through F-4. Estimates of the cross-sections of these configurations have been computed using the techniques discussed previously in this report.

Dimensions (in wavelengths)						
	Carrots			Cones		
	#1	#2	#3	#1	#2	#3
L	2	4	8	2	4	8

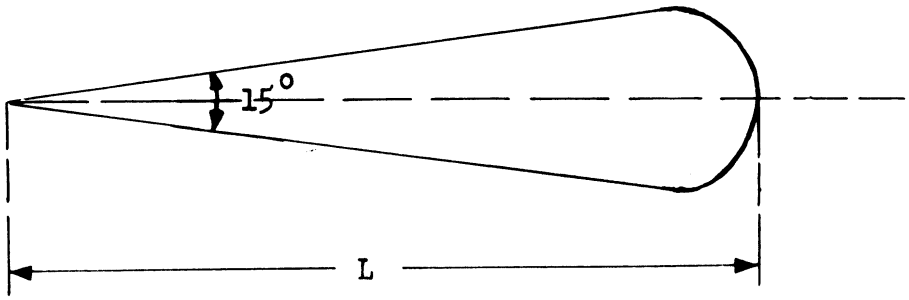

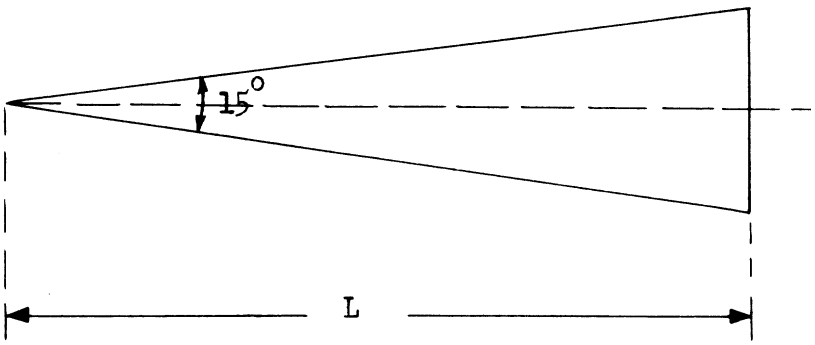

FIG F-1: CARROT AND CONE CONFIGURATIONS

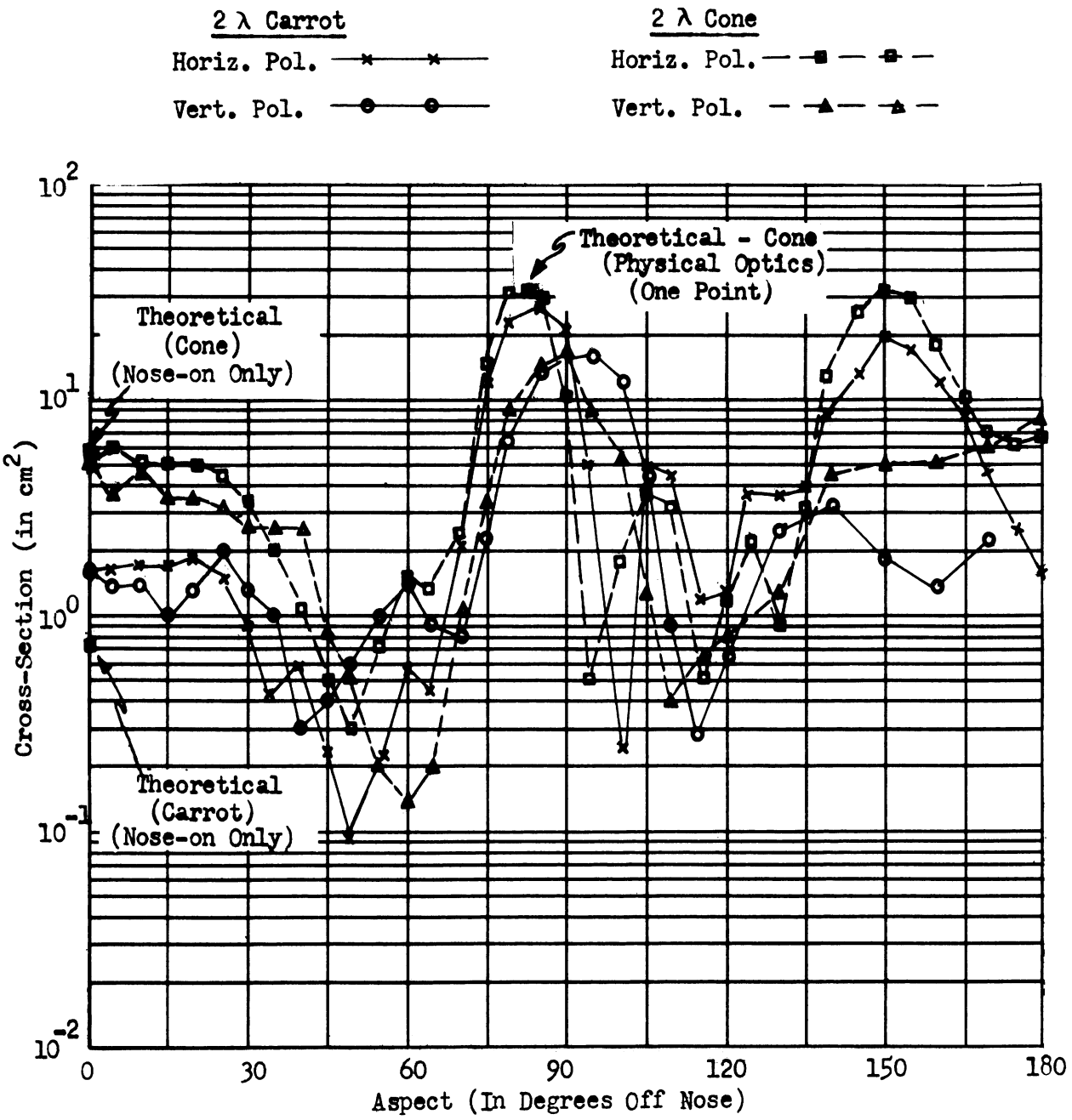

FIG F-2: 2 λ CONE AND 2 λ CARROT - (Ref. 22)
(λ = 3.2 cm)

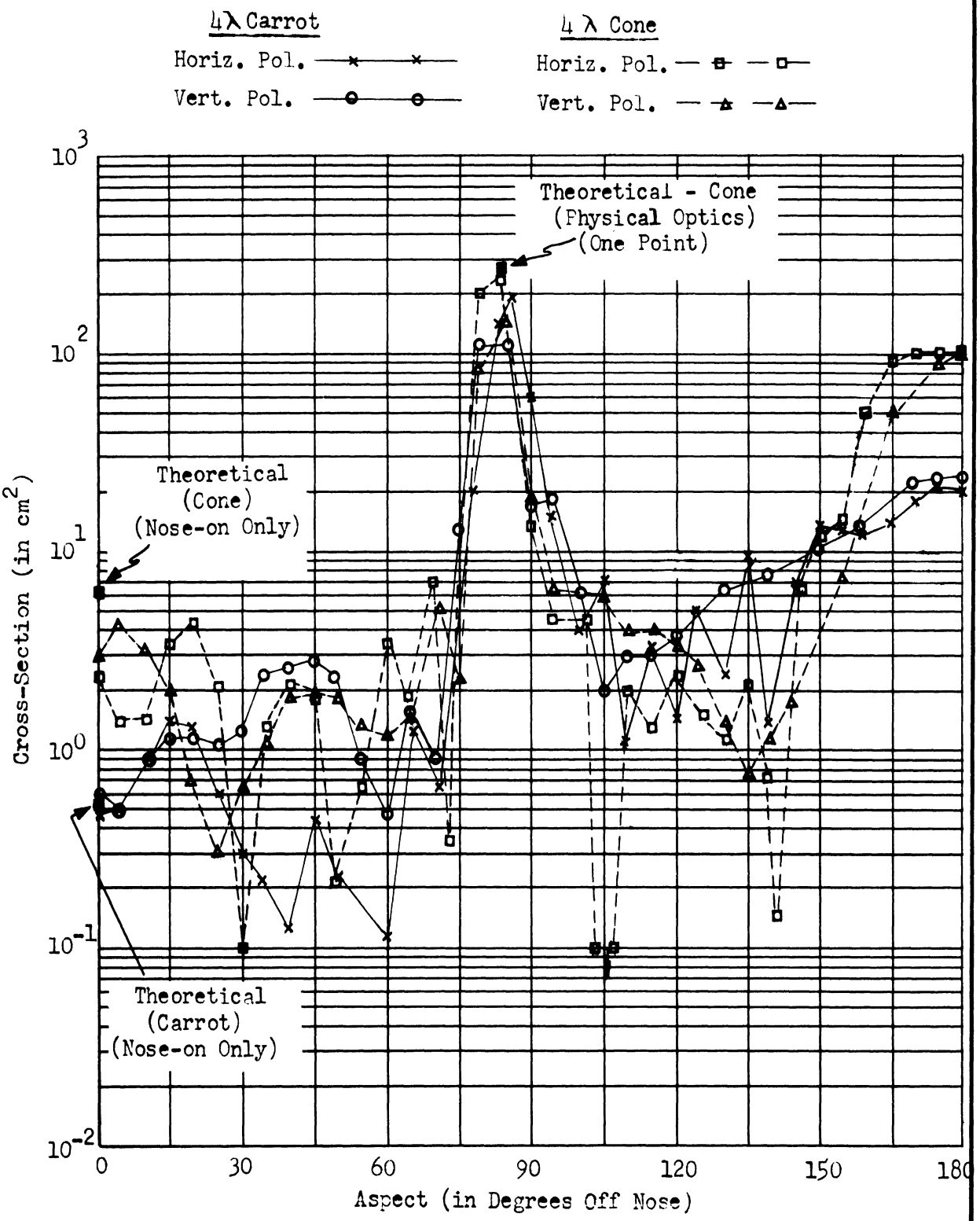

FIG F-3: 4λ CONE AND 4λ CARROT - (REF. 22)
(λ = 3.2 cm)

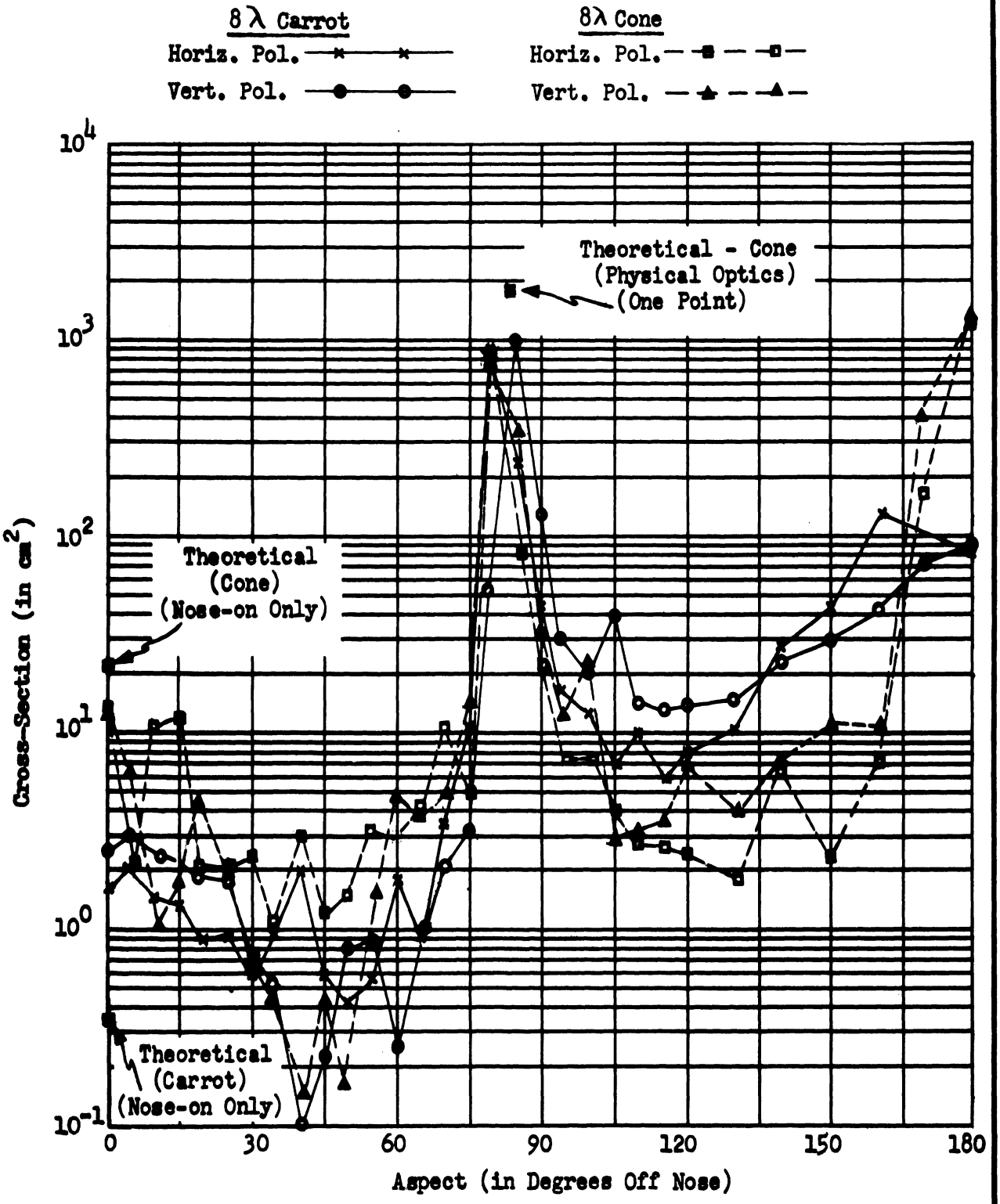

FIG F-4: 8λ CONE AND 8λ CARROT - (REF. 22)
(λ = 3.2 cm)

Theoretical estimates of the nose-on cross-section of the three finite cones are obtained, using the methods described previously in this report for thin cones. That is, an estimate of the graph of cross-section vs. a/λ, where a is the radius of the base, is constructed, using the resonant loop answers computed by Kouyoumjian (Ref. 12) faired into the theoretical estimate valid for small wavelengths (i.e., wavelengths for which λ/a is small) developed in Appendix D. The results of these computations are shown in Table F.1 where the nose-on cross-sections of these cones determined theoretically are compared with the experimental data given in Reference 22.

TABLE F.1 - THE NOSE-ON CROSS-SECTIONS OF THE 2λ, 4λ, AND 8λ CONES (λ = 3.2 cm)

BODY	CROSS-SECTIONS (IN CM^2)			
	Exp. Data*	Exp. Data**		Theoretical Estimate***
	Ver. Pol.	Hor. Pol	Ver. Pol.	
2λ cone	3.0	5.3	5.0	5.4
4λ cone	1.1	2.6	3.0	6.5
8λ cone	5.6	13.0	17.0	23.0

*Unpublished data obtained by Professor S. Silver, Dept. of Electrical Engineering, University of California.

**Reference 22.

***These theoretical values are also shown on Figures F-2 through F-4.

Theoretical estimates of the cross-sections of these cones at an aspect 82.5° off nose have been computed, using the optics formula derived in Reference 23

$$(8\pi L^3 \tan^4\alpha)/(9\lambda \sin^3\alpha)$$

where L is the altitude of the cone and α is the half-cone angle ($\alpha = 7.5°$). The theoretical values so obtained are shown on Figures F-2 through F-4.

It will be noted that the agreement between theory and experiment is excellent at both aspects; this can be seen by reference either to Table F.1 or Figures F-2 through F-4 for the nose-on case and to the figures for the 82.5° aspect.

For the three carrots involved in these experiments the technique described in Appendix E is employed to obtain estimates of the nose-on cross-sections. That is, the cross-section is assumed to be obtained from a contribution from the tip and a contribution which creeps around the rear. The contribution from the rear is estimated by using the theoretical sphere answer in the resonance region with the contribution from the first Fresnel zone removed. This results in the following estimate of the cross-section contribution which creeps around the rear (for $\sim 1 < ka < \sim 15$)

$$.033\ \lambda^2\ (\lambda/a)^{\frac{1}{2}} \quad \text{(Ref. 2)}$$

where a is the radius of the "hemispherical" stern.*

*As pointed out in Appendix E, the appropriate value of a is the radius of curvature at the shadow boundary. However, since this radius of curvature is approximately equal to one-half of the maximum thickness of the body for these carrots and since, as can be seen by reference to Appendix E, we are using an average estimate of this contribution, we can set a equal to one-half the maximum thickness of the body.

The estimates of the nose-on cross-sections of the three carrots obtained in this manner are shown on Figures F-2 through F-4 and in Table F.2. Table F.2, as well as the aforementioned figures, also contains the experimental data from Reference 22.

TABLE F.2 THE NOSE-ON CROSS-SECTION OF THE 2λ, 4λ, AND 8λ CARROTS (λ= 3.2 cm)

Body	Cross-Section (in cm^2)	
	Exp. Data (average of Hor. & Ver. Pol.)	Theoretical Estimate
2λ Carrot	1.7	0.72
4λ Carrot	0.53	0.51
8λ Carrot	2.2	0.36

Reference to Table F.2 shows that the agreement between theory and experiment is quite good.

F.3 The Radar Cross-Sections of 7-OC Type Warheads

Experimental data on the 7-OC warhead and modified versions of the 7-OC warhead were reported in Reference 2. These configurations are similar to the carrot and cone shapes discussed above. Sketches of thes configurations appear in Figure F-5. Theoretical estimates of the nose-on cross-sections have been determined by the methods described in Section F.2 - the finite cone methods for the 7-OC, and the 7-OC with a flat stern, and the formula for determining the contribution which creeps around the rear of the body for the 7-OC with a hemispherical stern. The results so

obtained are given in Table F.3; the experimental data for these configurations is included for comparison purposes. It will be noted that the agreement between theory and experiment is very good.

TABLE F.3 THE NOSE-ON CROSS-SECTIONS OF THE 7-OC TYPE WARHEADS (REFERENCE 2)*

Body	Wave-length (in cm)	Cross-Section (in cm^2)	
		Experiment	Theory
7-OC Warhead	30	12,000 - 15,000	10,000
7-OC Hemispherical Stern	30	60 - 100	140
7-OC Warhead	90	9,000 - 10,000	10,000
7-OC Hemispherical Stern	90	1,500 - 1,600	400
7-OC Warhead	133	4,000 - 9,000	10,000
7-OC Hemispherical Stern	133	250 - 1,800	900
7-OC Flat Stern	133	6,000 - 7,000	10,000

*The experiments are reported in Reference 2 ; they were performed by The Microwave Radiation Company, Inc., and by the Evans Signal Laboratory.

F.4 Other Experimental Data on Cones

F.4.1 Data From the Federal Telecommunications Laboratories, Inc.

W. Sichak in Reference 24 has reported the results of experiments conducted on three thin finite cones; these cones have half-cone angles of 5.1° and 9.6°. Sichak's data, together with the theoretical estimates obtained by the procedure described in Section F.2, are presented in Table F.4.

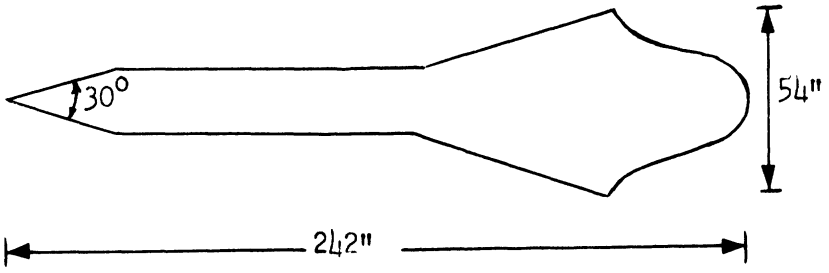

The 7-OC Warhead

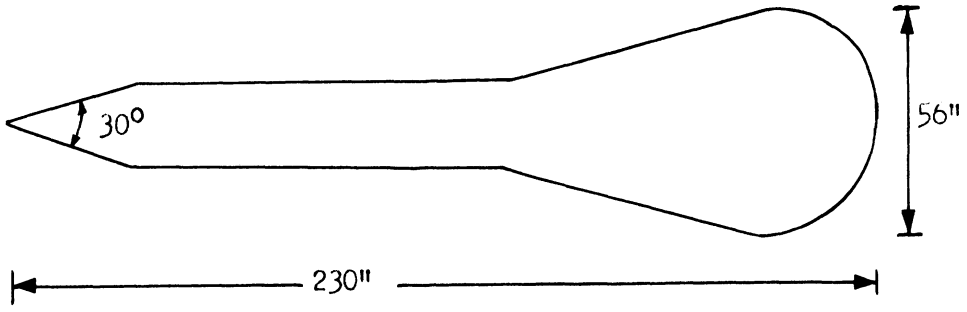

7-OC With a Hemispherical Stern

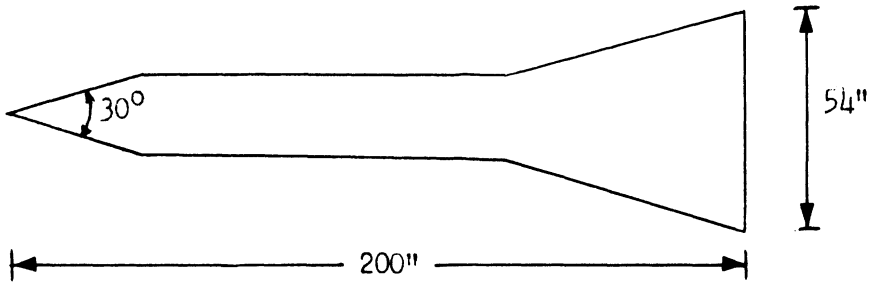

7-OC With a Flat Stern

FIG F-5: 7-OC TYPE MODELS

TABLE F.4 NOSE-ON CROSS-SECTIONS OF FINITE CONES USED IN FEDERAL TELECOMMUNICATIONS LABORATORIES EXPERIMENTS

Half-Cone Angle (in degrees)	Altitude of Cone (in cm)	Wavelength (in cm)	Cross-Section (in cm^2)	
			Experiment	Theory
9.6	15.25	1.25	4.0	13.0
5.1	15.25	1.25	0.6	3.6
9.6	7.63	1.25	0.9	3.4

F.4.2 Data From the Belmont Radio Corporation

The data from the Belmont Radio Corporation (Ref. 25) were obtained from an experiment conducted on a thin cone having a half-angle of $\sim 10^{\circ}$. The experiment was conducted at a wavelength of 1.26 cm and the radius of the base of the cone was equal to 0.59λ. The experimental value of the nose-on cross-section of this cone is 0.87 cm^2. Applying the techniques previously described in this Appendix, a theoretical estimate of 1.1 cm^2 is obtained.

F.4.3 British Experiments on Cones Capped With Cylinders

On a recent trip to England one of the authors (K.M.Siegel) was informed by J.S.Hey of the Radar Research Establishment of recent British experiments on cones faired into cylinders. From these experiments, which were conducted on four different cones capped with cylinders of varying length, average values were obtained. These values, together with theoretical estimates, are given in Table F.5. The theoretical estimates were obtained by using the expression derived in Appendix D (Equation 6 of Appendix D).

TABLE F.5 NOSE-ON CROSS-SECTIONS OF FINITE CONES FAIRED INTO CYLINDERS (UNPUBLISHED BRITISH EXPERIMENTAL DATA AND THEORETICAL ESTIMATES)

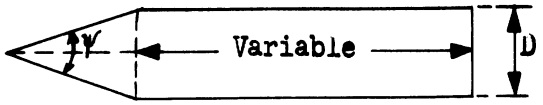

D (in λ)	$\Psi/2$	Cross-Section (in λ^2)		
		Experimental Est.	Theoretical Est.	
			Front Ring Only	Upper* Bound
1.8	10°	0.2	0.08	2.2
1.8	30°	0.3	0.4	3.1
3.0	10°	0.3	0.2	6.0
3.0	30°	0.5	1.0	8.8

F.4.4 Experimental Data on Thick Cones With Smoothly Rounded Bases

The work of C. J. Sletten (Ref.17) has indicated that if the cone angle is not too small and if $ka >> 1$, then the nose-on cross-section of a smoothly rounded cone is adequately predicted by the physical optics formula, $\lambda^2 \tan^4\theta/16\pi$, where θ is the half-cone angle. Sletten's experimental data are compared with this physical optics expression in Figure F-6.

* The upper bound was obtained by assuming that the tangential component of the incident field is propagated without attenuation to the sharp edge at the rear of the cylinder. The contribution from the front ring plus the contribution from the back ring thus obtained plus the maximum value of the resulting oscillating term yield the upper bound.

THE UNIVERSITY OF MICHIGAN
2428-19-T

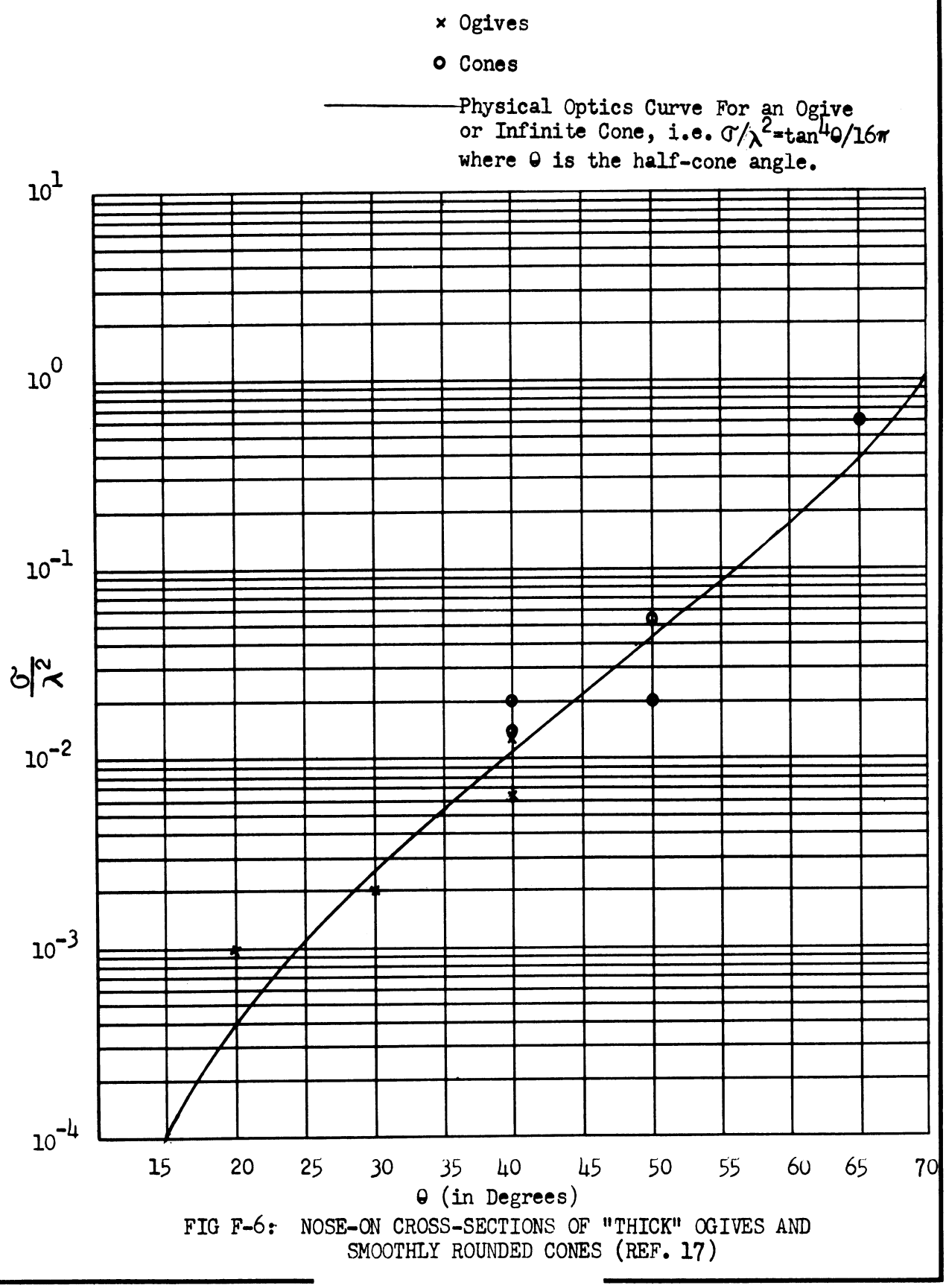

FIG F-6: NOSE-ON CROSS-SECTIONS OF "THICK" OGIVES AND SMOOTHLY ROUNDED CONES (REF. 17)

F.5 Conclusions

It has been observed in this appendix that the techniques employed to obtain theoretical estimates of the nose-on cross-sections of finite cones and finite cones which are smoothly terminated are in good agreement with experimentally determined values.

In addition it has been noted that there is, in general, at most one order of magnitude difference between the cross-sections of thin finite cones, smoothly rounded or not, if the over-all length of the configuration ranges from 2 to 8 wavelengths, especially for aspects out to 60° off nose. This is illustrated in Figure F-7. Thus, it is seen from the experimental data that if the radius of the base is comparable to the wavelength, the nose-on cross-section of the "carrot" is comparable to the nose-on cross-section of the comparable cone. If, on the other hand, the wavelength is small in comparison to this base-radius, the two nose-on cross-sections are considerably different. This trend can be seen from the material presented in Section F.4.

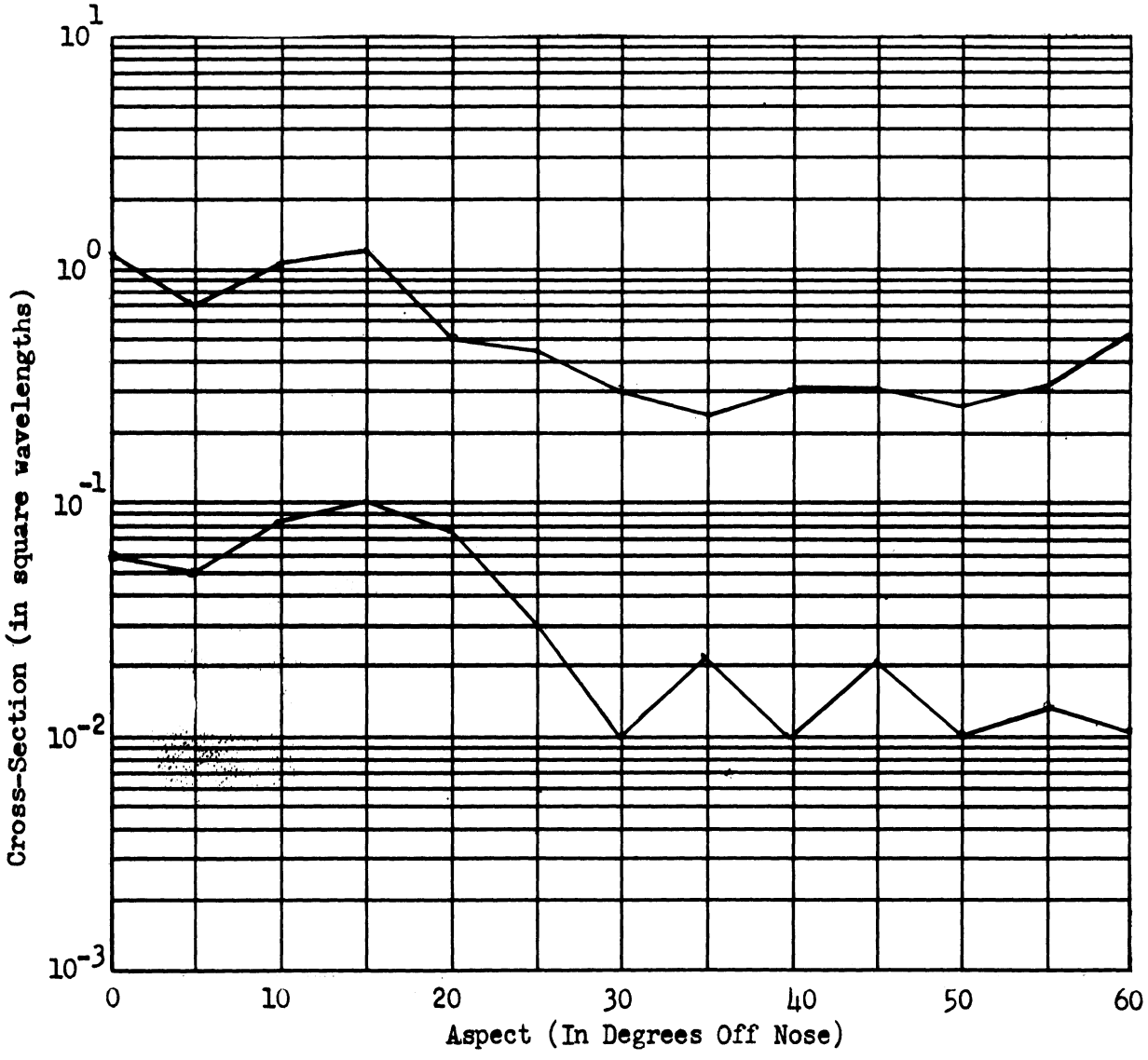

FIG F-7: LIMITS ON EXPERIMENTAL DATA FOR 7.5° CARROTS AND CONES
(Horizontal and Vertical Polarizations)

APPENDIX G

RADAR CROSS-SECTION OF AN OGIVE

We observed (Appendix E) that by using the diffraction contribution from the sphere together with the optics results for a cone, we could predict the cross-section of a shape which had a cone in front and was smoothly terminated in the rear (large ratio of radius of curvature to wavelength). When this radius of curvature (in the direction of Poynting's vector) at the shadow boundary was small, different techniques were required since the body "looked electromagnetically" like a sharply defined cone. "Sharpness" can only have meaning in terms of the sensitivity of the measuring instrument employed which, for electromagnetic energy, is wavelength.

One of the famous experiments involving discs shows that when a disc is illuminated by a point source in front, there is a bright spot in the rear. The student may ask, "how do you explain this 'bright spot behind the penny' when there has been a decay of the energy in the shadow region?" The answer is that at that particular angle of incidence a large amount of the lower order diffraction contribution has added in phase. To prove this, we rotate the penny slightly and the spot disappears. We can add a small discontinuity the order of the wavelength in the transition region (edge of penny) and bright spot disappears.

Now we are ready to discuss the ogive, that body formed by rotating a segment of a circle about its chord. We know the tip answer (see Appendix E). We expect the effects as we enter the transition region to remain very dependent on radii of curvature to wavelength ratios as discussed previously;

however, the point in the rear must be further investigated. This point clearly acts as a reflector to those waves which have crept along the body. Though these are second order effects we still must worry about "bright spot" effects. It seems clear that if the ogive is thin and not very long (in wavelengths) then in the case of axially symmetric back scattering one must expect such a "bright spot" effect as this case is such as to permit the in-phase addition of much of the creeping wave contribution. Thus we expect the nose-on cross-section for thin, relatively short ogives to be larger than we previously anticipated. To obtain a feel for this in-phase contribution, we obtained (see Appendix E) the maximum in-phase contribution from the diffraction term for a sphere. We believe that the effect of the creeping wave contribution for the ogive is greater than that for the corresponding sphere (sphere diameter equal to ogive diameter at thickest part) because the rear point of the ogive serves to reflect and focus energy back along the axis in phase. We predict that the maximum diffraction term for the sphere is of the right order to use, with the nose-on tip result, to obtain the ogive result. This then says that for the region $(ka)_1 > ka > \sim 15$ and $\alpha \leq \sim 20^\circ$ the ogive result is given by

$$\sigma = \frac{\lambda^2 \tan^4 \alpha}{16\pi} + \frac{a\lambda}{2}$$

where a is the radius of the ogive at its thickest part

α is half the ogive angle

$(ka)_1$ is, for fixed a, a lower limit on λ beyond which the rear contribution will be negligible.

As the direction of incidence moves off the axis of symmetry this in-phase "bright spot" contribution begins to decrease but simultaneously the tip contribution begins increasing according to the law

$$\sigma_{tip}(\theta) = \frac{\lambda^2 \tan^4\alpha}{16\pi \cos^6\theta(1-\tan^2\alpha \tan^2\theta)^3} \quad , \quad \theta < \frac{\pi}{2} - \alpha$$

where θ is the angle between the axis of symmetry and the direction of incidence. The contribution from the rear, $a\lambda/2$ decreases toward $\lambda^2/16\pi$. When the tip answer approaches the rear contribution, one might as well stop considering the rear contribution further. As θ increases even further, we can use previously derived optics laws as the effective resonance region is getting smaller and smaller (see Section IV). Thus when $\theta \geq \frac{\pi}{2} - \alpha$ we can use the following optics expressions (derived in Ref. 23)

$$\theta = \frac{\pi}{2} - \alpha$$

$$\sigma(\theta) = \frac{a^2}{4\pi \tan^2 \alpha/2}$$

$$\frac{\pi}{2} - \alpha < \theta \leq \frac{\pi}{2}$$

$$\sigma(\theta) = \frac{\pi a^2 (1+\cos\alpha)^2}{\sin^4\alpha}\left(1 - \frac{\cos\alpha}{\sin\theta}\right)$$

Considering the length of the ogive fixed and the wavelength fixed, $\sim 15 < ka < (ka)_1$ increasing the ogive angle so that the ogive approaches a sphere makes the resonance region become smaller. Thus the optics results can be applied for smaller and smaller values of ka until we find that the

region R: $\sim 15 < R < (ka)_1$ has shrunk to zero.

We have examined the effect of going from an intermediate range in ogive angle towards a sphere. The next question to be answered is what happens as the wavelength remains fixed while the ogive angle becomes smaller and smaller and the length becomes greater and greater. The cross-section of the ogive approaches that of a long thin wire. The wire results have been worked out for the case when the wavelength is larger than the wire radius (Ref. 11). The results of wire theory were used by us to obtain cone results in Section IV.

Ogive experiments have recently been performed by L. Peters at The Ohio State University (Ref. 4). The ogives used in these experiments are shown in Fig. G-1. In Figures G-2 through G-6 the experimental results are shown together with the results of our order analysis and the expected behavior of the curves.

The theory of Peters (Ref. 26) to explain his results will now be described.

The echo area of a long thin body is derived making use of existing concepts of antenna theory. The body is considered as a traveling-wave antenna. The position of the terminals of the antenna is chosen such that the component of power which is normally denoted as the scattered power may be neglected and thus the power that is flowing into the antenna terminals is computed (normally denoted as absorbed power). A portion of this power is reflected and consequently radiated as if the body were a transmitting antenna. This component of power is used to compute the echo area of the

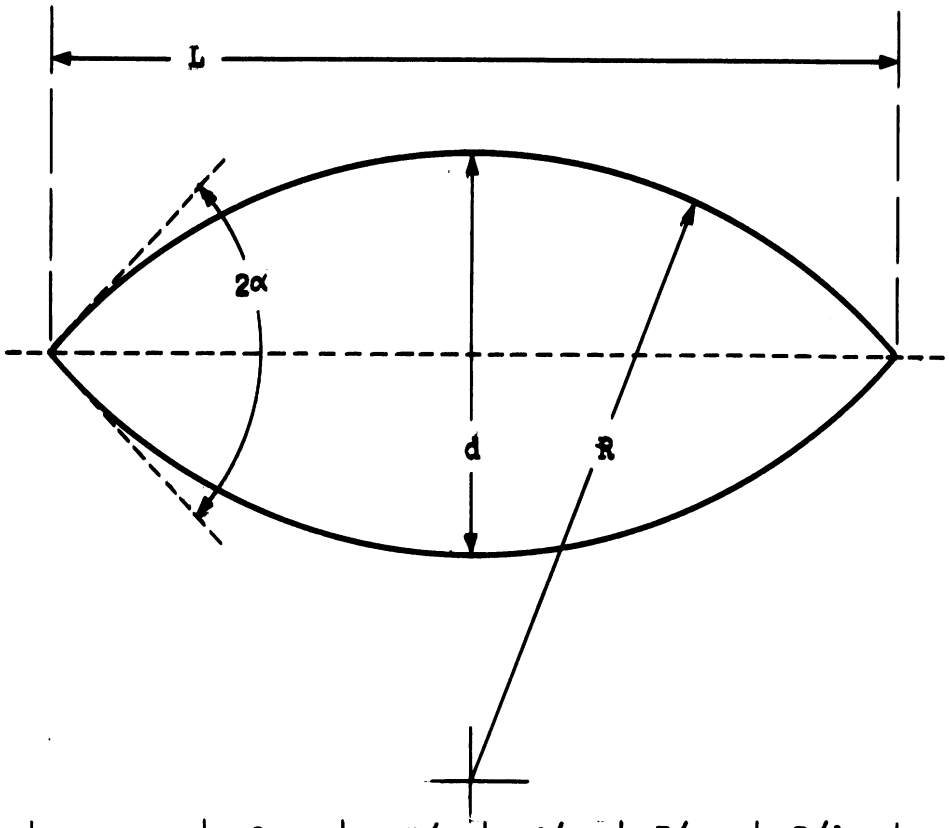

OGIVE No.	2α	L/λ	d/λ	R/λ	L/d
1	29.2°	32.0	4.2	62.0	7.6
2	29.2°	39.5	5.2	77.0	7.6
3	61.4°	36.6	9.8	36.6	3.7
4	88.8°	36.6	15.0	24.4	2.4
5	120.4°	36.6	21.0	21.0	1.7

FIG. G-1 OGIVES USED IN O.S.U. EXPERIMENTS

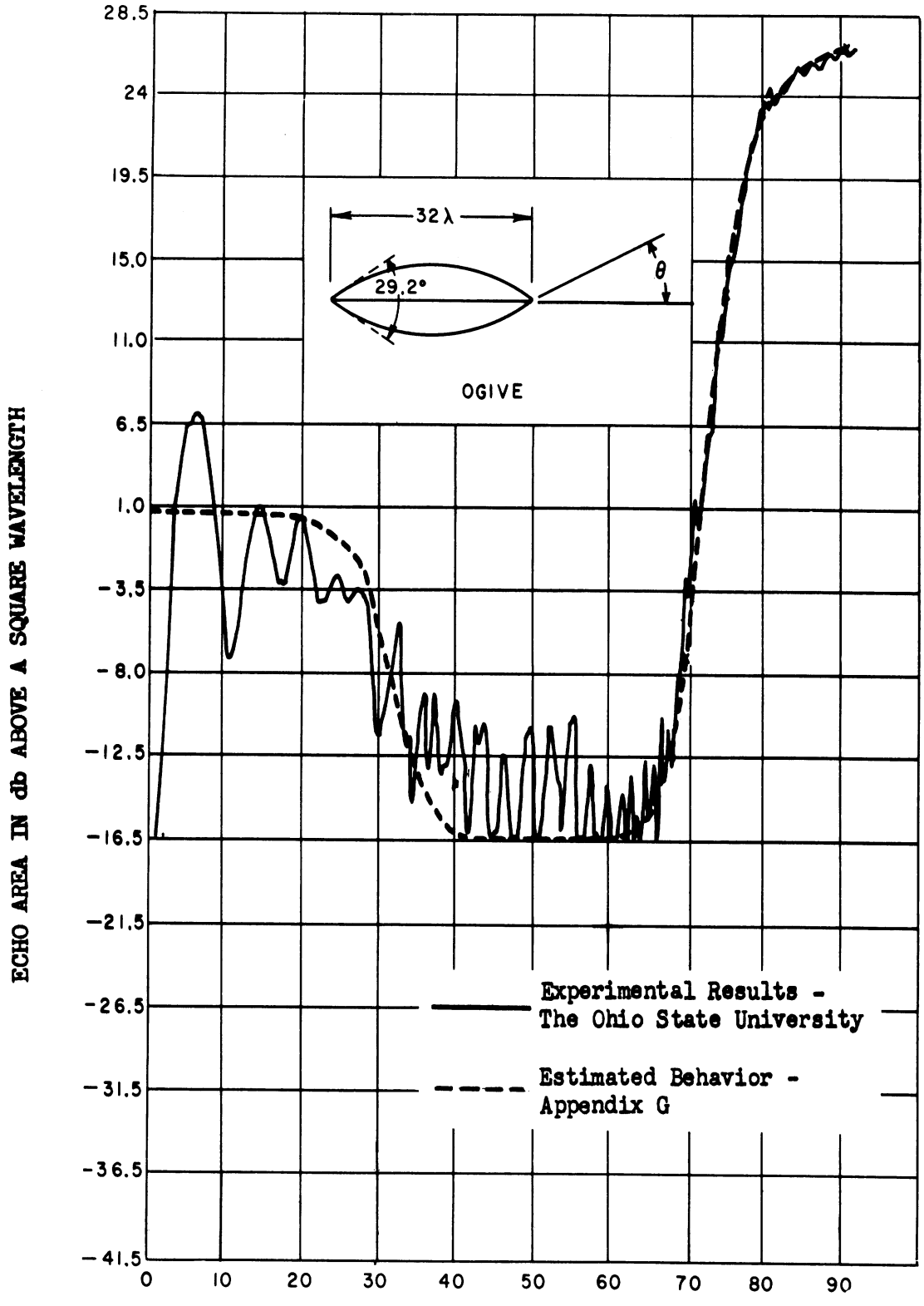

FIG. G-2 ECHO AREA PATTERN OF THE NO. 1 OGIVE

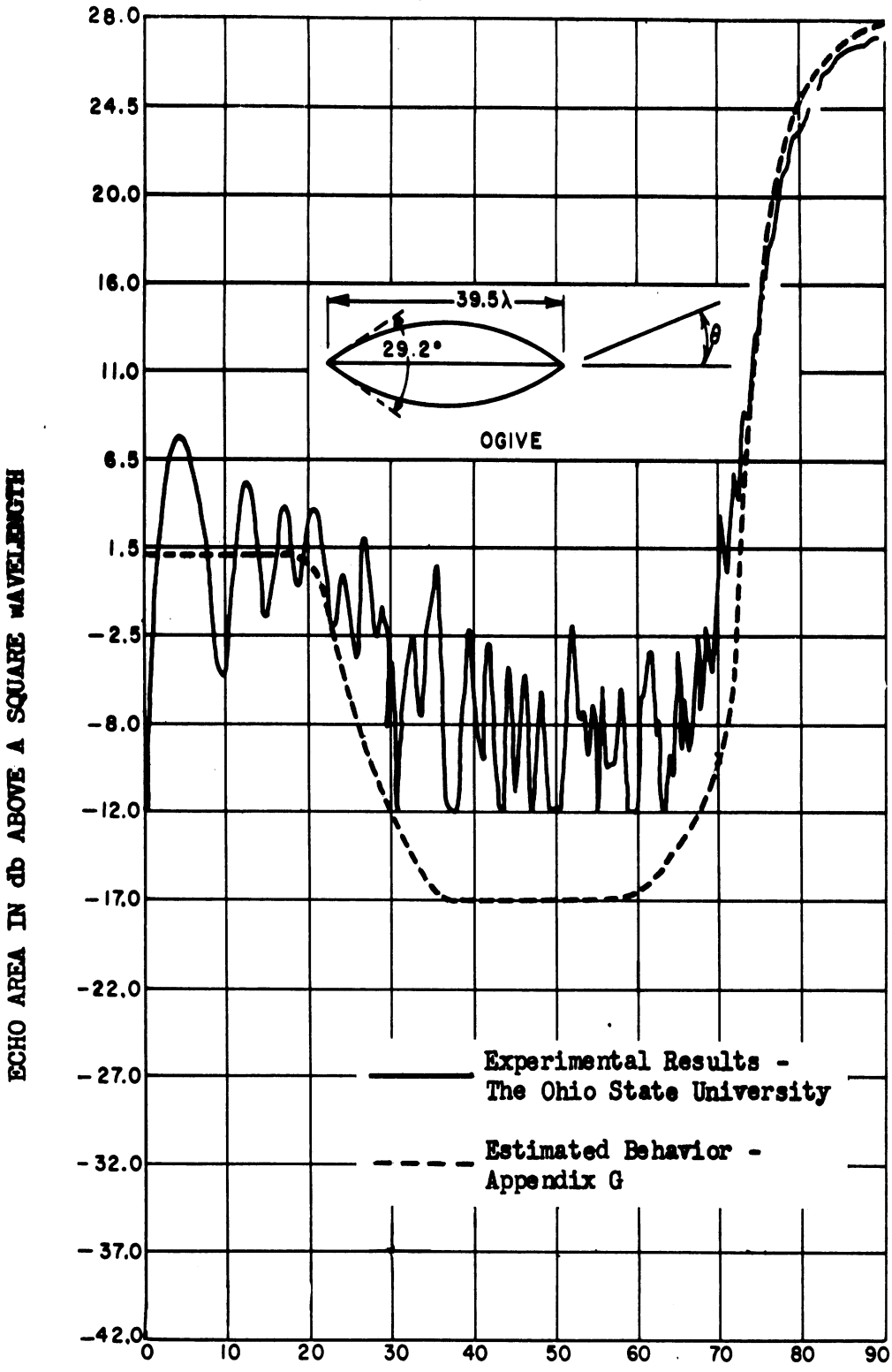

FIG. G-3 ECHO AREA PATTERN OF NO. 2 OGIVE

This Appendix is UNCLASSIFIED when detached from the remainder of the report.

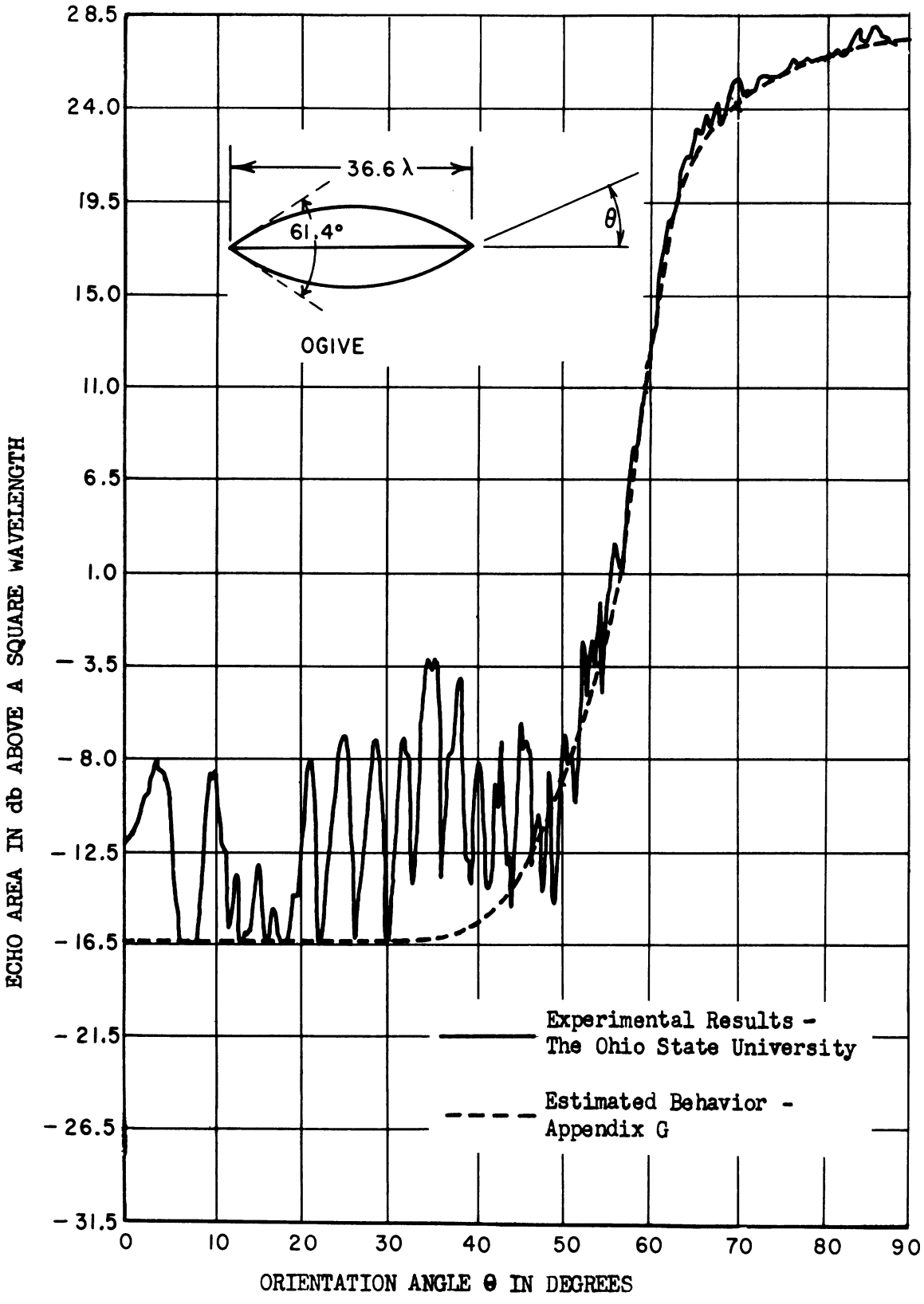

FIG. G-4 ECHO PATTERN OF THE NO. 3 OGIVE

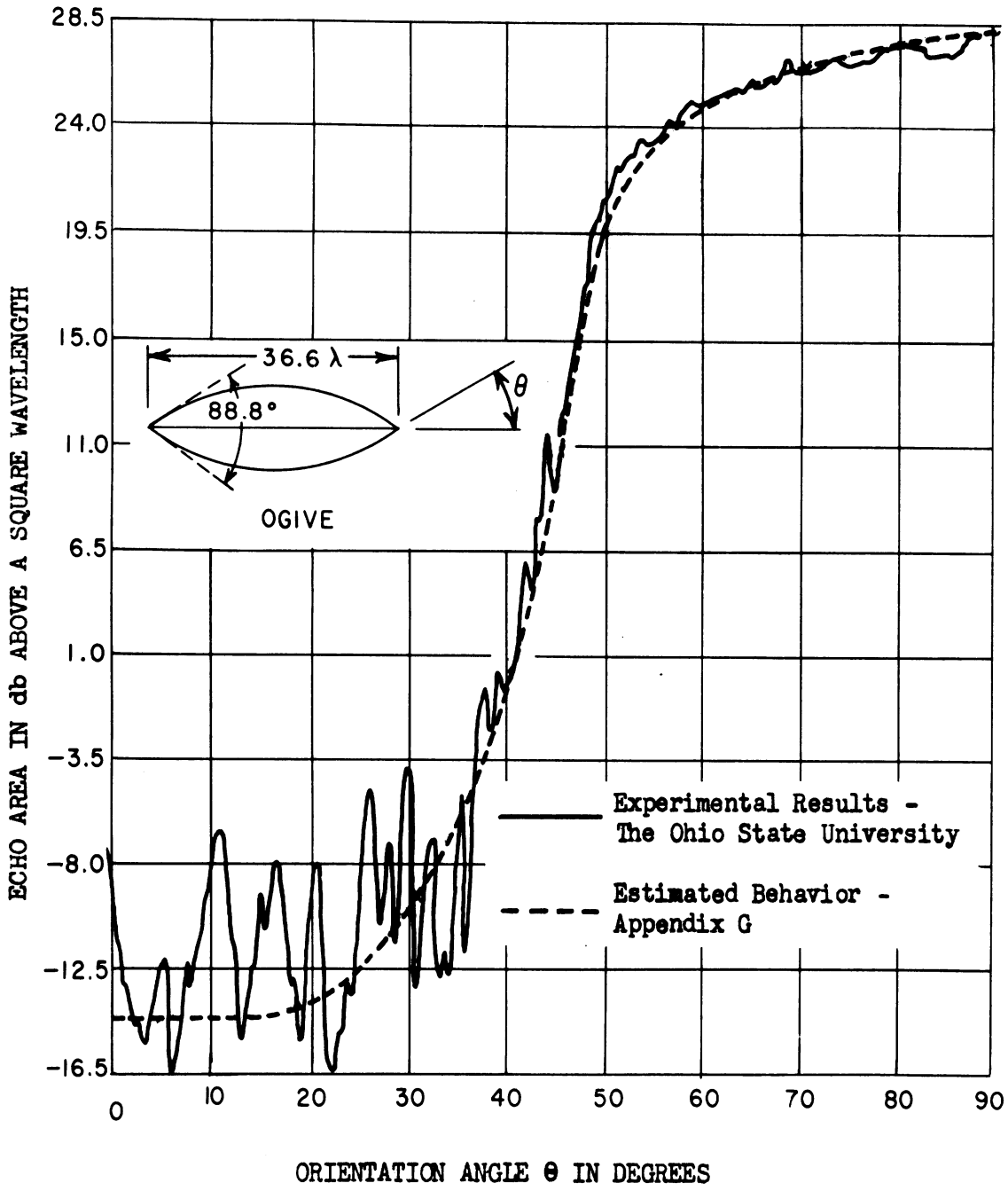

FIG. G-5 ECHO AREA PATTERN OF THE NO. 4 OGIVE

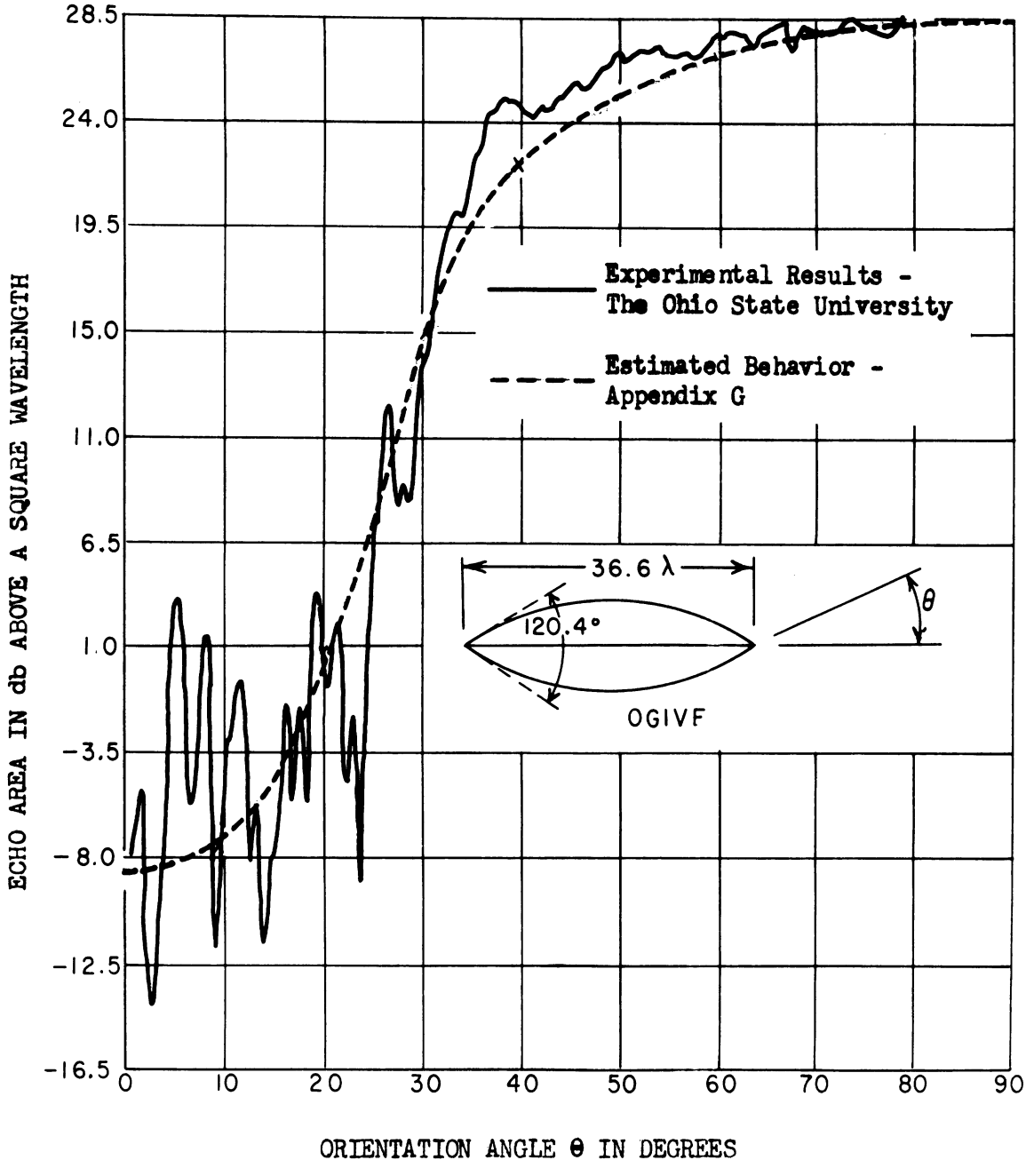

FIG. G-6 ECHO AREA PATTERN OF THE NO. 5 OGIVE

body. Since the magnitude of the power reflected from the terminals is proportional to the square of the voltage reflection coefficient, ν , he obtains for the cross-section

$$\sigma = \nu^2 \frac{G^2(\theta,\phi)}{4\pi} \lambda^2 .$$

The gain, $G(\theta, \phi)$ is determined from the magnetic field intensity of a thin traveling-wave antenna. This he (Peters) determines from purely theoretical arguments. In applying the technique to a specific body (for example an ogive 39 wavelengths long with a half-angle of 15°) the value of ν^2 is determined experimentally. To do this a flat plate of 0.9λ was placed at one end of the ogive, and the echo area measured both for the ogive with the plate and without. Assuming that, in the flat plate case, the voltage reflection coefficient is equal to one, the value of ν^2 for the ogive with no termination can be estimated. The results he so obtained are in good agreement with experiment in so far as predicting the maxima of the oscillations in echo area as a function of aspect out to about 50° off-nose.

This technique unfortunately can not be readily applied to the estimation of the return from any given ogive unless experimental equipment is available for the determination of the appropriate value of ν^2.

In the previous analysis of this appendix we insisted that in order for the ogive cross-section to contain a sizeable creep-transition region contribution, ka was such that $\sim 15 < ka < (ka)_1$. The next questions to raise are (1) why do we choose an upper limit to this range of ka? and (2) what formulas do we use for larger ka's? The answer to the second question is that

above the value of $(ka)_1$ we use the tip-scattering formulas and the optics formulas for $\theta = \frac{\pi}{2} - \alpha$ and $\frac{\pi}{2} > \theta > \frac{\pi}{2} - \alpha$. The reasoning for this follows directly from the reasoning we will use to answer question 1.

It was proposed by Schiff (Ref. 16) that these two contributions could be evaluated by assuming a current distribution on the body of the following form (illustrated symbolically in Fig. G-7). In the lit region the current, given by physical optics is constant as the shadow boundary is approached while in the shadow region the current distribution is assumed to match the optics value at the shadow boundary and go continuously to zero around the back of the body. The contribution from the rear, thus obtained, was of higher order in λ than the tip contribution hence negligible in the optics region.

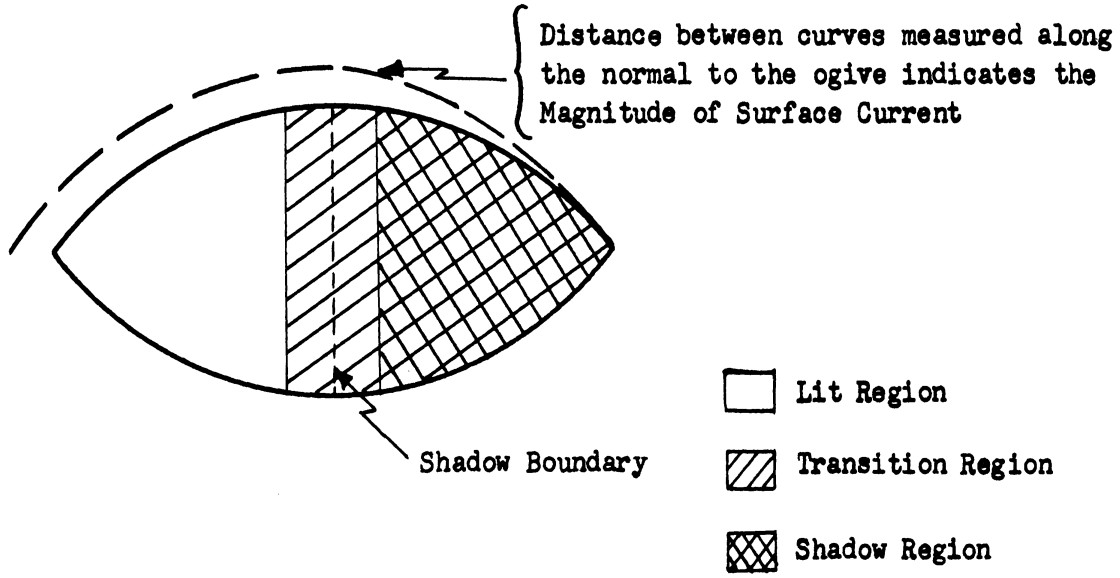

FIG G-7

From the work of Fock (Ref. 21) an estimate can be found for determining for a given ogive, a lower bound of ka for which the current on the rear has attenuated sufficiently to justify the neglect of the contribution from the rear. It is assumed that an attenuation of the current reaching the rear tip to less than one-tenth of the value of the current at the shadow boundary is required to insure that the front tip contribution dominates. Using Fock's expressions for the current on the rear of a sphere, the minimum ka for which an attenuation to one-tenth takes place is plotted against α, the half-angle of the ogive, in Fig. G-8. It is seen that for thin ogives, e.g., $\alpha < 30^{\circ}$, ka must be greater than 200 in order to be able to use the expression $\sigma \approx \frac{\lambda^2 \tan^4 \alpha}{16\pi}$ for the cross-section of an ogive. Thus we use Fig. G-8 to pick a value of $(ka)_1$ for each ogive of angle 2α.

Now, given an ogive of angle 2α, of major axis 2g and minor axis 2h, one can relate it to a prolate spheroid to learn about the first maximum. The Rayleigh elongation factor y (Appendix A) of the ogive is

$$y = \frac{\frac{3}{2}(\sin\alpha - \alpha\cos\alpha - \frac{1}{3}\sin^3\alpha)}{(1 - \cos\alpha)^3} .$$

Now we make the minor axis of the spheroid the same as that of the ogive, 2h, and we recall that in this notation the elongation factor of the spheroid is $\frac{\ell}{h}$, where ℓ, the semi-major axis of the equivalent spheroid, is given by

$$\ell = \frac{3h}{2} \frac{(\sin\alpha - \alpha\cos\alpha - (1/3)\sin^3\alpha)}{(1 - \cos\alpha)^3}$$

Now we have found the Rayleigh equivalent spheroid (that spheroid with the

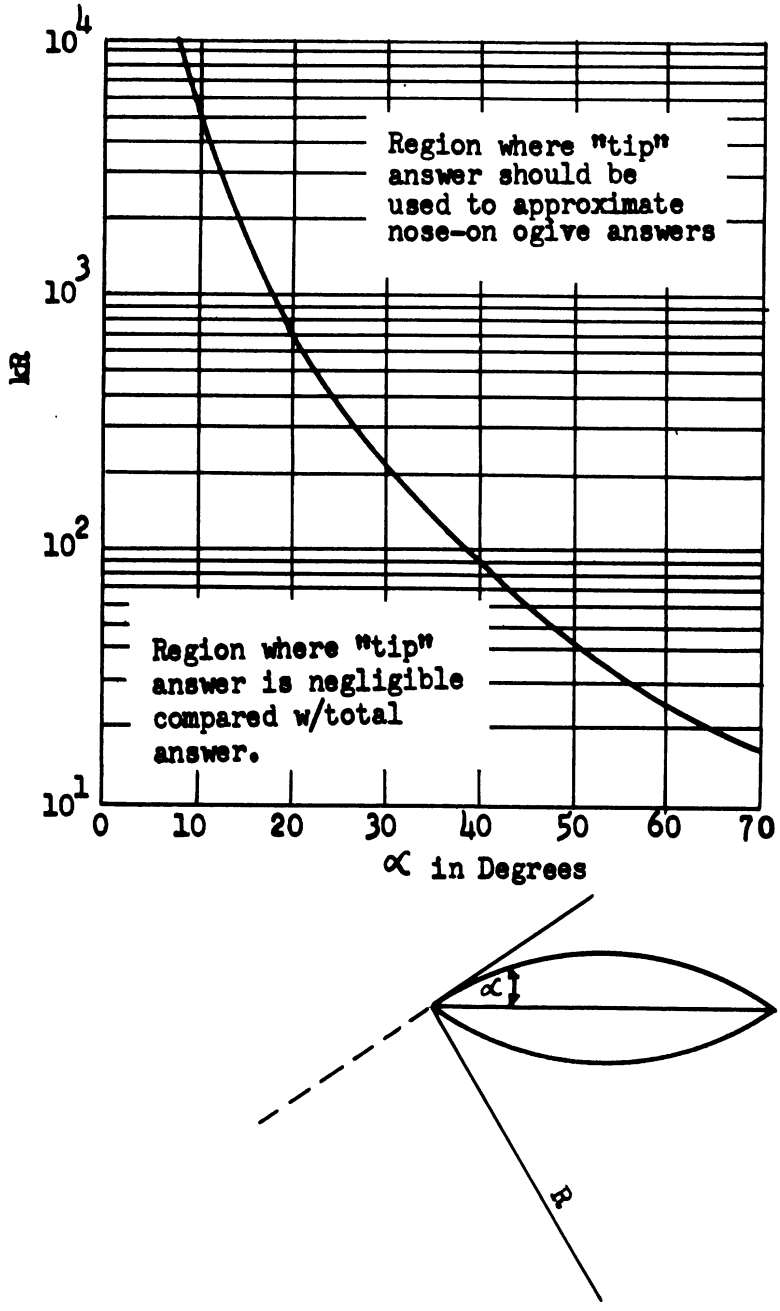

FIG G-8 APPLICABILITY OF OGIVE TIP RESULT TO TOTAL ANSWER

same cross-section in the Rayleigh region) for our ogive and can bring our previous analysis to bear. That is, we can find the abscissa of the first maximum by thin-wire theory (Ref. 11) and we can predict the amplitude of the first nose-on maximum by interpolation between the results of Mushiake (Ref. 27) and the 10/1 result (Fig. 4-1). We might even predict the abscissas of the first several maxima and minima by thin-wire theory and by interpolation predict the amplitudes of the first two maxima. To summarize: We have given our predictions, as a function of ka, for almost all nose-on cross-sections of ogives. We have made a Rayleigh region approximation. We have found an equivalent spheroid to predict results on the Rayleigh side of the resonance region. We have used the sphere results to predict an order for the intermediary resonance region results and average sphere diffraction term results to predict resonance results on the optics side. We then presented the optics results. We also presented the off-angle results except in the Rayleigh side of the resonance region. We have covered almost all other monostatic cases.

Many of the conclusions reached here should be further analyzed as more experience is gained in this field. We do feel we have obtained enough information to answer questions raised in the classified sections of this report.

REFERENCES

1. K.M.Siegel, M.L.Barasch, H.Brysk, J.W.Crispin, T.B.Curtz, and T.A.Kaplan, "Studies in Radar Cross-Sections XIX - Radar Cross-Section of a Ballistic Missile - II", The University of Michigan, Engineering Research Institute, Report No. 2428-3-T (January 1956). SECRET

2. K.M.Siegel, M.L.Barasch, J.W.Crispin, I.V.Schensted, W.C.Orthwein, and H.Weil, "Studies in Radar Cross-Sections XIV - Radar Cross-Section of a Ballistic Missile", The University of Michigan, Engineering Research Institute, Report No. UMM-134 (September 1954). SECRET

3. J.Honda, S.Silver, and F.Clapp, "Measurement of Scattering Cross-Sections of Figures of Revolution", University of California (work supported by ONR Contract N7-ONR-29529), Presented at Joint Meeting of URSI and the IRE, Washington, D. C. 30 April-2 May 1956.

4. L.Peters, "Memorandum on the Echo Area of Ogives", The Ohio State University Research Foundation, Report No. 601-7 (January 1956). UNCLASSIFIED

5. K.M.Siegel, F.V.Schultz, B.H.Gere, and F.B.Sleator, "The Theoretical and Numerical Determination of the Radar Cross-Section of a Prolate Spheroid", Proceedings of the Symposium on Electromagnetic Wave Theory, June 20 - 25, 1955 at The University of Michigan, Trans. of the IRE - PGAP, Vol. AP-4, No. 3 (July 1956).

6. B.B.Gorr and Lt.P.Blacksmith,Jr., "Radar Cross-Section of a Ballistic Missile", Antenna Laboratory, Air Force Cambridge Research Center, Technical Memorandum ERD-CRRD-TM-56-113 (4 June 1956). SECRET

7. R.I.Primich, J.E.Keys, and P.Robillard, "Scattering From ICBM Warheads", Radio Physics Laboratory, Defence Research Board of Canada, Memorandum to J.C.W.Scott (27 April 1956). SECRET

8. "Radar Cross-Section Measurements - Final Report", Cornell Aeronautical Laboratory, Inc., (CAL-University of Michigan Subcontract on Prime Contract AF-04(645)-33) Report No. UB-1071-P-1, (September 1956). SECRET

9. K.M.Siegel, H.A.Alperin, R.R.Bonkowski, J.W.Crispin,Jr., A.L.Maffett, C.E.Schensted and I.V.Schensted, "Studies in Radar Cross-Sections VIII - Theoretical Cross-Section as a Function of Separation Angle Between Transmitter and Receiver at Small Wavelengths", The University of Michigan, Engineering Research Institute, Report No. UMM-115 (October 1953). UNCLASSIFIED

10. A.F.Stevenson, "Solution of Electromagnetic Scattering Problems as Power Series in the Ratio (Dimension of Scatterer)/Wavelength", Journal of Applied Physics, 24, 1134 (1953).

11. J.H.Van Vleck, F.Bloch, and M. Hammermesh, "Theory of Radar Reflection from Wires or Thin Metallic Strips", Journal of Applied Physics, 18, 274 (1947).

12. R.G.Kouyoumjian, "The Backscattering from a Circular Loop", The Ohio State University Research Foundation, Report No. 662-5 (1956). UNCLASSIFIED

13. J.W.Strutt, Baron Rayleigh, "On the Incidence of Aerial and Electric Waves Upon Small Obstacles in the Form of Ellipsoids or Elliptic Cylinders and on the Passage of Electric Waves Through a Circular Aperture in a Conducting Screen", Philosophical Magazine, 44, 28 (1897).

14. J.A.Stratton, Electromagnetic Theory, McGraw-Hill, New York pp. 432-435 (1941).

15. A.L.Maffett, M.L.Barasch, W.E.Burdick, R.F.Goodrich, W.C.Orthwein, C.E.Schensted, and K.M.Siegel, "Studies in Radar Cross-Sections XVII - Complete Scattering Matrices and Circular Polarization Cross-Sections for the B-47 Aircraft at S-Band", The University of Michigan, Engineering Research Institute, Report No. 2260-6-T (June 1955). CONFIDENTIAL

16. W.Hansen and L.Schiff, "Theoretical Study of Electromagnetic Waves Scattered from Shaped Metal Surfaces", Stanford University, Microwave Laboratory, Quarterly Report No. 3, ATI-104410 (May 1953). UNCLASSIFIED

17. C.J.Sletten, "Electromagnetic Scattering from Wedges and Cones", Air Force Cambridge Research Center, Report No. 5090 (July 1952). UNCLASSIFIED

18. W. Franz and K. Deppermann, "Theory of Diffraction by a Cylinder as Affected by the Surface Wave", Annalan der Physik, 10, 361 (1952).

19. I. Imai, Z. Phys., 137, 31 (1954).

20. V.E.Pound, Internal Cornell Aeronautical Laboratory, Inc., Memorandum No. 830-141 (18 June 1956). UNCLASSIFIED

21. V. A. Fock, Journal of Physics, 10, 130 and 399 (1946).

22. "Radar Backscattering Cross-Sections of Three Configurations", Microwave Radiation Company, Inc., Report No. 203 (Work performed for Cornell Aeronautical Laboratory, Inc., under Contract No. DA-30-115-ORD-543), July 1955. SECRET

23. C.E.Schensted, J.W.Crispin, and K.M.Siegel, "Studies in Radar Cross-Sections XV - Radar Cross-Sections of B-47 and B-52 Aircraft", The University of Michigan, Engineering Research Institute, Report 2260-1-T (August 1954). CONFIDENTIAL

24. W.Sichak, "Missile Detection - Final Report", Federal Telecommunications Laboratories, Inc., Contract W-36(038)-sc-32119, ATI 42811 (August 1948). SECRET

25. "Research Investigations on Counter-Battery and Fire Control Radar", Belmont Radio Corporation, Final Report (May 1948). SECRET

26. L. Peters, "End-Fire Echo Area of Long Thin Bodies", The Ohio State University Research Foundation, Report No. 601-9 (June 1956) UNCLASSIFIED